HEI energy

NUMBER 231
DECEMBER 2025

RESEARCH REPORT

Assessing Source Contributions to Air Quality and Noise in Unconventional Oil Shale Plays

Meredith Franklin, Gunnar Schade, Detlev Helmig, Lara Cushing, and Jill Johnston

INCLUDES A COMMENTARY BY THE HEI ENERGY REVIEW COMMITTEE

www.healtheffects.org
www.HEIenergy.org

Assessing Source Contributions to Air Quality and Noise in Unconventional Oil Shale Plays

Meredith Franklin, Gunnar Schade, Detlev Helmig, Lara Cushing, and Jill Johnston

with a Commentary by the HEI Energy Review Committee

Research Report 231
Health Effects Institute
Boston, Massachusetts

Trusted Science · Cleaner Air · Better Health

Publishing history: This report was posted at *www.healtheffects.org* in December 2025.

Citation for report:

Franklin M, Schade G, Helmig D, Cushing L, Johnston J. 2025. Assessing Source Contributions to Air Quality and Noise in Unconventional Oil Shale Plays. Research Report 231. Boston, MA: Health Effects Institute.

ISSN 2688-6855 (online)

CONTENTS

ABOUT HEI ENERGY

The Health Effects Institute's Energy Research program (HEI Energy) was formed to identify and conduct high-priority research on potential population exposures and health effects from the development of oil and natural gas in the United States. Since 2022, HEI Energy has supported population-level exposure research in multiple oil and gas regions. This research followed an extensive planning process that included preparing reviews of the scientific literature, hosting multisector workshops to learn about research priorities, and developing an online curated database and spatial bibliography to advance both public and scientific understanding. The research scope of HEI Energy is expanding beyond oil and gas to other forms of energy development, with an overarching goal of providing impartial knowledge about the benefits and drawbacks associated with various technologies.

The scientific review and research provided by HEI Energy contribute high-quality and credible science to the public debate about unconventional oil and natural gas development and provide needed support for decisions about how best to protect public health. To achieve this goal, HEI Energy has put into place a governance structure that mirrors the one successfully employed for nearly 40 years by its parent organization, the Health Effects Institute (HEI), with several critical features:

- Balanced funding from the US Environmental Protection Agency under a contract that funds HEI Energy exclusively and from the oil and natural gas industry, with other public and private organizations periodically providing support
- An independent Board of Directors consisting of leaders in science and policy who are committed to fostering the public–private partnership that is central to the organization
- A research program governed independently by individuals having no direct ties to or interests in sponsor organizations
- An HEI Energy Research Committee, consisting of internationally recognized experts in one or more subject areas relevant to the Committee's work, that has demonstrated the ability to conduct and review scientific research impartially and has been vetted to avoid conflicts of interest
- Research that undergoes rigorous peer review by HEI Energy's Review Committee, which is not involved in the selection and oversight of HEI Energy studies
- Staff and committees that participate in open and extensive stakeholder engagement before, during, and after research and communicate all results in the context of other relevant research

In addition, HEI Energy publicly shares all literature reviews and original research that it funds, along with summaries written for a general audience. Without advocating policy positions, it provides impartial science targeted to make better-informed decisions.

HEI Energy is funded separately from the Health Effects Institute's other research programs (*www.healtheffects.org*), with financial support from the US Environmental Protection Agency, the oil and gas industry, and private foundations.

ABOUT THIS REPORT

The HEI Energy Research Report 231, *Assessing Source Contributions to Air Quality and Noise in Unconventional Oil Shale Plays*, presents a research project funded by HEI Energy and conducted by Dr. Meredith Franklin at the University of Toronto, Canada, and her colleagues. The report contains three main sections:

The **HEI Statement**, prepared by staff at HEI Energy, is a brief, nontechnical summary of the study and its findings; it also briefly describes the HEI Energy Review Committee's comments on the study.

The **Investigators' Report**, prepared by Franklin and colleagues, describes the scientific background, aims, methods, results, and conclusions of the study.

The **Commentary**, prepared by members of the HEI Energy Review Committee with the assistance of HEI staff, places the study in a broader scientific context, points out its strengths and limitations, and discusses the remaining uncertainties and implications of the study's findings for public health and future research.

This report has gone through HEI Energy's rigorous review process. When an HEI Energy-funded study is completed, the investigators submit a draft final report presenting the background and results of the study. Outside technical reviewers first examine this draft report. The report and the reviewers' comments are then evaluated by members of the Review Committee, an independent panel of distinguished scientists who are not involved in selecting or overseeing HEI Energy studies. During the review process, the investigators have an opportunity to exchange comments with the Review Committee and, as necessary, to revise their report. The Commentary reflects the information provided in the final version of the report.

Although this report was produced with partial funding by the United States Environmental Protection Agency under Contract No. 68HERC19D0010 to the Health Effects Institute, it has not been subjected to the Agency's peer and administrative review and may not reflect the views of the Agency; thus, no official endorsement by the Agency should be inferred. This report also has not been reviewed by private party institutions, including those that support HEI Energy, and may not reflect the views or policies of these parties; thus, no endorsement by them should be inferred.

CONTRIBUTORS

HEI ENERGY RESEARCH COMMITTEE

George Hornberger, Chair *Distinguished Professor Emeritus, Vanderbilt University*

Shari Dunn-Norman* *Associate Professor, Department of Geological Sciences and Engineering, Missouri University of Science and Technology*

Stefanie Ebelt Sarnat* *Associate Professor, Department of Environmental Health, Rollins School of Public Health, Emory University*

Alfred Eustes *Associate Professor Emeritus, Petroleum Engineering Department, Colorado School of Mines*

Julia Haggerty *Associate Professor of Geography, Department of Earth Sciences, Montana State University*

Howard Hu* *Professor and Flora L. Thornton Chair, Department of Preventive Medicine, Keck School of Medicine, University of Southern California, Los Angeles*

Kirsten Koehler *Professor, Department of Environmental Health and Engineering, Bloomberg School of Public Health, Johns Hopkins University*

Judy S. LaKind* *Adjunct Associate Professor, Department of Epidemiology and Public Health, University of Maryland School of Medicine*

Christopher Paciorek *Adjunct Professor and Research Computing Consultant, Department of Statistics, University of California, Berkeley*

Armistead (Ted) G. Russell *Howard T. Tellepsen Chair and Regents Professor of Civil and Environmental Engineering, Georgia Institute of Technology*

Peter S. Thorne *University of Iowa Distinguished Chair and Professor, Department of Occupational and Environmental Health, University of Iowa College of Public Health*

Yifang Zhu *Professor of Environmental Health Sciences, UCLA Fielding School of Public Health, University of California, Los Angeles*

HEI ENERGY REVIEW COMMITTEE

Isabelle Cozzarelli, Chair *Senior Research Scientist Emerita, USGS Geology, Energy, & Minerals Science Center*

Elizabeth Mannshardt† *Adjunct Associate Professor, Department of Statistics, North Carolina State University*

Jim Crompton *Affiliate Professor, Petroleum Engineering Department, Colorado School of Mines*

Albert Presto *Director, Center for Atmospheric Particle Studies, and Research Professor, Department of Mechanical Engineering, Carnegie Mellon University*

Christine Wiedinmyer *Director of UCAR Community Programs, University Corporation for Atmospheric Research (UCAR)*

Jun Wu *Professor, Department of Environmental and Occupational Health, University of California, Irvine*

HEI PROJECT STAFF

Donna J. Vorhees *Director of HEI Energy (Study Oversight)*

Dan Crouse *Senior Scientist (Report Review)*

Kristin C. Eckles *Senior Editorial Manager*

Hope Green *Editorial Project Manager*

Tara Hamilton *Consulting Editor*

*Shari Dunn-Norman, Stefanie Ebelt Sarnat, Howard Hu, and Judy S. LaKind rotated off the Research Committee before this report's publication.

†Elizabeth Mannshardt rotated off the Review Committee before this report's publication.

PREFACE

HEI's Research to Assess Community Exposures Associated with Unconventional Oil and Gas Development

INTRODUCTION

The scale and rate of onshore oil and natural gas development since the early 2000s differ markedly from earlier development, stemming from technological changes involving the increased use of hydraulic fracturing combined with horizontal drilling. While hydraulic fracturing has captured much public attention, this process alone is not new. Neither is horizontal drilling or the extraction of oil and gas from unconventional formations, such as tight (i.e., low permeability) sandstone and shale. What is new is the use of high-volume (millions of gallons of water per well), multistage hydraulic fracturing combined with horizontal drilling (thousands of feet in length).

This combination of technological innovations has influenced the scale of development and where development is feasible. With their extensive number of fracture stages along lengthy horizontal wells, today's unconventional oil and gas wells intersect more of the targeted oil- or gas-bearing rock than earlier vertical wells, which involves the following:

- Larger well pads with extensive amounts of equipment that are transported to and from the pad
- More raw materials that must be transported to the well pad for drilling, cementing, and hydraulically fracturing the target hydrocarbon-bearing formation to produce the oil or gas
- More liquid and solid waste from multiple wells drilled on one well pad that must be captured, transported, and treated, for reuse or ultimate disposal
- A longer period of industrial activity is required at a single well pad when multiple wells are developed on it and
- Increased truck traffic, changing demands on community infrastructure, and other possible community effects associated with population mobility.

Consequently, unconventional oil and gas development (UOGD) can be associated with a wide range of potential exposures to chemical and nonchemical agents. The rapid expansion of this development has given rise to concerns about potential effects on human health.

Current evidence indicates that people can be exposed to chemical agents (e.g., criteria and hazardous air pollutants, radioactive material, indicators of produced water, and odorous compounds) and nonchemical agents (e.g., noise, light, and vibration) released from UOGD processes. HEI Energy compiled this evidence in two extensive literature reviews (HEI Energy Research Committee 2019, 2020). But despite this literature and considering the recommendations of a wide variety of government, industry, and academic stakeholders at three HEI-hosted research planning workshops, HEI Energy concluded that important gaps remain in our understanding of who might be exposed, the full range of exposures, which processes lead to exposures, and how exposures vary over time and across regions. Specifically, few studies to date provide the information necessary for linking chemical or nonchemical agents from UOGD processes with exposed communities. In addition, the applicability of study results to UOGD operations, geographic areas, and populations beyond those investigated in the studies is not clear. Given the current state of knowledge, HEI issued complementary requests for applications in 2020 (*RFAs E20-1 and E20-2*) to improve the understanding of human exposure to UOGD.

OBJECTIVES OF THE RFAs

HEI solicited studies that can document one or more complete exposure pathway(s), should one exist, between UOGD process(es) and a population(s) potentially exposed to UOGD chemical emissions to air, chemical releases to water, or noise. The research should inform future health studies and be designed in an efficient way to maximize understanding of the variability in potential human exposures under routine operating conditions, while also being capable of capturing exposures associated with accidental scenarios.

OBJECTIVES OF RFA E20-1

RFA E20-1: Community Exposures Associated with Unconventional Oil and Natural Gas Development solicited studies that apply a combination of approaches

to quantify the spatial and temporal variability in human exposures to UOGD-generated atmospheric chemical concentrations and noise. To maximize the generalizability of the research, HEI encouraged research that couples established rigorous methods to measure air and noise exposure at multiple spatial scales with equally rigorous fate and transport modeling. The RFA had five major objectives:

1. Identify the UOGD processes that have resulted or might result in releases of chemicals or noise to outdoor air and the potential for human exposure resulting from such releases.
2. Quantify the magnitude, frequency, and duration of potential exposures to chemicals in outdoor air and to noise released from specific UOGD processes at multiple spatial and temporal scales.
3. Quantify the influence of various factors (e.g., varying meteorology, topography, operational characteristics, proximity to populations, and population behavior) on potential UOGD-related human exposures to characterize variability in exposures and enable the results of the research to be generalized to other conditions.
4. Estimate community exposures from UOGD sources across spatial and temporal scales relevant to a current or future assessment of potential health effects.
5. Distinguish potential UOGD exposures from other conventional oil and gas development and any other background source to the extent practicable.

OBJECTIVES OF RFA E20-2

RFA E20-2: Community Exposures Associated with Unconventional Oil and Natural Gas Development solicited studies that involve the synthesis and modeling of existing data and original research to better understand the nature, extent, and frequency of potential exposures related to UOGD impacts on water quality. The RFA had four major objectives:

1. Determine the UOGD processes that have resulted or might result in releases to groundwater or surface water and potential for leading to human exposure.
2. Quantify the magnitude, frequency, and duration of potential exposures to chemicals in surface water or groundwater released from specific UOGD processes.
3. Quantify the influence of various factors (e.g., varying geology) on potential human exposures to maximize the generalizability of the research and inform decision-making.
4. Distinguish potential UOGD exposures from conventional oil and gas development and any other background sources to the extent practicable.

STUDIES FUNDED UNDER RFA E20-1

HEI Energy funded three research teams to collaborate on improving our understanding of community exposures associated with air quality and noise from UOGD. The collaboration, "TRAcking Community Exposures and Releases (TRACER) from UOGD" (1) quantified acute and chronic human exposures in three regions of the United States, and (2) developed a model that captures our collective understanding of UOGD emission sources, estimates their impacts on local and regional air quality, and can be updated as UOGD operations and UOGD governance change over time.

"Measuring and Modeling Air Pollution and Noise Exposure Near Unconventional Oil and Gas Development in Colorado," Jeffrey L. Collett Jr., Colorado State University, USA The research team assessed population exposures to chemicals and noise in air associated with specific UOGD processes over the UOGD life cycle at four well pads in the Colorado North Front Range, located within the Denver-Julesburg Basin. With the cooperation of well pad operators, the team conducted fixed-site air and noise monitoring and mobile air monitoring at multiple locations surrounding multiwell pads to connect specific UOGD processes with air monitoring results. These processes included well drilling, hydraulic fracturing, coiled tubing/millout operations, flowback, and early production. The team obtained samples of drilling mud and compared emissions from different formulations. In addition to the monitoring program, they collaborated with Dr. Hildebrandt Ruiz to provide preproduction input data to the TRACER model, developed a preproduction emissions model designed for use by a variety of stakeholders to forecast HAPs and other VOC emissions from planned drilling and well completion operations and to assess whether efforts to reduce emissions achieve the desired goals. The team applied the model to simulate emissions and dispersion around specific well pads and estimate effects on local air quality, interpreting findings in the context of Colorado's regulatory setback distances separating UOGD from residences, schools, and other forms of development.

"Assessing Source Contributions to Air Quality and Noise in Unconventional Oil Shale Plays," Meredith Franklin, University of Toronto, Canada The research team assessed population exposures to ambient air pollution, radioactivity, and noise associated with UOGD. The team has coupled air, noise, and radioactivity measurements with meteorology and land use data to characterize UOGD sources of human exposure in the study regions: Permian Basin, Texas, and Eagle Ford Shale, Texas. To understand temporal variability in chemical concentrations in air, radioactivity, and noise levels, they conducted time-resolved fixed-site monitoring in the Permian Basin and leveraged ongoing fixed-site monitoring in the Denver-Julesburg basin. To understand spatial variability, they deployed passive samplers in both study regions. They linked monitoring data with satellite observations to characterize the location and magnitude of flaring.

"Predictive, Source-Oriented Modeling and Measurements to Evaluate Community Exposures to Air Pollutants and Noise from Unconventional Oil and Gas Development," Lea Hildebrandt Ruiz, University of Texas at Austin, USA The research team utilized a combination of measurement and modeling approaches in diverse study sites to assess the quality of an emission and dispersion modeling tool (TRACER model), which was advanced and refined from an existing model for methane emissions. The capabilities of the preexisting model were expanded from modeling emission and dispersion of methane from single UOGD well pads to assess community exposures. The expanded capability of the model included additional sources of emissions, regional scale modeling, a broad suite of pollutants of concern to human health, including secondary pollutants, and an assessment of the model for exposure assessment in future health studies. The original scope of work focused on the Eagle Ford Shale region in Texas; the project was later expanded to also include monitoring in the Permian Basin in New Mexico and modeling in the Marcellus Shale Region in the Northeastern United States, in close collaboration with the other two studies funded under this RFA.

DESCRIPTION OF THE RESEARCH PROGRAM

Three studies were funded under RFA E20-1, and two studies were funded under RFA E20-2 to cover the various RFA objectives; they are summarized below (**Preface Table**). The study locations stretch across several major oil and gas producing regions of the United States (**Preface Figure**).

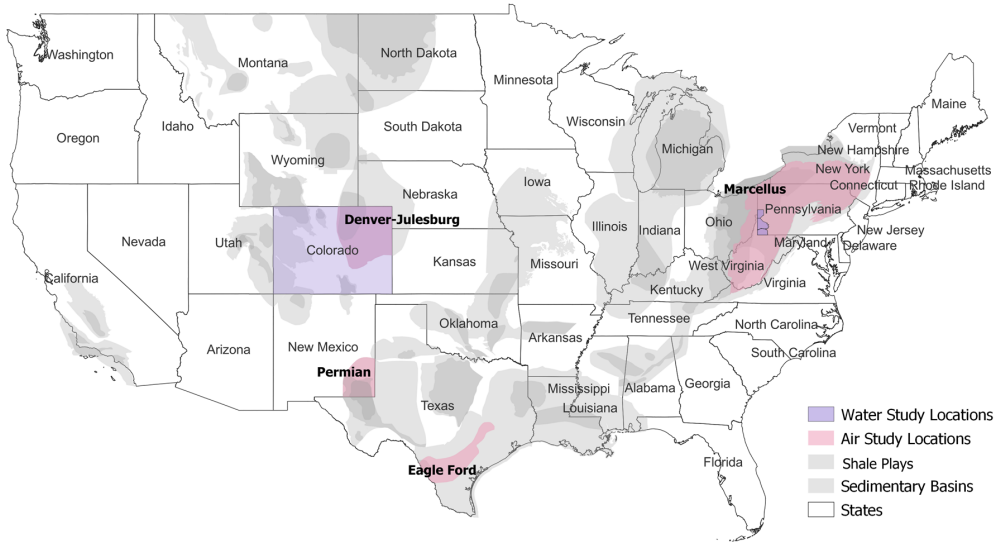

Preface Figure. Map of RFA E20-1 and E20-2 study locations and associated plays and basins across the United States.

STUDIES FUNDED UNDER RFA E20-2

HEI funded two studies in Colorado and Pennsylvania to combine existing water quality data and modeling to assess community exposures associated with UOGD releases to water. Both studies provide frameworks for identifying areas of potential water contamination, apportioning the sources of contamination, and identifying exposure pathways that connect UOGD to community water sources.

"Using Geoscientific Analysis and Community Engagement to Analyze Exposures to Potential Groundwater Contamination Related to Hydrocarbon Extraction in Southwestern Pennsylvania," Jennifer Baka, Susan L. Brantley, and Lingzhou Xue,* The Pennsylvania State University, USA The research team assessed linkages between UOGD and potential water contamination in a tri-county region of Southwestern Pennsylvania with a long history of industrial activity. Using an existing database of greater than 28,000 groundwater samples, the team investigated whether they could distinguish constituents associated with UOGD from other regional sources of similar contaminants (e.g., conventional oil and gas development and coal mining). The research team used statistical analysis and a machine learning tool (nonnegative matrix factorization, NMF) to isolate the influences of natural and anthropogenic processes on groundwater chemistry and identify potential linkages between UOGD and water contamination. The team hosted focus groups to elicit community concerns regarding UOGD, water contamination, and public health, and they considered what they learned in completing their assessment of potential community exposures associated with UOGD.

"Assessing the Effects of Unconventional Oil and Gas Development on Community Water Sources," Joseph Ryan, University of Colorado, USA The research team used existing data to assess the potential for community exposure to releases attributable to UOGD in ground and surface waters used as community water supplies. The team used monitoring data for water quality near oil and gas development, records of community water supplies, and records related to oil and gas operations in the Denver-Julesburg, Piceance, San Juan, and Raton Basins (e.g., well construction and integrity) to assess temporal and spatial correlations with water quality issues affecting communities. They identified chemicals of possible concern detected in the water quality dataset and coupled those with multiphase subsurface fluid flow and transport models to predict the likelihood of complete transport pathways in the Denver-Julesburg Basin.

*Co-principal investigators.

REFERENCES

HEI-Energy Research Committee. 2019. Potential Human Health Effects Associated with Unconventional Oil and Gas Development: A Systematic Review of the Epidemiology Literature. Special Report 1. Boston, MA: Health Effects Institute.

HEI-Energy Research Committee. 2020. Human Exposure to Unconventional Oil and Gas Development: A Literature Survey for Research Planning. Communication 1. Boston, MA: Health Effects Institute.

Preface Table. Key Characteristics of HEI's Research to Assess Community Exposures Associated with Unconventional Oil and Gas Development

Principal Investigator	Location	Study Period	Study Population	Main Pollutants in Air or Water	Monitoring Data	Exposure Assessment
RFA E20-1: Community Exposures Associated with Unconventional Oil and Gas Development — Air Quality and Noise						
Collett	Northern Front Range, Colorado (part of the Denver-Julesburg basin)	2022–2024	All subpopulations in the study location	VOCs, methane, $PM_{2.5}$, NO_x, A- and C-weighted noise	Fenceline fixed-site and mobile	TRACER emissions model and local air quality modeling
Franklin	Carlsbad-Loving, New Mexico (part of the Permian basin), Eagle Ford Shale region, Texas	2022–2024	All subpopulations in the study location	VOCs, methane, $PM_{2.5}$, NO_x, A- and C-weighted noise, ozone, H2S, radioactivity (alpha)	Regional fixed-site (NM) and passive (TX)	Non-negative matrix factorization for source apportionment
Hildebrandt Ruiz	Eagle Ford Shale region, Texas, Permian Basin, New Mexico, and Marcellus Shale Region	2022–2024	All subpopulations in the study location	VOCs, methane, PM_1, NO_x, A- and C-weighted noise, ozone, H2S, black carbon	Fixed-site (TX) and mobile (TX and NM)	TRACER emissions model and local and regional air quality modeling
RFA E20-2: Community Exposures Associated with Unconventional Oil and Gas Development — Water Quality						
Baka, Brantley, and Xue	Beaver, Greene, and Washington Counties in Southwestern Pennsylvania	2022–2024	All subpopulations in the study location	VOCs, metals	Existing state-level data	Machine learning and statistical modeling
Ryan	State of Colorado	2022–2024	All subpopulations in the study location	VOCs, metals	Existing state-level data	Chemical transport model and statistical tests

HEI STATEMENT

Synopsis of Research Report 231

Characterizing Air Pollution, Radiation, and Noise Associated with Unconventional Oil and Natural Gas Development (UOGD)

BACKGROUND

Unconventional oil and natural gas development (UOGD) has been associated with a wide range of potential exposures to air pollutants, greenhouse gases, radioactivity, and noise. The rapid expansion of UOGD activities in recent decades has caused concerns about their potential effects on human health. In August 2020, HEI Energy issued Request for Applications E20-1, the goal of which was to better understand the nature, extent, and frequency of potential exposures related to UOGD on air quality and noise.

This Statement highlights a study led by Dr. Meredith Franklin at the University of Southern California* and colleagues. Franklin and colleagues proposed to address critical research needs by improving the characterization of UOGD-related exposures in oil-producing regions over space and time. They proposed to use stationary, passive, and satellite monitoring along with modeling approaches to estimate potential human health exposures. The main focus of the study was to characterize air pollutants, greenhouse gas emissions, airborne radioactivity, and noise associated with UOGD in two shale production basins, the Permian Basin (eastern New Mexico and western Texas) and Eagle Ford Shale (south central Texas). These two production basins are among the most active drilling and oil production regions in the United States.

APPROACH

To obtain detailed concentration and exposure data, Franklin and colleagues conducted sampling campaigns at a field laboratory and various locations in populated areas close to UOGD activities. At the field laboratory, they used a combination of continuous fixed-site monitoring instruments to identify UOGD processes that resulted in outdoor air pollution, radioactivity, and noise. This laboratory was deployed on an area of active UOGD activity in the Permian Basin and was in operation from May 1, 2023, to May 31, 2024. The investigators measured approximately 30 different components, including 20 volatile organic compounds. They also compared their observations with measurements collected at other UOGD sites and in nearby urban areas.

The investigators recruited local volunteers to deploy passive samplers for approximately 1 year at 12 locations in populated areas in the Permian Basin and Eagle Ford Shale. They coupled the resulting measurements of 15 hydrocarbon concentrations with data on meteorology and well density within about 10 km of the samplers to better understand the factors influencing UOGD-related exposures in the area and to inform future health studies.

What This Study Adds

- Franklin and colleagues measured air pollutants such as ozone and volatile organic compounds; greenhouse gas emissions such as methane, carbon dioxide, and nitrous oxide; airborne radioactivity; and noise associated with UOGD activities in two shale production basins during a yearlong study period.
- Concentrations of most of the air pollutants and noise varied during the day and between seasons, with frequent occurrences of high concentrations (spikes).
- The investigators conducted source apportionment analysis, which allowed them to identify and quantify specific sources of emissions contributing to environmental pollutant data observed at the field laboratory.
- The study showed that UOGD, along with older oil and gas operations, is the dominant source of air pollution in the study area.

This Statement, prepared by HEI Energy, summarizes a research project funded by HEI Energy and conducted by Dr. Meredith Franklin at the University of Southern California* and colleagues. Research Report 231 contains the detailed Investigators' Report and a Commentary on the study prepared by the HEI Energy Review Committee.

*Dr. Franklin is now based at the University of Toronto.

The investigators also conducted source apportionment analysis — which is a statistical technique to identify and quantify the contributions of different sources (e.g., traffic exhaust or industrial emissions) — to observed environmental pollutant data to see how much each source contributed to the observed sample.

A third component of the study focused on flaring, which is the burning of waste gas (mostly methane) from wells. This is a common waste disposal practice associated with oil and gas development, but its effect on air quality is not well characterized. To address this question, the investigators used remote sensing observations of thermal sources to identify gas flaring locations associated with UOGD. They combined these observations with concentration data collected from the stationary and passive sampling of flaring emissions to identify exposures related specifically to flaring.

KEY RESULTS

Franklin and colleagues observed high daily and seasonal variability in the average concentrations of most components measured over the year of sampling. There were frequent occurrences of short-term spikes in concentrations among many of these components. The means and medians during the study period, however, remained below health benchmarks.

The investigators collected over 300,000 1-minute observations of noise levels during the study period. Average noise levels were approximately 60–70 decibels, which is generally comparable to what might be experienced as background noise in a typical office setting.

The radioactivity data, measured as alpha radiation, showed high daily and seasonal variability, with values ranging from below the detection limit up to 173 Becquerel m^3 for gas-phased radioactivity and up to 99 Becquerel m^3 for particle-associated radioactivity. For reference, and in the absence of a health-based benchmark for radon in outdoor air, the EPA estimates that the average concentration of indoor radon among homes in the United States is about 50 Becquerel/m^3, and they recommend that action be taken to mitigate concentrations in homes greater than 150 Becquerel/m^3.

Many of the components measured at the field laboratory were significantly correlated with each other, which suggested that nearly all the components measured were emitted from similar or co-located sources.

Measurement of hydrocarbons in populated areas close to UOGD activity indicated that concentrations of n-hexane and 2-methylpentane were the highest and most variable, whereas concentrations of ethylbenzene and the xylenes were the lowest. The concentrations of most hydrocarbons were strongly correlated with each other. The highest average concentrations were found at sites with higher numbers of wells in the surrounding area. For example, concentrations of benzene were highly correlated (r = 0.87) with the number of wells within 10 km of the samplers.

In the source apportionment analysis, the investigators identified five factors representing various sources of UOGD emissions. These factors together explained about 95% of the overall variance in the data: oil and gas fugitive emissions and venting (45%); handling, storage, and evaporation from produced water ponds (39%); traffic emissions (10%); flaring (9%); and widespread combustion and radon emissions (4%) (**Statement Figure**). Note that the sum of factor-specific variance explained values can exceed 100% due to shared explanatory power between factors.

Franklin and colleagues detected a total of 71,401 gas flares during the study period and collected detailed information on temperature, source area, and radiant heat for each flare. They found that nightly average concentrations of several volatile organic compounds (benzene, ethane, and ethene), methane, carbon monoxide, carbon dioxide, nitrogen oxides, and total radioactivity were correlated with the number of flares and with the estimated flared gas volume within 50 km of the field laboratory.

INTERPRETATION AND CONCLUSIONS

In its independent evaluation of the report, the HEI Energy Review Committee identified several strengths of the study design. One strength was the use of multiple measurement methods, such as stationary, passive, and satellite monitoring. Others were the long, continuous sampling period of over 1 year and the use of creative and novel exposure modeling approaches. Committee members were impressed with the large number of components the investigators measured, including several criteria air pollutants and many volatile organic compounds, along with detailed measurements of weather and noise, using a wide variety of different instruments.

The Committee also appreciated the comparisons of samples collected at the study sites with those collected at locations in other UOGD regions and with urban air quality stations. An additional strength of the study was the involvement of volunteers from the local communities to support the collection of samples.

The Committee thought the detailed analysis of flaring events was an important contribution. They also liked the analyses that linked well pad locations and their levels of activity with the measured concentrations of air pollutants and noise. This approach was effective for linking these components directly to the UOGD activities.

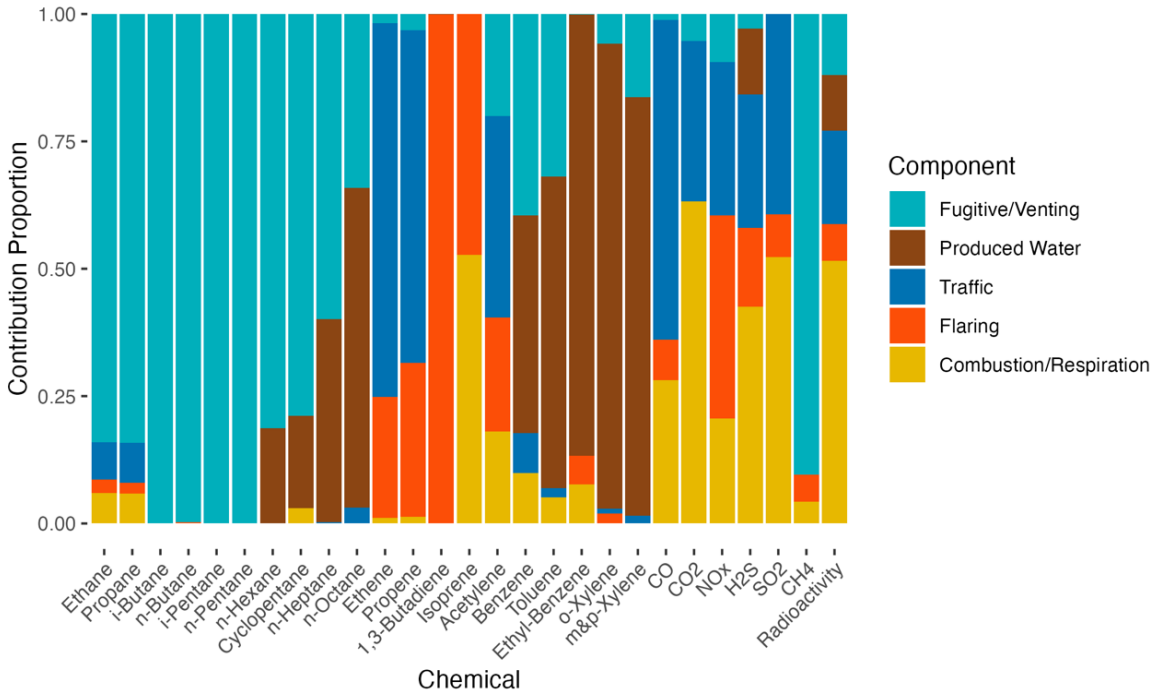

Statement Figure. Contribution proportions of each compound to the five factors identified through the source apportionment analysis. Source: Investigators' Report, Figure 32.

In summary, this study contributed to knowledge about potential exposures to a variety of emissions from UOGD activities at local and regional scales. It showed that UOGD, along with older oil and gas operations, are the dominant source of air pollution in this study area. The Committee agreed with the findings and conclusions, which should be of value to industry, local landowners, and community members, and to potential policymakers.

INVESTIGATORS' REPORT

Assessing Source Contributions to Air Quality and Noise in Unconventional Oil Shale Plays

Meredith Franklin[1], Gunnar Schade[2], Detlev Helmig[3], Lara Cushing[4], Jill Johnston[5]

[1]University of Toronto, Canada; [2]Texas A&M University, USA; [3]Boulder AIR, USA; [4]University of California, Los Angeles, USA; [5]University of Southern California, USA

ABSTRACT

Introduction Unconventional oil and gas development (UOGD*) has enabled the exploration of previously inaccessible or uneconomic oil and gas resources in shale rock, resulting in thousands of extraction sites across the landscape, many near people's homes. Human exposure to air pollution and noise related to these activities poses a health risk. This study focused on characterizing air pollutants, greenhouse gas emissions, airborne radioactivity, and noise associated with UOGD in two shale production basins.

Methods During one year of stationary air monitoring in Loving, New Mexico, in the western part of the Permian Basin (PB), we characterized the magnitude, frequency, and duration of UOGD-related emissions at temporal scales from 1 minute to seasonal. Continuous monitoring was performed for meteorological variables, near-surface ozone, nitrogen oxides (NO_x), sulfur dioxide, hydrogen sulfide, 20 speciated volatile organic compounds (VOCs) in the ethane to octane volatility range, and noise. Airborne radioactivity was measured in the gas and particle phases. Source apportionment was performed using nonnegative matrix factorization (NMF). To disentangle sound frequencies, we developed spectrograms and conducted machine learning regression to analyze sound sources and relationships to air pollutants. A network of passive hydrocarbon samplers that collected weekly measurements of 15 hydrocarbons was established throughout populated regions of both the PB and Eagle Ford Shale (EFS) areas to measure regional pollutant concentrations and their spatial gradients around UOGD. Visible Infrared Imaging Radiometer Suite (VIIRS) Nightfire (VNF) data were acquired to quantify gas flaring activity throughout the region during our field measurement period. VNF flares and estimated flare gas volume were linked to the stationary air quality measurements to examine associations.

Results Most of the monitored primary air pollutants showed high variability, with frequent concentration spikes that exceeded background mole fractions by up to three orders of magnitude. The frequency of concentration spikes, their maximum mole fractions, and averaged metrics (hourly, 8-hour, 24-hour, and annual) were higher than those reported from mostly urban comparison sites. Near-surface ozone measurements confirmed that this area of the PB is in nonattainment of the ozone national ambient air quality standard (NAAQS), exceeding the 70 ppb threshold more than 30 days of the year, and that this nonattainment is driven by UOGD-related emissions of VOCs and NO_x. The highest ozone values occurred during conditions of high temperatures, dry air, and slow advection of air masses across the PB from the south–southeast. VOC monitoring showed dominant impacts from saturated hydrocarbons, and associated NMF analysis identified five emission sources: a UOGD-related hydrocarbon source, two gas flaring sources, a general combustion source, and a road transportation/traffic source. These sources correspond well with identified spatial distributions of surface well pad activity, gas flaring during the study period, and road traffic in the area. Radioactivity measurements displayed diurnal and seasonal changes consistent with prior work; elevated levels were observed from the north-northwest sector. Airborne radioactivity correlated with aromatic VOCs, petroleum hydrocarbon alkanes, and CO_2. Our noise measurements were dominated by low frequencies (<100 Hz), which were most strongly associated with CO_2. The passive sampler network identified northwest-to-southeast increases in ambient hydrocarbon concentrations, in line with the identified UOGD and traffic density in the area. Benzene levels across the network at times exceeded health-based reference values and were significantly higher than benzene levels recorded during air monitoring in large Texas metropolitan areas. Average hydrocarbon levels were significantly correlated with the well density surrounding each site in both shale basins.

Conclusions Our extensive air quality research in the Permian-Delaware Basin revealed, at times, extraordinarily high levels of air pollution, including air toxics such as ben-

This Investigators' Report is one part of Health Effects Institute Research Report 231, which also includes a Commentary by the Review Committee and an HEI Statement about the research project. Correspondence concerning the Investigators' Report may be addressed to Dr. Meredith Franklin, Department of Statistical Sciences, 9th Floor, Ontario Power Building, 700 University Ave., Toronto, ON M5G 1Z5; email: *meredith.franklin@utoronto.ca*. No potential conflict of interest was reported by the authors.

Although this report was produced with partial funding by the United States Environmental Protection Agency under Contract No. 68HERC19D0010 to the Health Effects Institute, it has not been subjected to the Agency's peer and administrative review and may not reflect the views of the Agency; thus, no official endorsement by the Agency should be inferred. This report also has not been reviewed by private party institutions, including those that support HEI Energy, and may not reflect the views or policies of these parties; thus, no endorsement by them should be inferred.

* A list of abbreviations and other terms appears at the end of this volume.

zene, and frequent high ozone days in violation of the ozone NAAQS. Our analyses show that the overwhelming amount of this pollution is due to UOGD activities, including emissions from production and storage, gas flaring, and truck traffic.

INTRODUCTION

Oil and gas development in the United States has significantly expanded over the past few decades, driven by technological advancements such as hydraulic fracturing and horizontal well drilling. These unconventional oil and gas development (UOGD) methods have unlocked previously inaccessible shale rock formations that sit atop "tight oil shale plays," which refers to a low-permeability continuous shale that requires hydraulic fracturing to extract oil and gas. With thousands of extraction sites across relatively small geographic areas (Jones et al. 2015), the oil and gas boom has transformed the United States into the world's top producer (EIA 2023). Regions such as the Permian Basin (PB; eastern New Mexico and western Texas) and Eagle Ford Shale (EFS; south central Texas) have become epicenters of UOGD activity **(Figure 1)**. Oil and gas extraction has also become more common near where people live and work (Czolowski et al. 2017), affecting local communities and increasing the potential for human exposure to air contaminants (Moore et al. 2014; Schade and Heienickle 2023) and noise (Allshouse et al. 2019; Hays et al. 2017). There is growing evidence of health risks associated with living in proximity to UOGD, such as adverse birth outcomes (Cushing et al. 2020; McKenzie et al. 2014, 2019; Willis et al. 2023), as well as socioeconomic and racial disparities (Johnston et al. 2020; McKenzie et al. 2016). Approximately 1.4 million people, nearly 40% of whom identify as Hispanic, live in these areas.

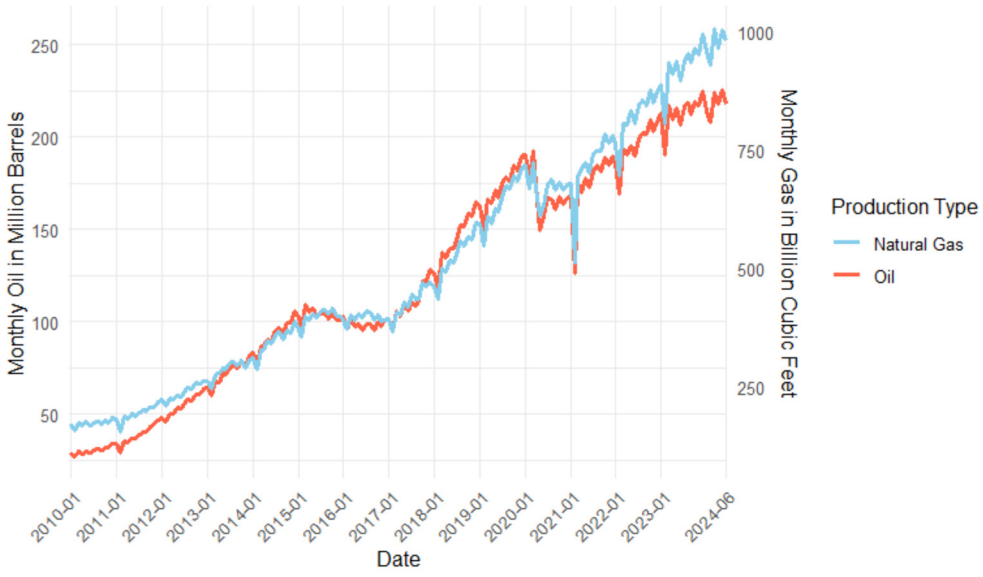

Figure 1. Oil and natural gas production from wells in the Permian Basin and Eagle Ford Shale since 2010. Source: US Energy Information Agency.

The impacts of oil and gas production on air quality and noise result from a multitude of activities: drilling, hydraulic fracturing, production, storage and leaks at well pad sites, burning of waste gas (i.e., flaring), operation of compressors, and emissions from transportation equipment needed to bring supplies and water or remove oil, gas, and waste. Air pollutants of concern include primary emissions of nitrogen oxides (NO_x), black carbon (BC), and hydrocarbons, including benzene, toluene, ethylbenzene, and xylenes (BTEX), and polycyclic aromatic hydrocarbons (PAHs) (Adgate et al. 2014; Helmig 2020). Secondary air pollutants, such as ozone (O_3), generated in the near-surface atmosphere from precursor emissions, are also a concern, as are greenhouse gas emissions of methane (CH_4) and carbon dioxide (CO_2). Combustion processes, including flaring, have been shown to release NO_x and volatile organic compounds (VOCs), the precursors contributing to the formation of O_3, which in turn is linked with adverse effects on the respiratory, cardiovascular, reproductive, and nervous systems. Benzene is a well-established carcinogen (Agency for Toxic Substances Control Registry 2007; Kim et al. 2013) and has also been linked to birth defects (Lupo et al. 2011, 2012). Noise from UOGD has been linked with health effects, including annoyance, sleep disturbance, and cardiovascular disease (Hays et al. 2017). Increases in beta radiation on collected airborne particles have been found in proximity to UOGD (Li et al. 2020), posing a human health risk from the inhalation of airborne radioactive particulate matter.

Pollutant emissions differ by well pad activity; for example, in a Colorado field study, overall VOC emissions were found to be greater during the flowback stage when material exited the well, compared to the fracturing stage when material was injected into the well. BTEX were highest during flowback and showed emissions spikes during the fracturing stage (Hecobian et al. 2019). Flaring, the intentional combustion of waste gases, emits NO_x (Schade and Roest 2018; Zhang et al. 2019) and VOCs (Knighton et al. 2012), as well as particulate matter in the form of BC (Fawole et al. 2016; Weyant et al. 2016). Transportation equipment, such as diesel trucks, emits NO_x and BC (Allshouse et al. 2019). Many stages of UOGD create noise pollution from the operation of heavy equipment such as diesel compressor engines and diesel trucks. The multitude of stressors from UOGD operations raises the possibility of cumulative health effects and underscores the importance of measuring multiple toxicants, including radioactivity and noise. Recent research

has also demonstrated that the timing of exposure and peak values of exposure can be critical to assessing health impacts. For instance, exposure during critical windows of development in utero has been linked with higher risks of diabetes, cardiovascular disease, respiratory problems, and other illnesses in adulthood (Gillman et al. 2005). Our prior work has linked short-term exposure to flaring during pregnancy with preterm birth (Cushing et al. 2020). Other theoretical work (e.g., Brown et al. 2015) and our monitoring in proximity to UOGD have shown that the exposure to released chemicals is largely dominated by occurrences of short concentration spikes. During those events, pollutant concentrations can increase up to a factor of 1,000 over their background levels (Helmig et al. 2014, 2025; Schade and Roest 2016).

A comprehensive evaluation of the health risks from UOGD sources considers geographic differences and the variety of sources and temporal variability in resulting pollutants. Most prior work on emissions has focused on methane (e.g., Alvarez et al. 2018; Brandt et al. 2014, 2016; Zhang et al. 2020), with a dearth of studies addressing hazardous air pollutant emissions, noise, and radioactivity from UOGD operations, particularly in oil shale basins, as well as impacts of flaring. Previous assessments of UOGD pollution have also relied on measurements of average exposure using integrated or sporadic air quality assessments, neglecting the potential importance of short-term exposures to elevated levels of pollutants that occur repeatedly over long periods of time. Our project addresses this gap by using monitoring at high time resolution coupled with spatial data sources to characterize processes that affect air quality across both space and time.

SPECIFIC AIMS

This study focused on the US oil shale regions Permian Basin (PB) and the Texas Western Gulf Basin (Eagle Ford Shale; EFS). Collected data were also compared to measurements in the Denver–Julesburg Basin (DJB). The PB and EFS are among the most active drilling and oil production regions in the country, collectively accounting for over 180,000 active wells that currently produce approximately 7 million barrels of oil per day, more than a seven-fold increase over 2010 (Figure 2). The epicenter of DJB has high oil and gas well density, with many wells located close to urban areas, especially the Denver metro region. Extensive air monitoring has been implemented in populated areas affected by the DJB to better understand air quality impacts from UOGD. In contrast, despite high productivity, air quality impacts from UOGD in the PB and EFS have been less well studied. Flaring is a common waste disposal practice in the EFS and PB, and air pollutant impacts from flaring associated with production are not well characterized. We sought to improve the spatial and temporal characterization of UOGD air pollution, radioactivity, and noise in predominantly oil-producing shale regions via stationary, distributed passive, and satellite monitoring alongside modeling that can be leveraged to assess human health exposures.

1. **Aim 1: Characterize the impact of UOGD activities on ambient air pollution, radioactivity, and noise by collecting high temporal resolution data from a stationary monitoring platform in the Permian Basin.**

   Hypothesis: We hypothesize that chemical and noise signatures near UOGD will show high temporal variability and will differ from DJB composition.

   Through a combination of automated, continuous, stationary atmospheric monitoring and source apportionment modeling, we identified UOGD processes that result in ambient air pollutants, radioactivity, and noise. Using source apportionment techniques, we distinguished UOGD-related pollution from other local sources such as vehicle traffic.

2. **Aim 2: Understand the spatial distributions of targeted petroleum hydrocarbons in ambient air, leveraging a dense network of time-integrated passive samplers.**

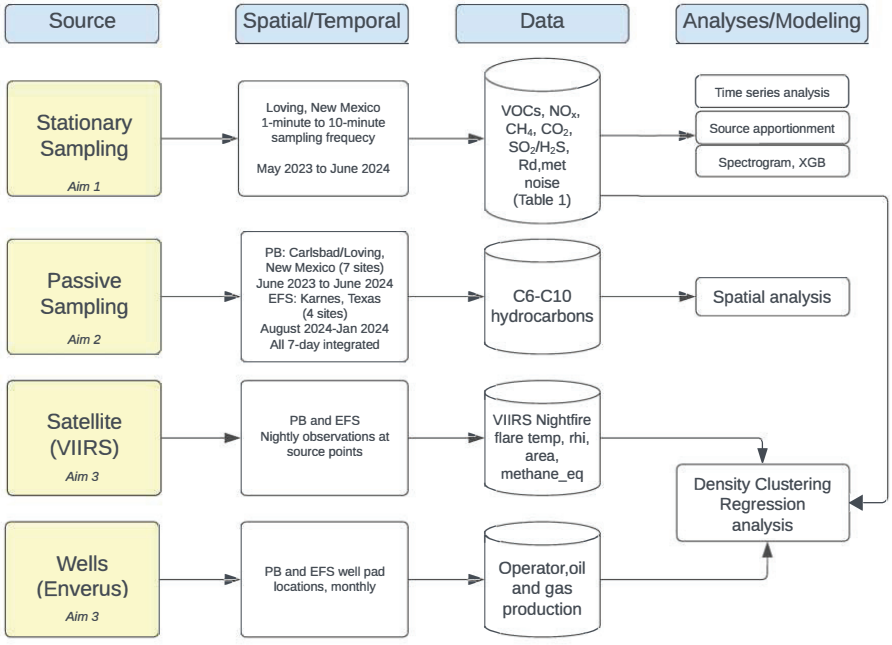

Figure 2. Overview of study showing data collected with spatial and temporal scales and methods applied. References to aims, figures, and tables are shown. EFS = Eagle Ford Shale; PB = Permian Basin; VIIRS = Visible Infrared Imaging Radiometer Suite

Hypothesis: We hypothesize that spatial distributions of concentrations of petroleum hydrocarbons will be different between shale areas and will have distinct seasonal patterns.

By deploying a spatially dense set of passive samplers and coupling these measurements with meteorology, well density, and population characteristics, we characterized exposures over basins and seasons to better understand the factors influencing UOGD exposures and inform subsequent health studies.

3. **Aim 3: Leverage satellite observations coupled with surface air pollution data to characterize the location and magnitude of flaring and its impact on air quality and radioactivity from UOGD.**

   Hypothesis: We hypothesize that flaring, as identified from satellites, is related to enhanced air pollutant concentrations nearby, and that flaring observations can be used to estimate occurrences of flaring-related air pollutants and radioactivity.

   By leveraging unique remote sensing observations of thermal sources, we identified locations of UOGD flaring, which is a regular practice in the EFS and PB. Combining these observations with the stationary and passive sampling of flaring emissions, including radioactivity, enables us to assess exposures related specifically to flaring at fine spatial and temporal resolutions.

STUDY DESIGN AND METHODS

STATIONARY SAMPLING PLATFORM FOR AIR QUALITY, GREENHOUSE GASES, NOISE, AND RADIOACTIVITY

The stationary sampling platform was installed, maintained, and overseen (including quality control) by Boulder Atmosphere Innovation Research (Boulder AIR) scientists. This mobile field laboratory ("trailer") housing instruments, calibration gases, and data logging systems started on April 16, 2023, and operated continuously from May 1, 2023, through May 31, 2024. The trailer was located at the north end of the town of Loving, New Mexico, in Eddy County (**Figure 3**, top). The trailer, with its exterior and interior shown at the bottom of Figure 3, is referred to as LNM (for Loving, New Mexico) or the LNM site.

Research Roadmap

Aims and Research Conducted	Methods Description
Aim 1	
Characterize the impact of oil and gas activities on ambient air pollution, radioactivity, and noise by collecting high temporal resolution data from a stationary monitoring platform in the Permian Basin	Stationary sampling platform: see section under Study Design and Methods: "Data Collection Methods for Stationary Sampling Platform for Air Quality, Greenhouse Gases, Noise, and Radioactivity" Source apportionment: see section under Data Analysis and Statistical Methods: "Source Apportionment Using Nonnegative Matrix Factorization" Noise frequency: see section under Data Analysis and Statistical Methods: "Noise Frequency Analysis" Additional methodological details for Aim 1 can be found in Appendix A
Aim 2	
Understand the spatial distributions of targeted petroleum hydrocarbons in ambient air, leveraging a dense network of time-integrated passive samplers	Passive sampling network design and sampling techniques: see section under Study Design and Methods: "Passive Sampling Network Design and Data Collection Methods" Spatial and temporal analysis of the collected passive sampling data: see section under Data Analysis and Statistical Methods: "Analysis of Passive Sampling Data" Additional methodological details and results can be found in Appendix B
Aim 3	
Leverage satellite observations coupled with surface air pollution data to characterize the location and magnitude of flaring and its impact on air quality and radioactivity from UOGD	Satellite data design and methods: see section under Study Design and Methods: "Satellite-Based Flaring Identification" Satellite flare clustering, flare gas volume estimation, and association with measured concentrations: see Data Analysis and Statistical Methods: "Analysis of Satellite Flaring" Additional results can be found in Appendix C

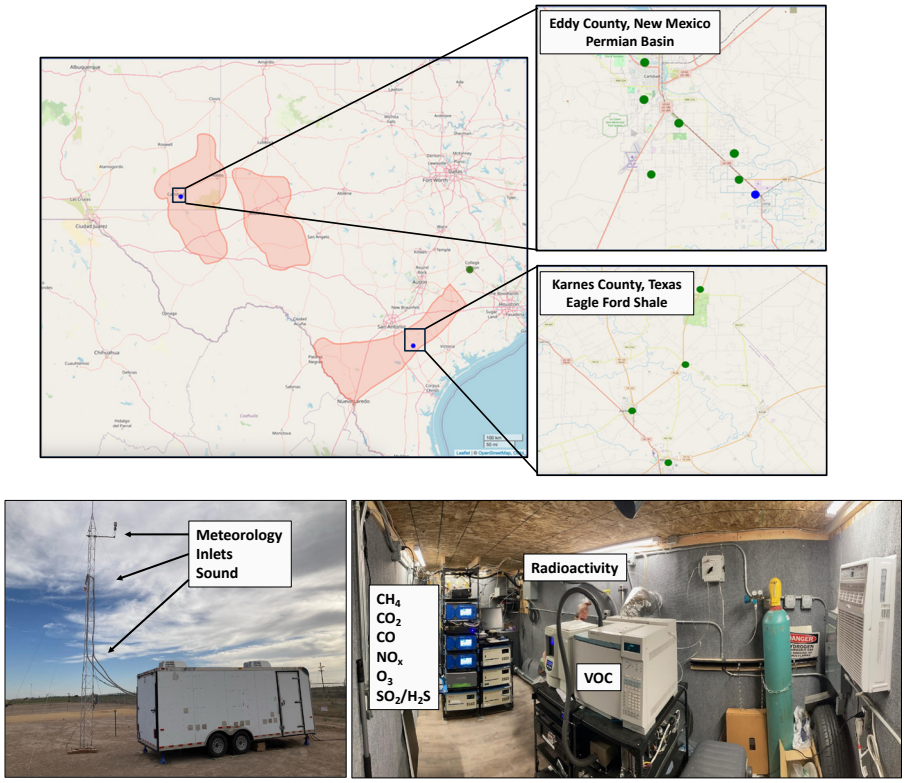

Figure 3. Top: Maps showing the study region, including the Permian Basin and Eagle Ford Shale (pale red regions) with markers for the stationary platform (blue dot) and passive samplers (green dots); Bottom: Trailer exterior (left) and interior (right) with annotations of the instruments.

Meteorological sensors and air sampling inlets, except for the radioactivity measurements, were installed onto a 10-m triangular lattice tower that was connected to the trailer. Wind conditions, temperature, relative humidity, barometric pressure, and incoming solar radiation were captured by instruments mounted on the tower at 8.7 meters (m) above ground level (agl). The tower also held inlets for ambient air for all analyzers, except radioactivity, at approximately 6 m agl.

Inside the trailer were gas analyzers for O_3, CH_4, CO_2, carbon monoxide (CO), hydrogen sulfide (H_2S), sulfur dioxide (SO_2), and nitrogen oxides (NO_x, including NO and NO_2). VOCs were measured with a custom-made VOCs enrichment/gas chromatography (GC) instrument with flame ionization detection (FID). Twenty VOCs were routinely tracked and quantified. Data represent the mean VOC mole fractions over the 10-minute sample collection period, with the recorded timestamp at the middle of that sampling period. The set of selected VOC tracers entailed ethane, propane, butanes, pentanes, n-hexane, n-heptane, n-octane, benzene, toluene, acetylene, ethene, propene, isoprene, cyclopentane, ethylbenzene, m,p-xylene, o-xylene.

Airborne radioactivity was measured as alpha radiation, both in the gas phase and on a filter collecting particles, with two separate monitors. The gas phase radioactivity was measured as alpha radiation emitted from radon gas (Rn-222 and Rn-220); a second instrument was used to measure alpha radiation emitted from radon progeny associated with airborne particles (collected in the form of total suspended particulate matter, PM). Counting data from both instruments was accumulated over a 10-minute interval, then averaged to the desired period (e.g., hourly).

Sound pressure levels were monitored with a Brüel & Kjær 2250-L sound level meter, which consisted of a unidirectional microphone, a preamplifier, and a main processor. The instrument was positioned on the tower at 4 m in height. Data were collected for ⅓ octave band frequencies from 12.5 hertz (Hz) to 16 kilohertz (kHz) in decibels (dB). Hertz is a unit of frequency defined as one sound vibration or cycle per second. The sound level meter's internal sound processing software applies frequency and time weightings to the signal according to international standards (IEC 61672-1) to compute A-weighted and C-weighted levels, including their maxima, minima, and peaks. Frequency weighting adjusts how the sound level meter responds to different sound frequencies. For example, A-weighted levels better capture human-perceived sound by emphasizing mid-frequencies (500 Hz–4 kHz), which are audible, and reducing low- and high-frequency bands. C-weighted levels measure overall loudness, including low frequencies, but remove high-frequency bands.

All measurements continuously collected data at 1-minute time resolution or were averaged to 1-minute intervals, except radioactivity and VOCs. VOCs were measured over

a 10-minute sampling interval once every hour. We used regulatory-approved monitoring equipment and followed regulatory protocols and calibration methods (40 Code of Federal Regulations Part 58) where applicable, or, alternatively, we adhered to guidelines and calibration scales established by the World Meteorological Organization's Global Atmospheric Watch program. Data collection was automated and continuous. Data logging devices used custom-written software (O_3, NO_x, CO, H_2S, SO_2, VOCs, radioactivity) or manufacturer-provided software (meteorological variables, CH_4 and CO_2, noise). **Table 1a** provides an overview of the compounds measured, including the instruments and methods used. Details of the instruments and methods can be found in Appendix A (available on the HEI website).

Monitoring data were continuously logged to a computer inside the trailer that was accessible remotely. **Table 1b** shows the data coverage completeness from each sensor, which was approximately 90% for VOCs and >95% for all other sensors. Data were reported in real time on a website that was specifically developed for this project (https://bouldair.com/loving.htm). The web portal was updated with numerical data collected from the sensors and monitors every 5 minutes. Tabulated data included the most recent measurement and the prior 8- and 24-hour averages. Time series data graphs displayed the prior 3 and 30 days of data. Another set of time series graphs compared the LNM data with concurrently sampled observations from the Boulder AIR-operated monitoring sites in the DJB. Other website tabs provided information on the motivation for the study, monitoring methods, pollution source analyses, and contacts. The website received approximately 4,400 visits over the 1+ year period while public.

PASSIVE SAMPLING NETWORK DESIGN AND DATA COLLECTION METHODS

Permian Basin

Local volunteers from the Carlsbad-Loving, New Mexico, region were recruited using local advertisements, outreach to community-based organizations, and word of mouth to help deploy a network of (ultimately) seven passive samplers. All stations were located at or near residential locations across inhabited areas between Loving and Carlsbad, with five locations on a volunteer's private property next to their occupied dwellings, one location in a business yard, and one location next to the LNM stationary air quality measurement location (Figure 3). Not all sampling sites were established at the same time. The initial five locations were established in late spring 2023, and an additional two locations were established in fall 2023. All stations were at or near populated areas and were operated into late spring 2024, which provided an annual record for the initial stations and a 6- to 7-month record for the additional two stations added in fall 2023. Each station consisted of a shepherd hook that supported an assembly holding two (replicate) samplers comprising Radiello yellow diffusion tubes with standard Radiello Carbograph 4-filled adsorption cartridges inside, covered with a shield/baffle to keep out rainwater and reduce solar radiative load on the samplers **(Figure 4)**. This setup and operation had been tested in three previous projects in Texas and Colorado (Sablan et al. 2020; Schade and Heienickle 2023). Temperature sensors were deployed at two stations to supplement the meteorological measurements made at LNM. The small white sensors (HOBO MX2300 loggers) were deployed to the shepherd hook bar approximately 1.2 m above ground level and were expected to experience similar solar radiative loading as the diffusion tubes themselves.

Samplers at all locations were exchanged on an approximately weekly basis by a local volunteer, safely packed, and express-shipped to College Station, Texas, for hydrocarbon analysis. This field sampling protocol was approved by the Research Ethics Board at the University of Toronto (protocol #41867). Written informed consent was obtained from all participants who hosted a sampler, and volunteers were provided with a $50 gift card in acknowledgment of their participation.

Sample handling and analysis were very similar to the protocol used in our previous project (Schade and Heinickle 2023), entailing inspection and transfer to thermal desorption tubes, followed by thermal desorption and preconcentration. These steps were followed by GC separation (60-m wide-bore RTX-1 column, HP 6890 Series II GC) with FID. Calibration samples, diluted gas mixtures quantitatively sampled onto carbonaceous adsorbents, were processed with each set of weekly field samples. The calibration samples used one of two certified gas standards, each containing n-hexane and toluene, which were used to quantify alkanes and aromatic compounds, respectively, in each field sample. The gas standards were intercompared with each other, and one was shared with Boulder AIR, where its composition was evaluated in a single-blind experiment to compare reference standards between the two groups performing hydrocarbon measurements. These experiments revealed excellent intra- and interlaboratory transferability. The hydrocarbons quantified in all field samples included the alkanes 2-methylpentane, 3-methylpentane, n-hexane, 2,4-dimethylpentane, 2-methylhexane, n-heptane, n-octane, the naphthenes cyclohexane and methyl-cyclohexane, and the aromatics benzene, toluene, ethylbenzene, m,p-xylene, and o-xylene, for a total of 15 hydrocarbons.

After analysis, all field samplers were cleaned via an additional thermal desorption under clean carrier gas flow, repacked, and express-shipped back to the volunteer to maintain an approximately 1 week turnaround period. Sample chromatograms and their integration were stored in PDF format, and peak areas were transferred to spreadsheets for concentration calculations. To convert measured hydrocarbons' mass loads on each passive sampler to ambient mole fractions, tabulated sampling rate values were used as provided by the Radiello systems' manufacturer for the given diffusion tube-adsorption cartridge combination. Averages between the two field replicates were calculated and converted to molar mixing ratios using local average air density

Table 1a. List of Components Measured at LNM, Including Instruments Used, Detection Limits, Analytic Methods, and Calibration Details

Component	Instrument	Detection Limit(s)	Calibration Scale	Calibration Protocol
Ozone (O_3)[a]	Thermo Scientific 49C	1 ppb	EPA Region 8	Daily zero and span checks; annual transfer standard
Nitrogen Oxides (NO, NO_2, NO_x)	Teledyne T200UP	0.05 ppb	Linde, EPA-grade	10 ppm NO standard; daily zero and span checks every 3 days; biweekly conversion efficiency checks; quarterly full calibrations
Hydrogen Sulfide (H_2S)	Teledyne T101	0.1 ppb	Praxair, EPA-grade	5 ppm standard; zero and span checks every 3 days; monthly span calibrations
Sulfur Dioxide (SO_2)	Teledyne T101	0.1 ppb	Praxair, EPA-grade	5 ppm standard; zero and span checks every 3 days; monthly span calibrations
Methane (CH_4)[a] Carbon Dioxide (CO_2)[a]	PICARRO G2301	0.05 ppm	NOAA GML	Calibration checks every 2 days; 6-month linearity check
Carbon Monoxide (CO)	Thermo Scientific 48C	30 ppb	Linde, EPA-grade	2.6 ppm standard; 6-hour autozero; monthly span checks
VOCs, e.g., Ethane Propane Benzene	Agilent 6890 TD-GC-FID	0.01–0.05 ppb	Multicomponent gas standards, UK National Physics Laboratory	4 ppb; zero air and standard runs every 3-4 days; monthly primary standard calibrations
Radon and Particle Radioactivity	AlphaGUARD/Alpha PM	2 Bq/m^3	Factory-calibrated	Detection limit for 10-minute signal integration
Meteorology Winds, Pressure, Temperature, RH, Solar Radiation	METSENS500 multi-sensor, pyranometer	±3% or better	Factory-calibrated	
Noise	Bruel & Kjaer 2250	1 dB	Factory-calibrated	Bruel & Kjaer Sound Calibrator type 4231 ± 0.2 dB
C_6–C_8 Hydrocarbons, Passive Sampling	Radiello sampling followed by TD-GC-FID	0.01–0.05 ppb	Apel-Riemer	Multicomponent gas standards, weekly calibrations

dB = decibel; ppb = parts per billion; ppm = parts per million.

[a] Greenhouse gas.

for the elevation conditions in Loving. Differences between replicates were tracked for each compound and used in quality control. Data from the spreadsheets was read into *R* for analysis and plotting.

Eagle Ford Shale

Sampling in the Texas Eagle Ford Shale (EFS) area was very similar to the PB; however, fewer stations were deployed, and a shorter field monitoring period was executed. Four stations were set up in August 2024 across a south-north pattern from Kenedy, Texas, at the southern end of the shale production area where surrounding wells produce mostly gas, to a recreational vehicle (RV) park close to the northern end of the shale production area, where surrounding wells produce mostly oil (Figure 5). An additional site was established in urban College Station, close to Texas A&M's main campus, which is technically within the Eagle Ford Shale but has virtually no producing wells surrounding it and thus indirectly served as an urban reference station. All sites were maintained and visited weekly via day trips from College Station until January 2025. Temperature data were collected at two of the sites and compared to the local weather station measurements at the Texas Commission on Environmental Quality's (TCEQ)

Table 1b. Monitored Variables, Number of Collected Data Points, Hours of Observations, and Percentage Data Coverage from Each Sensor at LNM over the Campaign Period

Measurement	Count	Hours [a]	Coverage [b]
CO_2, CH_4, H_2O	592,334	9,831	99.9%
CO	568,615	9,640	98.0%
Temperature, Wind	589,735	9,781	99.4%
NO, NO_2, NO_x	570,507	9,683	98.4%
O_3	563,281	9,505	96.6%
Radioactivity	58,223	9,655	98.1%
VOCs	8,900	8,833	89.8%
H_2S	162,297	9,668	98.3%
SO_2	161,152	9,668	98.3%
Noise	355,118	6,576	~60%[c]

LNM = Loving, New Mexico; VOCs = volatile organic compounds.

[a] Number of hours between April 16, 2023, and May 31, 2024, containing observations of ambient air, not including sensor calibrations.

[b] Fraction of hours with observations of ambient air, out of 9,840 total hours between April 16, 2023, and May 31, 2024.

[c] Instrument was offline from November 13, 2023, to March 14, 2024, due to an instrument issue.

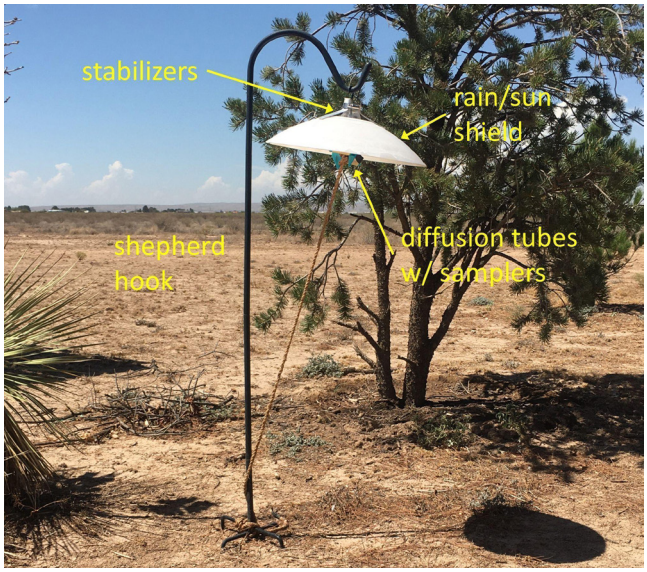

Figure 4. A network field site's passive sampling setup.

monitoring site in Karnes City. That site's hourly hydrocarbon measurement data served as a comparison to our data collected in Karnes City. All sampling, handling, and analysis were identical to the procedures described above for the PB network.

OIL AND GAS WELLS

We extracted information on well locations, types, and ages from Texas and New Mexico state databases maintained by the New Mexico Energy, Minerals, and Natural Resources Department and by the Texas Railroad Commission. Operator and production data were extracted from Enverus (*https://www.enverus.com*) for both PB and EFS and the Texas Railroad Commission (RRC) for hydrocarbon-producing wells in Texas.

Enverus provides data on wells, including geolocations, operator name (identified with an operator ID), well type (horizontal, vertical, directional, unknown), well status (active, inactive, plugged and abandoned), plug date (date production permanently ends), completion date or first production date (when well is ready for or begins production), and last production date. In a separate data portal, Enverus provides monthly production values by operator for oil and gas production.

For analysis with data collected at LNM, we first filtered the well data to include directional, vertical, and horizontal active wells that were within 10 kilometers (km) of the trailer. The identified wells were then merged with production data by operator ID and month. Monthly production values within the buffer were summed, creating values for oil production in million barrels (MBBL per month) and gas production in million cubic feet (MMCF per month).

Similarly, we evaluated producing wells surrounding the passive sampler network sites in the Permian and EFS: we determined the number of active wells and total oil and gas production during the sampling periods within 2-, 5-, and 10-km circular buffers surrounding each sampling location for comparisons to the measured ambient air pollutant concentrations.

Figure 5 shows an overview of oil and gas well locations (cyan dots) in the larger Carlsbad–Loving region, including sites identified from satellite data as having conducted gas flaring during our 2023–2024 field measurement period.

An analysis of Enverus data within a 50-km radius of the LNM site indicated that actively producing conventional wells (N = 3,212), defined as vertical wells with production recorded during the LNM sampling period, represented approximately 38% of the number of unconventional wells (N = 8,401) (Appendix C, Table C1). The conventional wells were primarily clustered near Carlsbad, to the NNW and N of the LNM site, as well as in a small area to the NE, although most were located farther from the site compared to the denser distribution of unconventional wells (Appendix C, Figure C1). During the LNM sampling period, active conventional wells accounted for 0.5% of total oil production and 0.5% of gas production relative to unconventional wells (Appendix C, Table C2). Prior works have found that (1) emissions from wells within 50 km accounted for 98% of average ethane concentrations at a central measurement site (Graves et al.

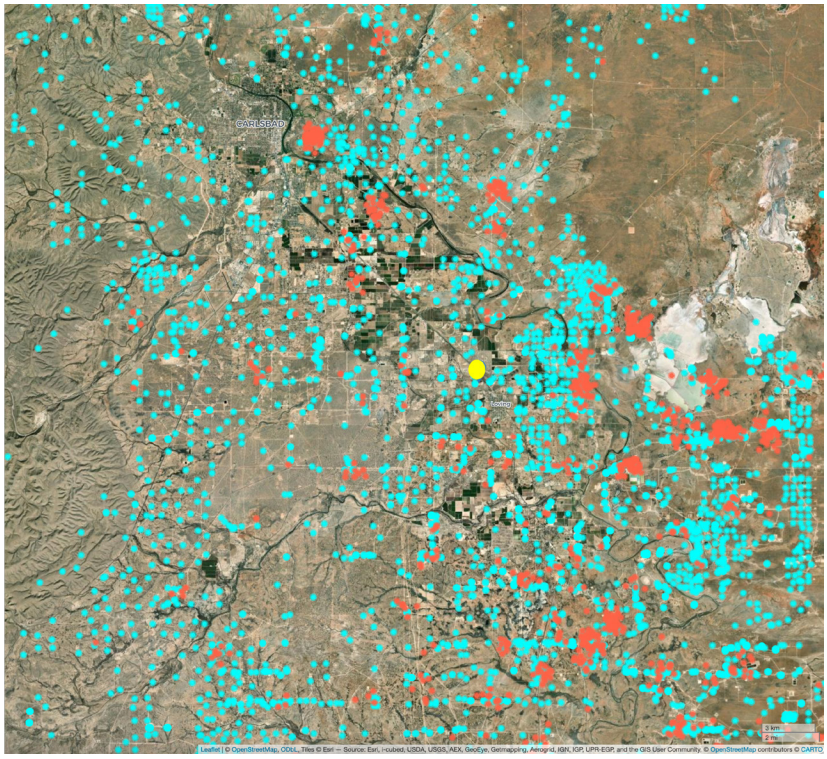

Figure 5. Active wells in the Carlsbad–Loving, NM, region from Enverus (cyan dots) and Visible Infrared Imaging Radiometer Suite Nightfire individual nightly flare detections during the monitoring period May 2023–June 2024 (red dots). The yellow marker shows the location of the LNM sampling site. VIIRS = Visible Infrared Imaging Radiometer Suite.

2025), and (2) methane emission intensities from conventional wells were nearly three times smaller than those from unconventional wells in Canada (Baillie et al. 2019). Based on these studies and our findings, we conclude that the air quality impacts from conventional wells in the region were likely minimal compared to those from unconventional wells.

RADIOACTIVITY IN OIL AND GAS EXPLORATION

Oil and gas production releases radon gas, primarily Rn-222, that is formed from the decay of U-238. Due to radon's short half-life, 3.83 days, its nonvolatile radioactive decay products can deposit and accumulate, known as scale, inside pipes and valves throughout the industry. Once radon is emitted, itself and its radioactive progeny, which quickly adhere to airborne particles, pose health concerns such as increased risk of lung cancer and cardiovascular effects (Blomberg et al. 2020; Harrison et al. 2007). These radionuclides travel preferentially with natural gas and natural gas liquids (NGLs) from the point of extraction through transportation and processing infrastructure, with potential radon emissions at facilities like compressor stations, refineries, and petrochemical plants (Gray 1993). Li and colleagues (2020) analyzed EPA RadNet data and found that for every 100 unconventional oil and gas development (UOGD) wells within 20 km upwind of a monitoring site, airborne particle-associated beta radioactivity increased by approximately 7%, compared to 1% for conventional wells. They observed exponentially higher radioactivity closer to wells, suggesting current monitoring underestimates exposure. A subsequent study found that airborne radioactivity was elevated two to three times above background levels in communities within 1 km of Colorado's largest oil refinery when winds were blowing from its direction upwind (Helmig et al. 2024).

SATELLITE-BASED FLARING IDENTIFICATION

In the last few decades, satellite-based observations have enabled the detection of flares globally, which has been instrumental in assessing their contribution to air pollutant and greenhouse gas emissions (Faruolo et al. 2022). Visible Infrared Imaging Radiometer Suite (VIIRS), which is a multispectral instrument, records near-infrared and short-wave infrared data in several spectral bands nightly with 750-m spatial resolution. Combustion sources are readily detected in the infrared data, and observed signals can be fully attributed to the combustion source. The VIIRS Nightfire (VNF) algorithm developed by Elvidge and colleagues (2013) leverages detections from all VIIRS spectral bands, collecting data at night, including the infrared and day/night bands. The algorithm detects the thermal anomalies, filters out nonflare sources, and estimates key parameters, including flare-specific temperature, source area, and radiant heat intensity. While the spatial resolution of VNF is nominally 750 m, the thermal detections are subpixel. This means the effective detection resolution depends on the flare intensity; UOGD flares have a high energy contribution and are thus detected below the native pixel size. Data on nightly flares were acquired from the Colorado School of Mines Earth Observation Group (*https://eogdata.mines.edu/products/vnf/*) using VNF v3.5.

Flaring is a significant environmental and public health concern as it contributes to greenhouse gas and air pollutant emissions. The boom in oil and gas production in the PB has been coupled with a rise in gas flaring, particularly since 2016 **(Figure 6)**. We conducted a comprehensive analysis of flaring activities in the PB for our measurement period, combining satellite observations from the VNF product with our field measurements to quantify flared gas volume as well as estimate the contribution of flaring to CH_4, NO_x, CO_2, and select VOCs at the LNM sampling site.

Figure 6. Top: Annual counts of flares observed in the PB by the Visible Infrared Imaging Radiometer Suite (VIIRS) from 2016 to 2023; Bottom: Spatial kernel density estimates of flares observed by Visible Infrared Imaging Radiometer Suite during the LNM sampling period. The blue marker denotes the location of the LNM trailer.

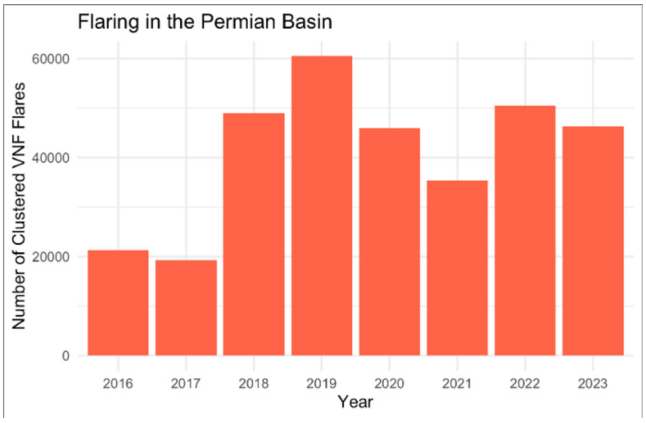

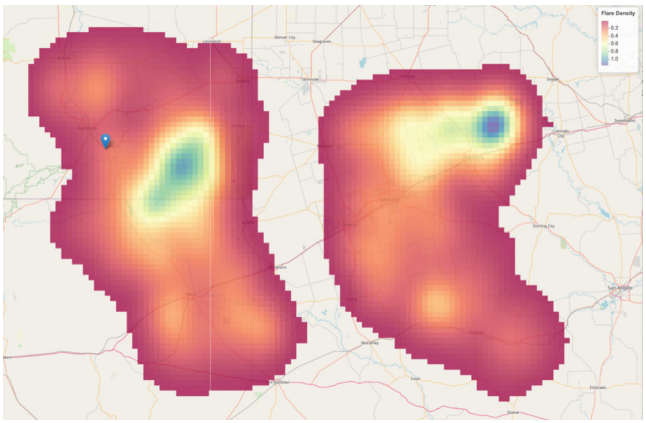

DATA ANALYSIS AND STATISTICAL METHODS

STATIONARY SAMPLING: ANALYSIS OF AIR POLLUTANTS, GREENHOUSE GASES, AND RADIOACTIVITY

Summary Statistics and Correlations To summarize the data measured over the yearlong sampling period at LNM, we calculated statistics of all components measured at LNM, including means, standard deviations, medians, quantiles, maxima, and minima. Correlations between key hydrocarbons were examined through scatterplots and compound ratio changes over time.

When linear regression analyses were performed, orthogonal distance regression (ODR) was used to account for errors in both the *x* and *y* variables as an alternative to the ordinary least squares (OLS) method, which only accounts for errors in the y variable. Orthogonal distance regression analyses were calculated using Python stats and SciPy packages. Specific formulas and residual variance (percentage of variance not explained by the correlation of variables, roughly analogous to 1-R^2, where R is the Pearson correlation coefficient) calculations can be found in Boggs and colleagues (1992).

Time Series Time series plots of the highly temporally resolved data are presented for methane and carbon monoxide to illustrate emission plumes and for O_3 to illustrate National Ambient Air Quality Standard (NAAQS) exceedances. Additionally, for several compounds, we illustrate diurnal concentration changes using box plots. Atmospheric measurements at UOGD sites commonly exhibit pronounced diurnal variability, with minimum concentrations in the afternoon and maxima during nighttime and early morning hours. This pattern is primarily driven by the diurnal evolution of the planetary boundary layer. At night, the suppression of convective mixing and the formation of a stable boundary layer reduce vertical dilution, allowing near-surface emissions to accumulate. Conversely, daytime convective turbulence enhances mixing and dispersion. Despite these cycles, elevated concentrations exceeding typical background levels by several-fold can occur at any hour, indicating continuous and/or episodic emissions from local and regional sources.

Furthermore, box plots with data binned by wind direction (degrees) were used to better understand advection from nearby and distant sources, including contributions from flaring and well density.

Polar Plots Bivariate polar plots were used to help visualize concentrations as a function of ambient wind speed and direction. The plots used polar coordinates, with wind speed in the radial dimension and wind direction in the azimuth dimension. To generate these plots, we used the OpenAir package (Carslaw and Ropkins 2012). Compound-specific concentrations were aggregated into wind speed and wind direction bins, and the mean or median in each bin was calculated. We used the default binning, interpolation, and smoothing settings in OpenAir, which uses wind direction bins of 10-degree intervals and 1-meter/second interval wind speed bins. The "min-bin" parameter specifies the minimum number of values in each bin required in the interpolation and is shown in the polar plot. In most cases, min-bin values >1 were selected to avoid outlier values biasing the results. Gray areas on the respective figures represent data that were removed because there were too few data points in the particular bin to meet the minimum bin threshold. Importantly, data with wind speeds less than 1 m s^{-1} were excluded from these analyses to ensure clear wind direction dependency results. If multiple 1-minute wind speeds and directions were associated with a measurement interval (e.g., the VOCs, which use a 10-minute sample), those wind observations within the measurement interval were vector averaged to obtain a single representative wind speed and direction to be paired with that measurement.

Comparisons with DJB Comparisons of the concentrations measured at LNM were made with five sites in the DJB that were operated at the same time. **Figure 7** shows the locations of the DJB comparison sites in relation to oil and gas pro-

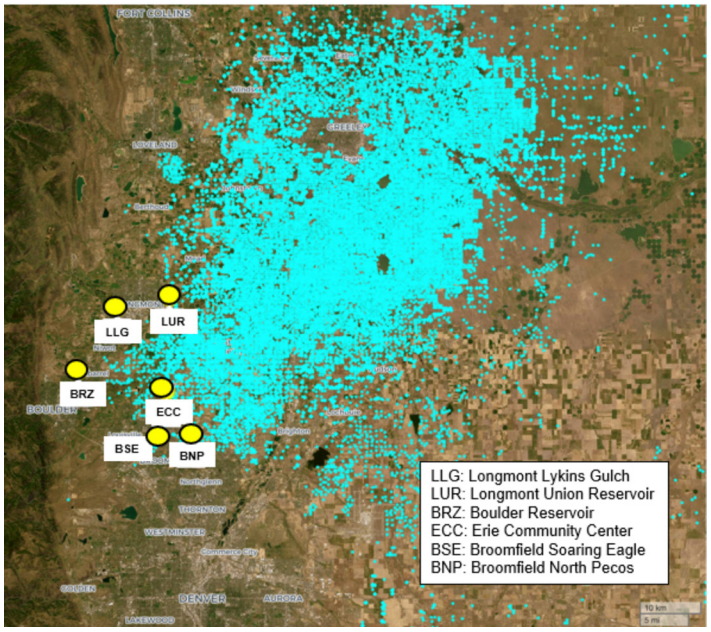

Figure 7. Map of the Denver-Julesburg Basin (DJB) comparison sites (yellow dots) with respect to oil and gas well locations (cyan dots).

duction and the Northern Colorado Front Range and Denver metro area.

Source Contribution Analyses Potential Source Contribution Function (PSCF) analyses determine the probability that an emissions source contributed to elevated concentrations of CH_4, O_3, select VOCs, or total radioactivity at a grid cell with a given latitude and longitude (Pekney et al. 2006). PSCF modeling was conducted using NOAA's 3-km gridded High-Resolution Rapid Refresh (HRRR) meteorology data as input to the Hybrid Single-Particle Lagrangian Integrated Trajectory (HYSPLIT) model to compute back trajectories. Hourly trajectories using a 5-m above ground level starting height were calculated going 12 hours backward in time to characterize where the air mass had traveled from. Each concentration of a given variable measured at LNM that met a specified criterion (e.g., exceeding the 50th percentile value of all observations) was paired with the back trajectory closest in time to the LNM observation time. Back-trajectory locations were then accumulated into a grid using all selected data. Gridded maps were generated for each compound analyzed, showing the probability that any given back-trajectory would have passed over a given pixel on the map. In essence, these maps show likely source regions for these compounds. More details about the PSCF modeling application can be found in Oltmans and colleagues (2021).

SOURCE APPORTIONMENT WITH NON-NEGATIVE MATRIX FACTORIZATION

Non-negative matrix factorization (NMF) is a widely used method for identifying and quantifying pollution sources from multipollutant data. NMF decomposes a dataset (a matrix typically denoted by **X**) of concentrations into a set of source profiles and their respective contributions while ensuring that all values remain non-negative, aligning with the physical constraint that pollution concentrations cannot be negative (Lekinwala and Bhushan 2022). Generally, **X** is an approximation of the product of a basis matrix **W**, which is the source profiles, and a coefficient matrix **H**, which is the source contributions: **X≈WH.** Through NMF, we minimize a loss function to find **W** and **H** such that their product best approximates **X** while ensuring all elements remain nonnegative. The rank, *k*, is chosen a priori to represent the number of factors (here: related to emission sources) that are extracted. For a given *k*, if **X** has dimension $m \times n$, then **W** is $m \times k$ and **H** is $k \times n$.

NMF or its equivalent counterpart, positive matrix factorization (PMF) has been used extensively by air quality researchers examining chemical speciation of particulate matter concentration to extract source signatures such as traffic emissions, industrial activities, or biomass burning (e.g., Chan et al. 2008; Lyu et al. 2021; Srivastava et al. 2025). In the context of studying UOGD sources, a previous study using NMF in the EFS revealed six consistent source factors, of which two were associated with preexisting local sources from car traffic and industry, three with regional oil and gas exploration, and one with diesel emissions (Schade and Roest 2018). In this study, we conducted NMF on a merged dataset with hourly resolution of 27 compounds (VOCs, CH_4, CO_2, CO, H_2S, SO_2, NO_x, and total radioactivity) measured at LNM. Several preprocessing steps based on Schade and Roest (2018) and Guha and colleagues (2015) were taken on the data. We denote individual concentrations as x_{ij} where i is an observation (i.e., concentration for each hourly timestamp t_i) and j is the component.

1. Missing observations were removed; if any component x_{ij} had a missing hourly concentration at time t_i, the entire hour was removed to ensure a complete matrix of data.

2. For each component x_{ij}, background concentrations were removed by subtracting its minimum concentration, $x_{min,j}$. If $x_{min,j} < 2\text{xLOD}$ (LOD is the limit of detection, found in Table 1a), we did not remove the background. Similarly, if the maximum concentration $x_{max,j} > 100\text{xLOD}$, we did not remove the background.

3. Any concentration below the detection limit was replaced with a random value between 0 and 0.5xLOD.

4. Each component of X was normalized using its minimum and maximum values through $x_{norm,j} = (x_{ij} - x_{min,j})/(x_{max,j} - x_{min,j})$, resulting in all concentrations being in the range [0,1] and ensuring no negative values. Normalization is done because input data originated from different instruments, with different ranges and different uncertainties (Guha et al. 2015).

In NMF, uncertainty for each x_{ij} concentration was introduced to give more importance to reliable data and less weight to less certain values. We constructed an uncertainty matrix **S** based on steps adopted from Williams et al (2010), and Guha et al (2015). For all compounds, the following steps were taken:

1. $s_{ij} = 2\text{xLOD}$ if $x_{ij} \leq \text{LOD}$
2. $s_{ij} = ((0.1x_{ij})^2+(\text{LOD})^2)^{0.5}$ otherwise

We applied NMF with weighted least squares to minimize $\sum_{ij} 1/{S_{ij}}^2 (X_{ij} - (WH)_{ij})^2$, which is computed using iterative least squares to solve for W and H iteratively We explored between four and six sources (i.e., the rank, k = 4, 5, or 6) and settled on the best result of five factors based on a balance of minimal reconstruction error (variance explained) and our expected number of sources as informed by previous studies. We calculated the total variance explained by looking at the ratio of the weighted residual sum of squares from the NMF to the weighted total sum of squares. To decompose the variance explained by each factor, we implemented a leave-one-out reconstruction approach. Because NMF factors are not orthogonal (unlike principal component analysis), the variance contributions estimated from the leave-one-out approach can overlap. As a result, the sum of factor-specific variance explained values can exceed 100%, reflecting shared explanatory power between factors.

To analyze sources with geographic features, we used box plots of each factor by 10-degree wind direction intervals. NMF analyses and visualizations of the NMF results were performed in R 4.4.2.

NOISE FREQUENCY ANALYSIS

Spectrograms, which are visual representations of how sound frequency signals change over time, were created to visually analyze the ⅓ octave band data in 32 frequencies from 12.5 Hz to 16 kHz, measured in dB. The x-axis of the spectrogram represents time, which in our data was 1-minute intervals. We examined different lengths of total time to look at short-term trends (1 day), medium-term trends (1 month), and long-term trends (4 months). There was a lapse in data collection between mid-November 2023 and mid-March 2024 due to an instrument error and calibration issue, so the longest consecutive time series is from mid-June 2023 through mid-November 2023. The frequency is on the y-axis of a spectrogram, and the intensity of the heatmap represents the amplitude of each frequency at a given time. The spectrogram was used to explore the evolution of the sound signal over different time periods. To quantify potential sources of noise from UOGD, we took a novel approach that associates source-specific air pollutants with the multifrequency noise data. As noise originates from the same source as many air emissions, sound frequencies have the potential to serve as distinct signatures of UOGD processes. For example, drilling and hydraulic fracturing operations use large compressors, generators, and engines that contribute the most noise at well pads (Radtke et al. 2017). Flaring is a large source of sporadic noise, while truck traffic can contribute to noise at every phase of oil and gas production (Allshouse et al. 2019). Hays and colleagues (2017) classified noise associated with UOGD into (1) construction and preparation (road construction, site and well pad preparation, truck traffic), and (2) production and completion (flaring, drilling, hydraulic fracturing, compressor stations). Previous studies of noise have focused on characterizing A- and C-weighted levels, finding that across all stages of production, levels exceed guidelines of 55 dB and 65 dB, respectively (Allshouse et al. 2019; Radtke et al. 2017). Octave band analysis in one study showed that the dominant frequencies for fracturing and completion were in the low-frequency range (<125 Hz) (Radtke et al. 2017). Production, which includes compressors and oil and gas movement through pipelines, was dominated by even lower frequencies (13–30 Hz) (Hays et al. 2017). Low-frequency noise can cause vibrations and travel long distances; it may be a greater human exposure problem than noise characterized by A-weighted measurements, given that most walls in buildings and homes are not able to attenuate these frequencies (Leventhall et al. 2003). Other stages of production that have machinery and pump noise exhibit mid-frequency signatures (150 Hz to 500 Hz) while flaring produces high-frequency noise (above 2 kHz) from turbulent mixing of gas being burned with air, creating rapid pressure fluctuations (Sorrels and Coburn 2019).

By leveraging the simultaneously measured high temporal resolution noise and air quality data collected at LNM, we explored UOGD pollution sources. In a prior study of traffic-related noise using machine learning, specifically extreme gradient boosting (XGB), we uncovered sources of pollution related to specific frequencies of noise (Fallah-Shorshani et al. 2024). The benefit of a machine learning approach like XGB is that we can include meteorological variables, which are a crucial component to understanding sound propagation and air pollution. We chose XGB because it has been used extensively in environmental prediction, including our prior work, showing optimal performance in modeling noise measurements (Fallah-Shorshani et al. 2022; Yin et al. 2020).

An additional consideration was the potential for high correlation among noise frequencies, particularly within low, mid, and high ranges. To address this, we conducted NMF on the ⅓ octave band frequencies and included the resulting factors in the XGB to compare with the results derived when using the individual frequencies.

All models were trained on 80% of the data and tested on the 20% of left-out data, and model performance statistics (R^2 and root mean square error [RMSE]) were reported on the test set. Variable importance by the frequency method (i.e., number of times a variable is used to split the data across all the trees in the boosted model) was performed to identify the dominant variables in predicting each of the pollutants. All

noise frequency analyses, including spectrograms and XGB, were conducted in Python 3.13.

ANALYSIS OF PASSIVE SAMPLING DATA

A total of 194 site-weeks of measurements (two replicates each) were collected between June 2023 and June 2024. An additional 24 site-weeks were either not taken or lost as samplers were damaged, the whole site's setup was damaged (e.g., due to extreme weather), or the volunteer was unable to replace damaged or missing parts in time. Alongside the 388 field samples, 102 blanks were processed, consisting of 35 field blanks and 67 lab blanks. A field blank was a sampler that was shipped and handled identically to field samples but never removed from its glass shipping container. A lab blank was a standard, cleaned adsorbent cartridge not exposed to ambient air. All blanks were run alongside the field samples and standards, and typically in between the two field replicates from one site to evaluate possible sample carry-over.

No alkanes were observed in the laboratory blanks and almost all field blanks, but many blanks contained small levels of aromatics. The laboratory blanks showed right-skewed distributions for benzene, toluene, and m,p-xylene, with typical 1-week exposure equivalent levels of <0.005 ppb for all compounds. Field blanks showed more uniform distributions with higher concentrations. Average (median) 1-week equivalent exposure mixing ratios for benzene, toluene, and m,p-xylene were 0.01 (0.01), 0.05 (0.02), and 0.06 (0.05) ppb, respectively. No correction to the data was made based on these findings. However, based on the possibility that blank values reflect contamination via ambient air diffusion into the capped glass tube cartridge holders during transport and storage, method detection limits (MDLs) for all aromatic compounds were assumed to be of the order 0.05 ppb.

Method precision was determined from the relative differences between the two field replicates and varied by compound. Mean (median) precision ranged from as low as 10% (5%) for high mixing ratio (1–10 ppb) compounds such as methylcyclohexane and n-hexane to as high as 42% (37%) for low mixing ratio compounds (<0.5 ppb) such as m,p-xylene. Mean (median) precision across all quantified compounds' average precisions was 21% (18%). This is consistent with prior experiences using this method of sampling under field conditions, which has led us to flag results when replicates deviate by more than 30% and exclude samples when a difference of more than 60% between replicates is observed, roughly equivalent to the average and median 95% level across all observed replicates and compounds.

Accuracy was evaluated using two calibration gases during this study: a working standard containing isoprene, n-hexane, and toluene prepared in 2014 (Scott-Marrin, Riverside, California), and a newer gas standard containing n-pentane, n-hexane, benzene, methylcyclohexane, and toluene prepared in 2022 (Apel-Riemer, Miami, Florida; certification accuracy of 5%), both in ultra-high purity nitrogen. The working standard was shared with Boulder AIR in fall 2023 in a single blind comparison. Boulder AIR provided both the correct compound ID and mixing ratios in the standard, finding levels within the manufacturer's stated accuracy of 2% except for toluene (7%). Based on the Boulder AIR analysis using two newer external gas standards, the working standard's toluene mixing ratio was reduced from its original 5.07 ppm certification to 4.7 ppm, reflecting the age of the standard and its reduced pressure. We compared the working standard against the 2022 standard several times during 2023 and 2024. The results showed no differences in response factors for n-hexane and toluene (after adjustment), implying confidence in the accuracy and comparability of hydrocarbon measurements across the two independent groups in this project.

Overall accuracy was estimated from error propagation using field precision, gas standard accuracy (5%), and flow dilution accuracy (5%) (all calibration curves had determination coefficients better than 0.99). Uncertainty ranged from better than 20% for compounds such as methyl-cyclohexane, n-hexane, benzene, and toluene to poorer than 30% for n-octane, ethylbenzene, and the xylenes.

Abundances of 15 hydrocarbons were analyzed at seven field sites across the Carlsbad, New Mexico area in the Permian Basin, a map of which is shown in **Figure 8.** The campaign's duration and data density allowed for both seasonal analysis and robust correlational analysis, as well as comparisons to similar data collected at air quality monitoring sites in Colorado and Texas, including our stationary field site (site code LNM).

Abundances of the same 15 hydrocarbons were also analyzed at four sites across the Karnes City, Texas, area at the center of the EFS, a map of which is shown in **Figure 9**. The southernmost site was located on private property in south-central Kenedy, Texas, a community of 3,500 people. The site in Karnes City (population: 3,200) was located on church property toward the eastern edge of town, 200 m from main Highway 181 and 900 m east-northeast from TCEQ's Karnes City air quality monitor. The HEL site was located at a historical site in Helena, a small community northeast of Karnes City. Lastly, the northernmost site was on the grounds of a small RV park with several permanent occupants off Texas Highway 80 south of Gillett. An additional site was operated in urban College Station, Texas (population: 121,000) in the northeast corner of the EFS, providing a reference location with very few active oil and gas wells in the vicinity. In the EFS case, the campaign's duration and data density did not allow for a complete seasonal analysis; however, a robust correlational analysis and comparisons to similar data collected at TCEQ's Karnes City air quality monitoring site were possible.

We examined descriptive statistics for VOC concentrations at all sites and calculated correlation coefficients between measured hydrocarbons. We plotted average concentrations of each compound on maps to visually assess variation in relation to wind direction, shale areas, gas flares, and known emission sources such as roadways. We also plotted time series of

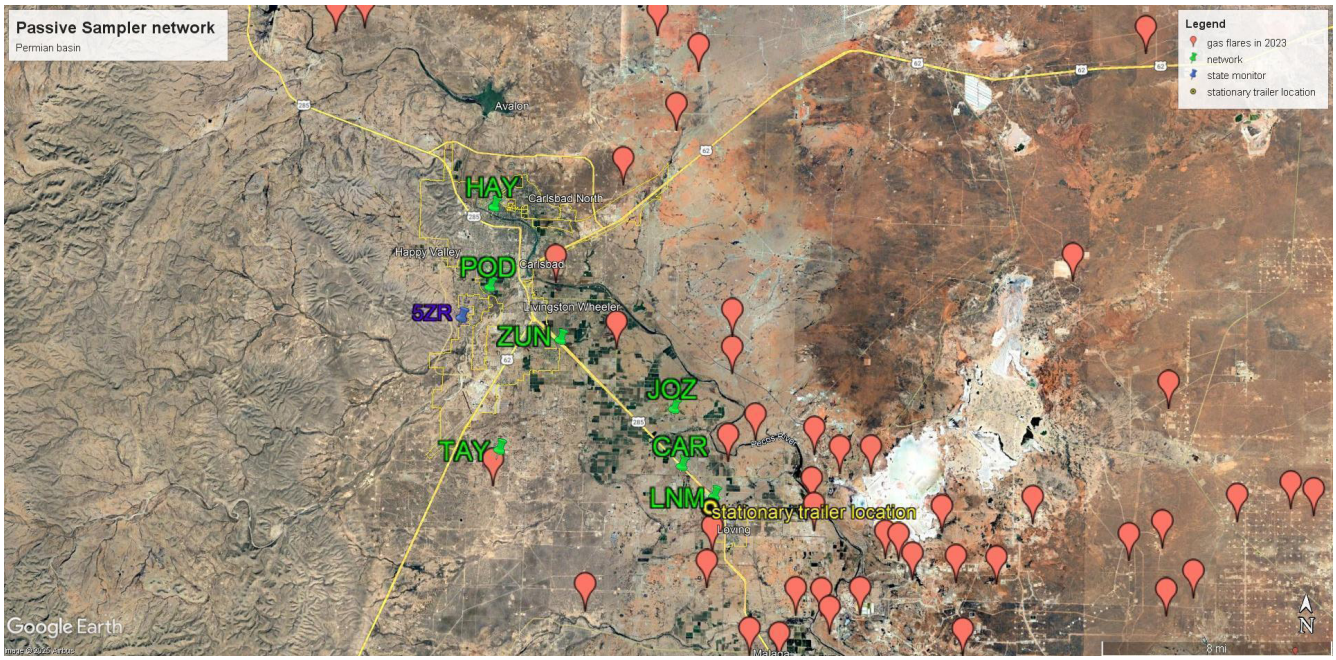

Figure 8. Passive sampler network (green markers and three-letter site codes) on satellite picture background of the Carlsbad, New Mexico area. Also indicated are the locations of a New Mexico state air quality monitor (site code 5ZR) southwest of Carlsbad, locations of oil and gas well site pads (faint white blotches), and VIIRS-identified active flares in the area in 2023 (red pins). The network stretched across a 17 km ×14 km = 238 km² area.

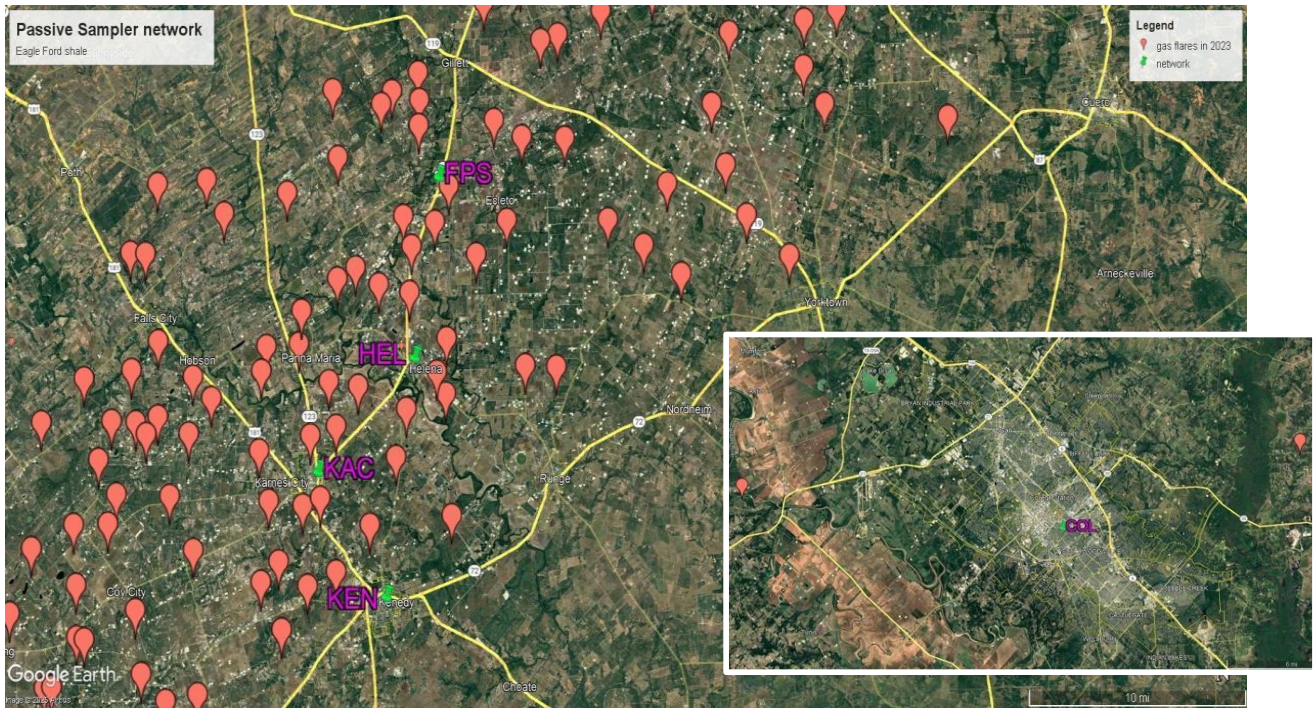

Figure 9. Passive sampler network (green markers and pink site codes) on satellite picture background of the Karnes City, Texas, area. Also visible are the locations of oil and gas well site pads (white blotches) and VIIRS-identified active flares in the area in 2023 (red pins) throughout the Eagle Ford Shale. The white border inset on the right shows the additional College Station site location 240 km to the northeast. In this case, the network stretched across a 10 km × 27 km = 270 km² area, not including the College Station site.

concentrations to assess seasonal variation. Data from the KAC site were compared to averaged hourly hydrocarbon levels measured at the nearest TCEQ air monitoring station in Karnes City, located approximately 900 m to the east-southeast of the KAC site (Appendix B). Lastly, we investigated relationships between average hydrocarbon mixing ratios at each field site, and oil and gas well densities in the area.

We used ArcGIS software to sum the number of active and inactive oil and gas wells and the volume of oil and gas produced over the study period within 2-, 5-, and 10-km circular buffers at each passive sampling site. Data were collected in a spreadsheet for each basin; additional plots of the locations of these wells in the different buffers are provided in the Appendix.

ANALYSIS OF SATELLITE FLARING

HDBSCAN (Hierarchical Density-Based Spatial Clustering of Applications with Noise) is a flexible and powerful clustering algorithm that groups georeferenced data points based on their spatial density. The additional benefits of this algorithm are that it has only one tuning parameter (minimum number of points in a cluster) and it produces a cluster membership probability. This means that if a spatial point does not have a high probability of being in a cluster, it is deemed noise. Using a similar approach to our previous work in the Eagle Ford Shale (Franklin et al. 2019), we first excluded VNF detections less than 1,600 K, then applied HDBSCAN to all nightly detections in the PB on data for the year of our stationary platform measurements in 2023–2024. We tuned the minimum number of cluster points between two and eight to minimize the number of noise points while maintaining a reasonable number of clusters.

With an optimally tuned algorithm, we removed the noise points and examined the clustered flares through the following:

1. **Methane equivalents estimation:** VNF Version 3.5 includes per-flare estimates of methane equivalents, which is a metric of the rate of methane combustion (in $m^3\ s^{-1}$) (Elvidge et al. 2013). To derive methane equivalents, the Earth Observation Group geospatially matches VNF detections to the Global Gas Flaring Catalog (*https://www.worldbank.org/en/programs/gasflaringreduction/global-flaring-data*), which provides known gas flaring locations based on reported and remote sensing data. Then, a calibration curve is used to estimate flared gas volume based on the detected flare's radiant heat, which is then converted to methane equivalents using the Global Warming Potentials for methane (IPCC 2021). We used the VNF estimates of methane equivalent to quantify inefficient flares that release incomplete combustion products. However, as methane equivalent was only reported for a subset of the flares in the VNF dataset, we also examine its relationship with VNF temperature and source area using a regression method we developed to estimate flared gas volume in the EFS (Franklin et al. 2019)

$$methane\ equivalent = \beta_0 + \beta_1 T + \beta_2 T^2 + \beta_3 T^3 + \beta_4 S + \epsilon$$

where T = flare temperature in degrees K; S = flare source area in m^2; β = regression coefficients that we estimated; ε = the residual error. This model was trained on 80% of the data, maintaining HDBSCAN clusters, and tested on the remaining 20%. Using this equation, we estimated methane equivalents for the flares that did not have a value.

2. **Assessing the relationship between satellite flares and air emissions at the LNM site**: We created 5-km, 10-km, 20-km, 30-km, and 50-km buffers around LNM and calculated the following flare-related variables:
   - The number of flares within each buffer
   - The number of downwind flares in each buffer, using the nighttime wind direction at LNM
   - The median methane equivalent of the flares in each buffer

   We also calculated the inverse distance-weighted monthly oil and monthly gas production levels for wells within 10 km of LNM. These metrics were merged with averaged (daily and nightly) concentrations of key tracers and the flaring source factors derived from NMF. Night was defined as 00:00 to 06:00 to represent concentrations that coincide with the VIIRS overpass time, which, based on the observation timestamp, was anywhere from 01:00 to 04:00 local time. We fit multivariable regression models testing the best combination of these predictors to maximize the R^2. In this inferential analysis, we did not tune the models but rather report statistically significant regression coefficients determined by $\alpha \leq 0.05$.

RESULTS

STATIONARY SAMPLING

Summary statistics of all components measured at LNM are shown in **Table 2**. Mean values of VOCs were highest for compounds with low carbon numbers (e.g., ethane and propane) and lowest for compounds with high carbon numbers (e.g., octane and xylenes). High compound variability was encountered for nearly all species, signifying an environment of strong air pollution sources affecting the measurements.

We discuss and compare selected observations at the LNM site in terms of

- absolute values and their comparison to air quality standards, where applicable
- mixing ratio distributions and their comparison to Colorado Front Range sites
- mixing ratio distributions as a function of air mass origin as evaluated from wind data
- diurnal and seasonal changes
- similarities and differences to other compounds

Table 2. Summary Statistics of Air Pollutants and Select Meteorological Parameters Measured at LNM, Using Data from the Entire Campaign

Measurement	Unit	Count	Mean	Standard Deviation	Minimum	Percentiles					Maximum
						5th	25th	50th	75th	95th	
Carbon Dioxide CO_2	ppm	592,334	432	9	413	422	426	430	436	448	554
Methane CH_4	ppb	592,334	2,668	1,305	1,919	1,981	2,080	2,283	2,865	4,428	139,140
Carbon Monoxide CO	ppb	568,615	170	99	20	94	122	150	196	301	10,420
Ethane C_2H_6	ppb	8,900	94	133	0.78	3	16	44	124	319	2,060
Ethene (Ethylene) C_2H_4	ppb	8,900	0.74	0.85	0.01	0.01	0.16	0.47	1.07	2.36	17
Propane C_3H_8	ppb	8,900	58.2	80.7	0.22	1.8	9.6	27.9	77.3	204.8	1211
Propene (Propylene) C_3H_6	ppb	8,900	0.15	0.18	0.01	0.01	0.04	0.09	0.21	0.46	5.53
1,3-Butadiene C_4H_6	ppb	8,900	0.01	0.02	0.01	0.01	0.01	0.01	0.01	0.032	1.21
i-Butane (Isobutane) C_4H_{10}	ppb	8,900	10.1	15.8	0.03	0.34	1.57	4.58	12.8	36.8	377
n-Butane C_4H_{10}	ppb	8,900	26.2	39.4	0.06	0.80	4.02	11.9	33.4	94.6	537
Acetylene C_2H_2	ppb	8,899	0.56	0.57	0.02	0.09	0.21	0.37	0.72	1.60	13.7
Cyclopentane C_5H_{10}	ppb	8,900	0.53	0.73	0.01	0.02	0.09	0.25	0.70	1.89	13.5
i-Pentane (Isopentane) C_5H_{12}	ppb	8,900	7.91	11.88	0.02	0.25	1.20	3.50	10.1	28.8	216
n-Pentane C_5H_{12}	ppb	8,900	8.98	13.58	0.02	0.25	1.28	3.90	11.5	32.9	259
n-Hexane C_6H_{14}	ppb	8,900	2.96	4.51	0.02	0.08	0.40	1.25	3.84	11.04	93.4
Isoprene C_5H_8	ppb	8,900	0.01	0.01	0.01	0.01	0.01	0.01	0.01	0.02	0.40
n-Heptane C_7H_{16}	ppb	8,900	1.09	1.63	0.00	0.03	0.15	0.46	1.44	4.01	37.3
Benzene C_6H_6	ppb	8,900	0.67	0.82	0.01	0.04	0.15	0.35	0.89	2.29	12.3
n-Octane C_8H_{18}	ppb	8,693	0.35	0.48	0.00	0.02	0.06	0.16	0.47	1.27	8.87
Toluene $C_6H_5CH_3$	ppb	8,741	0.65	0.81	0.00	0.03	0.12	0.32	0.89	2.29	11.1
Ethylbenzene $C_6H_5C_2H_5$	ppb	8,900	0.06	0.07	0.00	0.00	0.01	0.03	0.08	0.20	0.94
m&p-Xylene $C_6H_4(CH_3)_2$ (isomers)	ppb	8,900	0.22	0.30	0.00	0.00	0.02	0.10	0.31	0.84	5.25
o-Xylene $C_6H_4(CH_3)_2$	ppb	8,900	0.08	0.10	0.00	0.00	0.00	0.04	0.11	0.29	1.19
Ozone O_2	ppb	563,281	33.3	21.30	0.50	0.5	15.6	33.2	48.9	69.1	112
Nitrogen Oxide NO	ppb	570,507	5.1	20	0.03	0.0	0.1	0.4	2.7	23.7	1,204
Nitrogen Dioxide NO_2	ppb	570,187	9.6	9.70	0.03	0.5	2.1	6.3	15.0	28.0	336
Nitrogen Oxides NO_x	ppb	570,187	14.6	25	0.03	0.6	2.5	7.3	18.7	47.7	1,382
Hydrogen Sulfide H_2S	ppb	162,297	1.02	1.14	0.20	0.20	0.43	0.73	1.27	2.82	78.7
Sulfur Dioxide SO_2	ppb	161,152	0.37	0.45	0.20	0.20	0.20	0.20	0.44	0.95	12.6
Gas Radioactivity Rn-222, Rn-220	Bq m-3	58,223	19.8	13.7	1.00	4.2	10.7	17.1	25.9	46.6	173
Particle Radioactivity	Bq m-3	55,533	9.6	9.5	1.00	1.0	2.5	7.0	13.0	28.5	98.5
Temperature	°C	589,735	19.8	7.6	-11.0	2.6	12.2	20.2	27.6	36.1	43.1
Wind Speed	m s-1	589,725	3.5	2.3	0.03	0.7	1.8	3.0	4.6	8.0	23.6

LNM = Loving, New Mexico; ppb = parts per billion; ppm = parts per million.

Summary Statistics

As an overview of the variability encountered in our air pollutant observations, polar plots are presented for CH_4, three VOCs (acetylene, ethane, benzene), O_3, and NO_x (**Figure 10**). We observed that methane and the three VOCs have similar yet distinct dependencies on air mass transport (winds), with the highest median values of each compound associated with light southeasterly winds up to 3 m s^{-1}. The relative enhancements of median values associated with these winds compared to other wind directions were approximately 1.5 times higher for methane, 5 times higher for acetylene, 10 times higher for benzene, and over 100 times higher for ethane. For NO_x, we observed a distinctly different pattern, with the largest median values associated with a narrow sector of southwesterly winds >5 m s^{-1}. This sector was in line with the neighboring well pad where intermittent gas flaring was observed, but at comparatively low intensity (note that this gas flare did not prominently appear in our VIIRS data analysis). Similar to the pattern observed with the VOCs, the highest ozone values were encountered under southeasterly airflows with winds <5 m s^{-1}. Airflow from this direction during summer daytime conditions regularly coincided with exceedance of the 2015 ozone NAAQS of 70 ppb. The southeasterly wind sector displayed 10–15 ppb higher ozone medians than values associated with other wind directions.

Results by Compound

Methane Methane showed high variability with many spikes (or plumes) of highly elevated mole fractions, sometimes exceeding 100 ppm. There were frequent occurrences of methane >20 ppm in nearly every month of the campaign, particularly during the winter. For comparison, among all of the Colorado Front Range sites, there was only one occurrence of methane exceeding 20 ppm in 2023.

In **Figure 11**, we show a complete time series of the methane data, a running monthly median illustrating seasonal changes, and the global background methane mixing ratio of 1.93 ppm during the campaign. The time series illustrates the high frequency of methane spikes throughout the campaign, the occurrences of clean air conditions, and the seasonally higher methane abundances in winter compared to summer. These features were reproduced by the saturated hydrocarbons we measured, such as ethane and propane, and were generally present for all VOCs measured.

Figure 12 shows a box-whisker plot of methane binned hourly. As with all hydrocarbons, methane showed a diurnal cycle with minimum values in the afternoon and maximum values at night and in the early morning hours, which likely reflects diurnal changes in the atmospheric mixing state. With the absence of thermal convection, nighttime mixing with air from aloft (dilution) is weaker than during the day, causing emissions to accumulate to higher levels near the surface. At all hours of the day, plumes with methane concentrations 2–5 times the 95th percentile values at that hour were observed. The nocturnal median methane levels of approximately 3 ppm suggest a large regional hydrocarbon emission source.

Analyzing methane by wind direction revealed that methane spikes above the 95th percentile not only occur at all hours of the day (Figure 12), but also from any wind direction, likely a feature of the LNM site's relatively central location to the oil and gas production area.

Figure 14 shows a box-whisker plot comparing methane at LNM with other monitoring sites in Colorado. The mean methane value observed at LNM exceeded the 95th percentile values at all Colorado Front Range sites. The 75th and 95th percentile values at LNM were approximately 50% and 230% larger, respectively, than the global background.

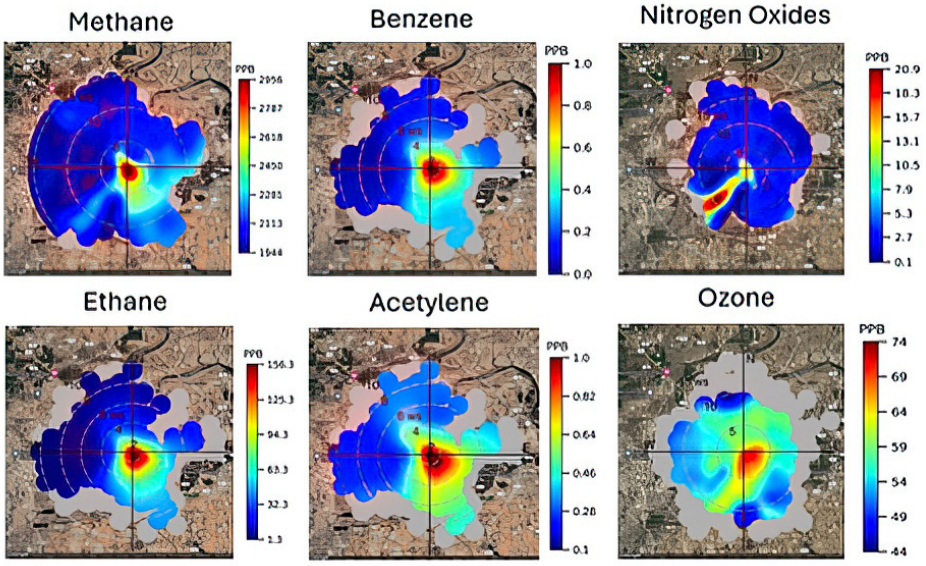

Figure 10. Bivariate polar plots showing the directional air mass transport impacts on acetylene, ethane, nitrogen oxides, methane, benzene, and ozone at LNM. All plots use a minimum bin of 2 and a minimum wind speed of 1 m s–1. The ozone plot comprises data from the summer season only (May 1–September 30, 2023) between 11:00–19:00 Mountain Standard Time (MST).

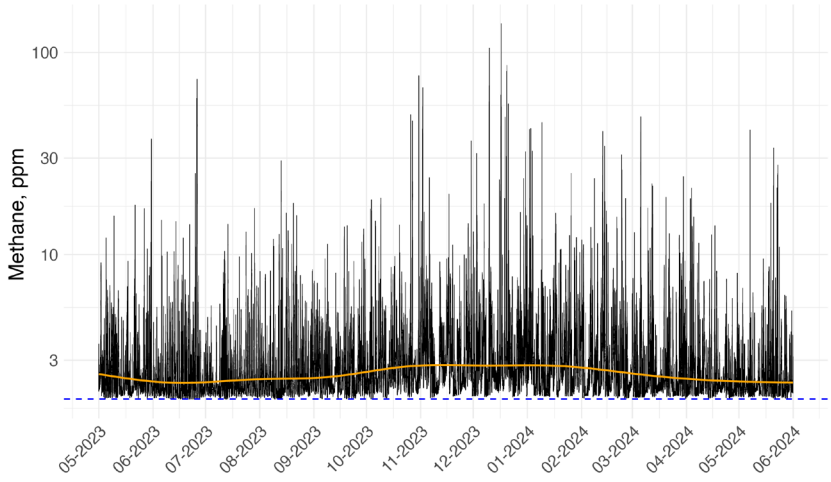

Figure 11. LNM-collected methane time series with running mean (orange line) and background level of 1.93 ppm (dashed blue line).

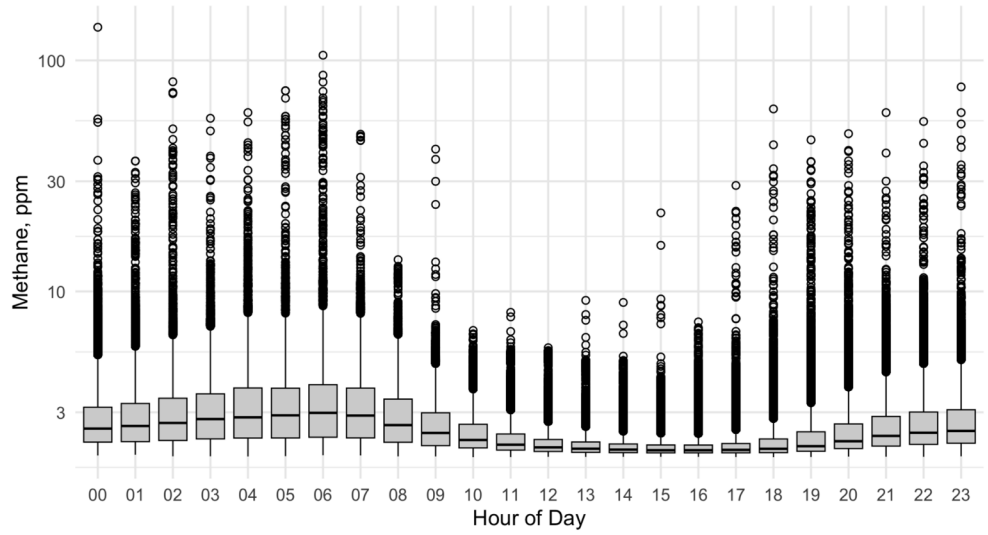

Figure 12. LNM-collected methane mole fractions binned by hour of day. The boxes at each hour reflect the interquartile range of the observations, the horizontal line indicates the median value, and the endpoints of the whiskers the 5th and 95th percentiles. Outliers above the 95th percentile are shown with open circles.

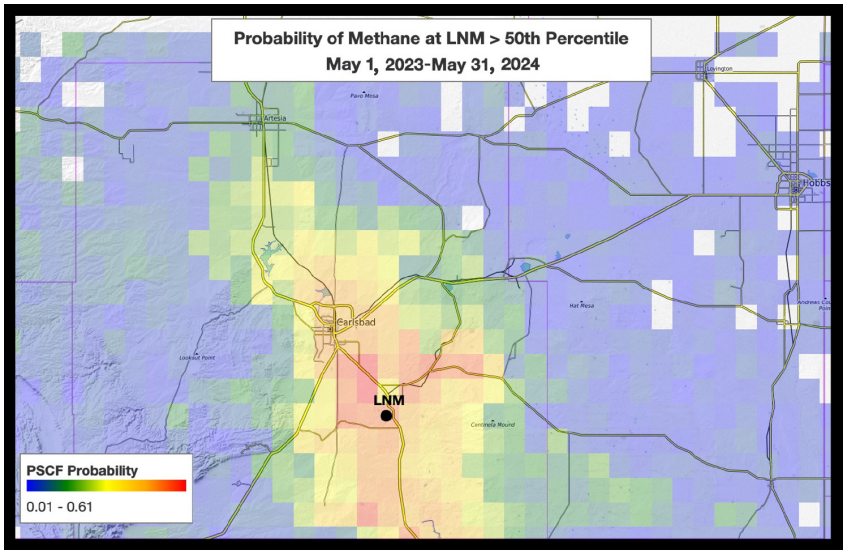

Figure 13. Potential Source Contribution Function (PSCF) analysis for transport origin of methane at LNM, using 3 km-resolution HRRR back trajectories paired with methane occurrences above the 50th percentile.

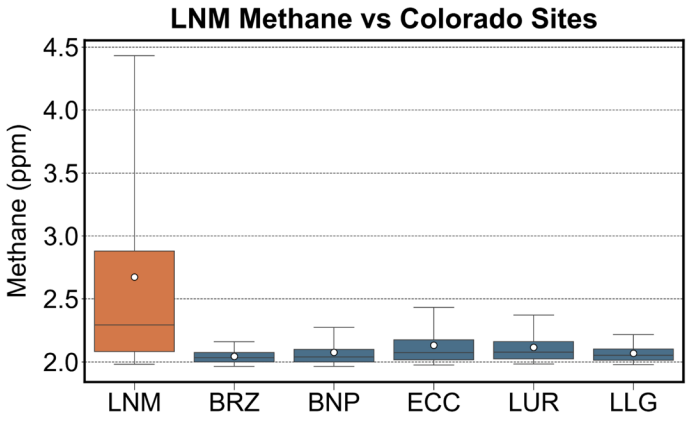

Figure 14. Box-whisker plot comparing methane statistics at LNM to other sites in the Colorado Front Range (blue). The white dots show the mean; the colored boxes show the 25th, 50th, and 75th percentiles; and the whiskers show the 5th and 95th percentiles of the data distribution. See Figure 7 for an explanation of the Colorado monitoring site three-letter codes.

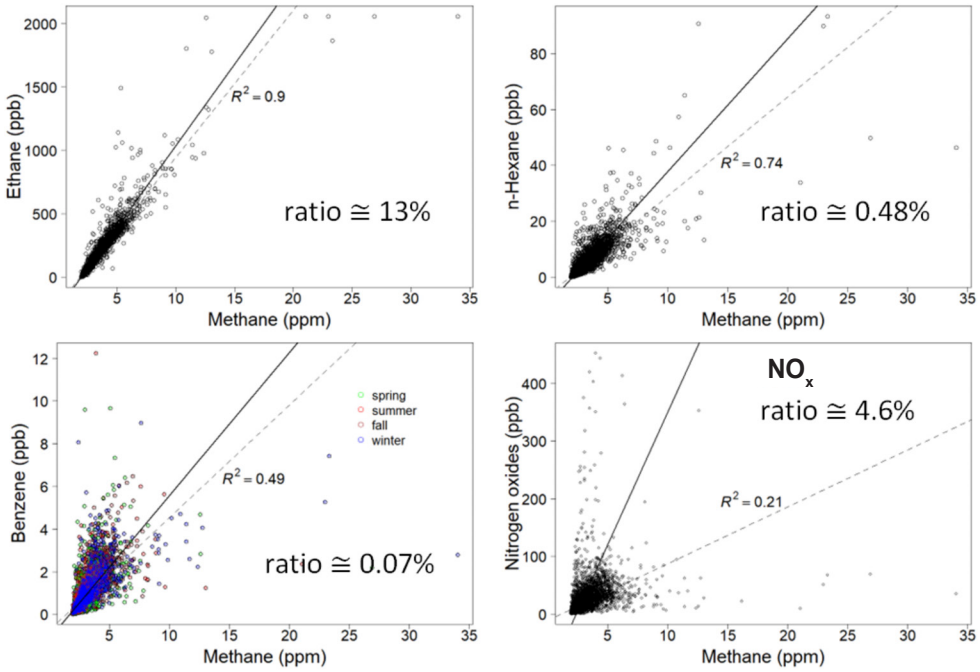

Figure 15. Orthogonal distance regression analysis between methane and select compounds. The percentage values depict the molar emission ratios (rounded), most uncertain for NO_x. Standard OLS regression and determination coefficients are provided via dashed lines.

Lastly, of all species measured, methane showed the tightest correlation with ethane (**Figure 15**). The slope of the regression indicates an ethane to methane mass emissions ratio of 25%. Ethane is a selective tracer for raw oil and gas emissions, meaning it is emitted directly from UOGD without alteration by atmospheric chemistry, combustion processes, or contributions from nonfossil sources. The close ethane-methane correlation is another clear indication that the observed methane enhancements originated from oil and gas sources with negligible contributions from other potential methane sources such as landfills or dairy operations, which do not release ethane.

Somewhat surprisingly, methane correlated significantly with nearly all measured species, including NO_x (Figure 15). This is a strong indication that virtually all compounds measured were emitted from similar, and/or co-located with, sources in the oil and gas industry.

VOCs All VOC species measured at LNM showed significantly higher mole fractions than measured at the Colorado Front Range sites. Both medians and means, as well as peak values observed for ethane and other VOCs at LNM, were significantly higher. However, relative differences were dissimilar between VOC species. **Figure 16** shows a box-whisker comparison of ethane between LNM and the DJB sites. The highest ethane observations among the DJB sites occurred at ECC, where the maximum value during the campaign period was 92 ppb, which was lower than the mean value of 94 ppb at LNM.

Aside from elevated mixing ratios in plumes, ethane (and methane) emissions were also observed from the nearby gas flare on the well pad site to the southwest.

Figure 17 shows a similar comparison of benzene between LNM and the DJB sites. The median benzene level at LNM was slightly higher than the 95th percentile value at ECC,

Figure 16. Box-whisker plot comparing ethane at LNM to other sites in the Colorado Front Range. See Figure 7 for an explanation of the Colorado monitoring site three-letter codes.

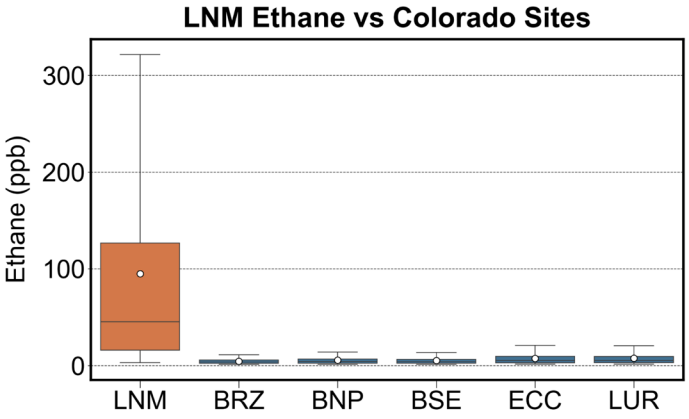

Figure 17. Box-whisker plot comparing benzene at LNM to other sites in the Colorado Front Range. See Figure 7 for an explanation of the Colorado monitoring site three-letter codes.

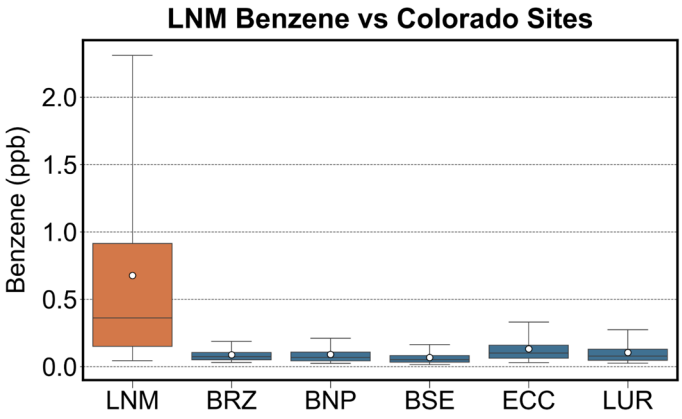

the DJB site with the highest recorded concentrations. In a broader context, analysis of 133 monitoring sites primarily in urban areas shows that typical ambient benzene concentrations range from 0.09 ppb to 0.39 ppb (10th to 90th percentiles; EPA, 2022). At LNM, measured concentrations were consistently above this level, with the 75th percentile reaching approximately 0.9 ppb, indicating significantly higher exposure than typical urban backgrounds. Additional comparisons are discussed below in the context of the passive sampling network data. Benzene is a known carcinogen with well-known health effects (ATSDR 2007; Bolden et al. 2015). As for other VOCs, the LNM site showed anomalously high levels of this pollutant compared to the DJB sites, with mean values at LNM approximately 5–15 times those in Colorado.

A common parameter investigated in connection with VOC emissions from UOGD activities is the isopentane to n-pentane ratio. While this ratio in urban areas is typically between 1.5 and 2 and dominated by emissions of processed petrochemical hydrocarbons (both evaporative and tailpipe) from traffic sources, upstream oil and gas production areas display ratios around one or less (Ghosh 2018; Gilman et al. 2013; Schade and Roest 2016). **Figure 18** shows the i-/n-pentane ratio as a function of binned wind directions for the LNM site data. Air transport from all directions carries a characteristic oil and gas signature. The isomeric pentane ratio shows a weak directional dependency, with relatively lower values (median of ~0.9) observed in air transported from the south, and progressively higher values transported in winds originating from the east and west, and lowest values from the north. This suggests that air originating from the south has been influenced generally more strongly by oil and gas emissions than air transported from the north.

Carbon Monoxide **Figure 19** shows the full time series record of carbon monoxide (CO) at the LNM site. The data collected at LNM showed that values stayed below 200 ppb approximately 75% of the time. In the 1-minute data, there were two instances when CO briefly exceeded 5 ppm, which were both during May 2024 (y-axis capped at 3,000 ppb to provide detail). The highest short-term peak value observed during the campaign was 10.4 ppm. The CO NAAQS is 9 ppm for an 8-hour average and 35 ppm for a 1-hour average. All LNM CO data remained below these CO threshold values.

CO showed a diurnal cycle similar to the hydrocarbons, with approximately 50% higher values in the early mornings compared to mid-afternoons. This suggests that CO emissions, a marker of incomplete combustion, continue at night, likely due to contributions from both gas flare and diesel compressor engine emissions.

Sulfur Compounds Sulfur dioxide mixing ratios stayed far below the SO_2 primary NAAQS of 75 ppb for all hourly averaged data and far below (0.4 ppb) the secondary standard of 10 ppb annually. Sulfur dioxide ranged between 0 and 13 ppb. It only exceeded 6 ppb a total of 20 times, most of which occurred between October 2023 and April 2024. Hydrogen sulfide was more variable, with maximum mixing ratios and order of magnitude above background levels. Elevated levels of 30–80 ppb appeared as transient spikes lasting only a few minutes. In total, there were 26 occurrences of hydrogen sulfide exceeding 10 ppb and 7 occurrences of it exceeding 20 ppb at LNM. In comparison, the highest value observed at the Broomfield site in the Colorado Front Range was 3.7 ppb. The odor threshold for H_2S is approximately 8 ppb for sensitive people. Consequently, during the 1-year observation window, there were several periods when this threshold value was exceeded and caused odors that were noticeable to citizens.

Figure 20 shows a bivariate polar plot analysis of summer 2023 data for hydrogen sulfide and sulfur dioxide. The highest median values of hydrogen sulfide were observed from a relatively narrow and well-defined sector, with northwesterly winds <5 m s^{-1} and east–northeasterly winds >8 m s^{-1}. Under these wind conditions, hydrogen sulfide concentrations were

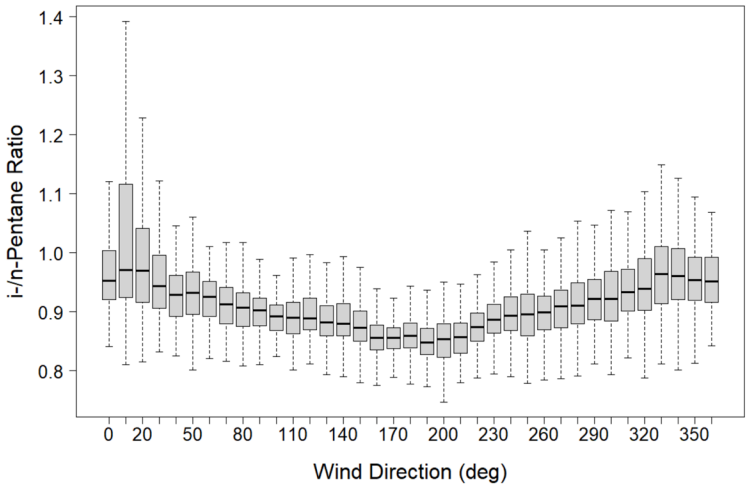

Figure 18. Wind direction binned i-/n-pentane ratio for the complete measurement period at the LNM site (mean = 0.9, outliers omitted from graph). Fewer than 1% of the data showed values exceeding a ratio of 1.5.

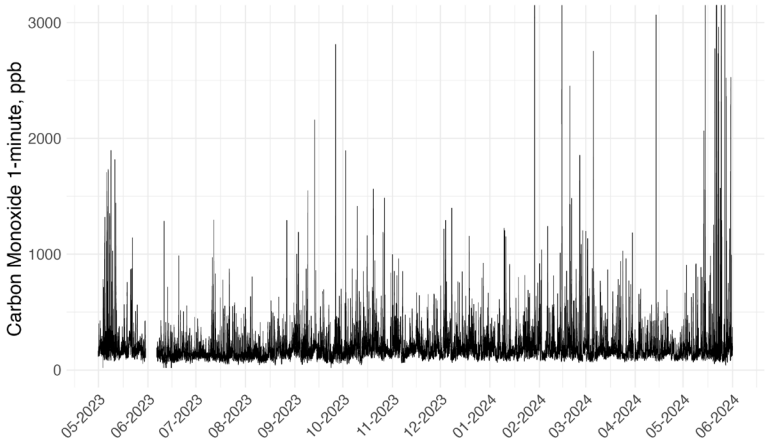

Figure 19. Carbon monoxide time series for the complete measurement period at the LNM site (y-axis capped to provide detail).

elevated about 4–5 times above background levels associated with westerly winds. The sulfur dioxide bivariate polar plot shows a similar signal of enhancement from northwesterly wind directions between 2–6 m s^{-1}, with median values of approximately 0.5 ppb compared to background values of 0.2 ppb for all other wind directions and speeds.

Ozone and Nitrogen Oxides Lastly, we consider ozone and its nitrogen oxides precursor. During the 2023 ozone season, there were 17 days when the maximum daily 8-hour average ozone (MDA8 O_3) exceeded 75 ppb, and an additional 14 days when it exceeded 70 ppb (**Table 3**). An area will exceed NAAQS if the 4th highest maximum daily 8-hour concentration each year, averaged over 3 years, is greater than 70 ppb.* The time series record of ozone (**Figure 21**) shows a long ozone season, with short-term values exceeding 70 ppb from April until early November, and MDA8 O_3 above 70 ppb from May into September.

Hourly ozone at the LNM site was similar to New Mexico state's air monitor at the 5ZR site southwest of Carlsbad (Appendix A, Figure A1), which would be expected due to the secondary formation origin of atmospheric ozone, resulting in relatively smaller geographical gradients than those of their primary precursor emissions.

Figure 22 shows a comparison of nitrogen oxides between LNM and the Front Range sites and two large metropolitan areas in Texas. Higher values of NO_x were observed at LNM, although by a smaller margin than the hydrocarbons discussed above. This was not driven by the observed elevated mixing

*40 C.F.R. § 50, Appendix U (2025); *https://www.ecfr.gov/current/title-40/chapter-I/subchapter-C/part-50/appendix-Appendix%20U%20to%20Part%2050*.

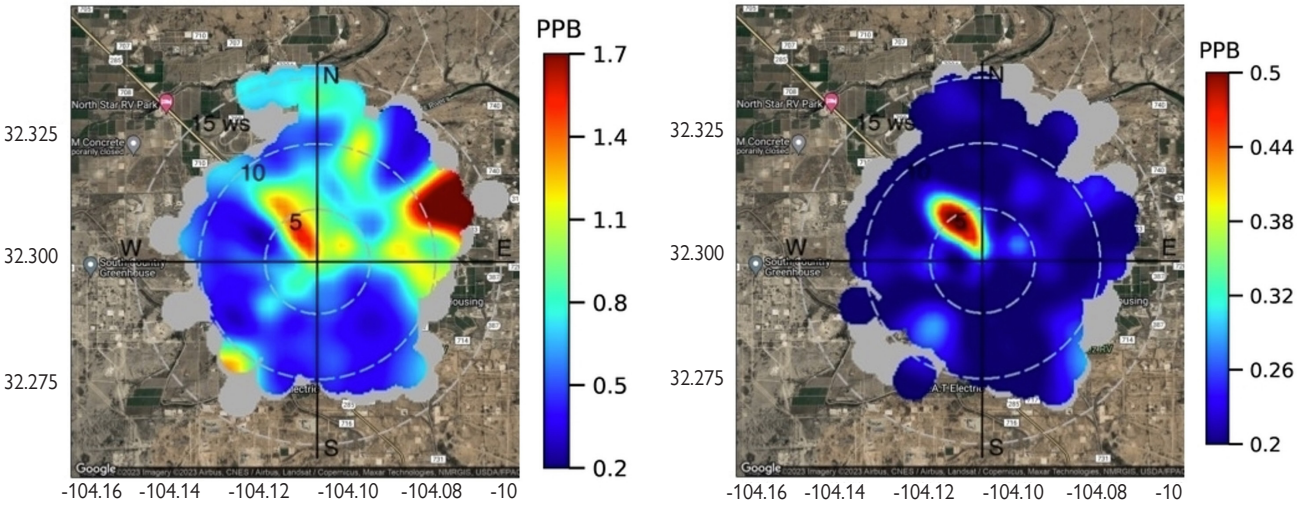

Figure 20. Bivariate plots of hydrogen sulfide (left) and sulfur dioxide (right) summer 2023 medians. Wind speeds are shown in m s–1.

Table 3. List of Monitoring Values and Dates During the 2023–2024 Campaign Year When Maximum Daily Average 8-Hour (MDA8) Ozone Exceeded 75 ppb and 70 ppb

Exceedance of 75 ppb		Additional Days with Exceedance of 70 ppb[a]	
MDA8 O_3	Date	MDA8 O_3	Date
87.1	August 31	75.8	May 9
86.7	September 9	75.7	May 12
84.3	August 30	75.7	August 15
82.1	August 27	75.6	August 8
81.6	September 17	74.0	May 16
79.7	July 23	73.5	May 24
78.9	September 3	72.9	August 4
78.6	May 1	72.6	May 21
77.9	August 26	72.0	August 6
77.8	September 6	71.8	July 14
77.7	August 7	71.7	July 10
77.7	June 6	71.3	August 25
77.3	September 15	71.2	September 2
77.2	September 10	71.0	July 3
76.6	May 2		
76.6	June 8		
76.0	July 4		
Total: 17 days		**Total: 31 days**	

MDA8 O_3 = maximum daily 8-hour average ozone; NAAQS = National Ambient Air Quality Standard; ppb = parts per billion.

[a]An area will exceed the 2015 National Ambient Air Quality Standard for ozone if the 4th highest maximum daily 8-hour concentration each year, averaged over 3 years, is greater than 70 ppb.

ratios of NO_x under southwest winds, with NO_x generated by the nearby gas flare. Eliminating those wind directions from the calculation only reduced the annual mean from 14.7 to 13.0 ppb and the median from 7.5 to 7.2 ppb NO_x. When a wind sector frequency-weighted mean of NO_x was selected, the polar plot (cf. Figure S1) in **Figure 23** shows directional impacts on NO_x also from the southeast to east sector, as well as the Highway 285 corridor, which extends toward the north–northwest and to the south–southeast from the LNM site (Figure 3, Figure 24).

Remarkably, NO_x levels in this region of New Mexico are higher than those in the Front Range and similar to large metro areas. The population density of Eddy County is only 5 people km^{-2}, whereas the population density of Denver, Colorado, is on the order of 1,800 people km^{-2}. Greater population density is associated with more vehicular traffic and power plants, which are major sources of NO_x in many regions (Lal and Patil 2001; Lu 2016). The high NO_x at LNM is indicative of a high number of sources and/or the strength of NO_x emissions in Eddy County.

Based on the directional analysis of the NO_x data, the high abundance of NO_x despite low population density, the correlation of NO_x with methane, and prior works (Dix et al. 2020; Francoeur et al. 2021; Dix et al. 2022), it is clear that UOGD activities contribute substantially to regional NO_x emissions and therefore to ozone formation. A PSCF analysis of ozone exceeding 70 ppb is shown in **Figure 24**. This graphic shows that the high ozone source region stretches deep into the Texas portion of the PB.

Radioactivity

The radioactivity data showed high variability, with values ranging from below the detection limit up to 173 Bq m^{-3} for gas-phase radioactivity and up to 99 Bq m^{-3} for particle-associated radioactivity. The two radioactivity measurements were strongly correlated, as shown in **Figure 25**. As in prior monitoring work (Helmig et al. 2024 and references therein), gas-phase radon radioactivity exceeded particle-phase radioactivity by approximately 50%. Particle-bound radioactivity represented approximately 31±19 % (1σ) of total radioactivity.

The total (sum of gas and particle phase) radioactivity exhibited strong diurnal variability (**Figure 26A**), with values reaching a minimum in the late afternoon (median ≈ 20 Bq m^{-3}) and a maximum in the early morning hours (median ≈ 40 Bq m^{-3}). The 95th percentile values were consistently 2–3 times the mean values throughout the day, again showing the highly variable nature of the observations. The data also exhibited seasonal variability (**Figure 26B**), with minimum values in June and July (median ≈ 20 Bq m^{-3}) and maximum values in November and December (median ≈ 35 Bq m^{-3}). These diurnal and annual cycles were driven largely by changes in atmospheric mixing, as solar heating during the summer months generates stronger turbulence in the lower atmosphere that helps to disperse pollutants, deepens the surface boundary layer, and dilutes surface emissions.

Bivariate polar plots for gas-phase, particle-associated, and total radioactivity are shown in **Figure 27A–C**. When winds were blowing from the west at >5 m s^{-1}, median gas-phase radioactivity of 5–10 Bq m^{-3} and particle-associated radioactivity of 2–4 Bq m^{-3} were observed, consistent with continental background radioactivity levels in air. However, northwesterly winds up to 5 m s^{-1} were associated with enhanced levels of both gas-phase (median ≈ 27 Bq m^{-3}) and particle-associated (median ≈ 11 Bq m^{-3}) radioactivity, which were approximately 3–5 times higher than the background levels. These figures comprise data over the entire campaign. Winter months showed higher median radioactivity values (>50 Bq m^{-3}) associated with northwesterly winds (not shown). When the radioactivity (gas to particle) ratio is plotted in the same manner (**Figure 27D**), both a north–south gradient and an elevated ratio toward the southwest are apparent. Higher

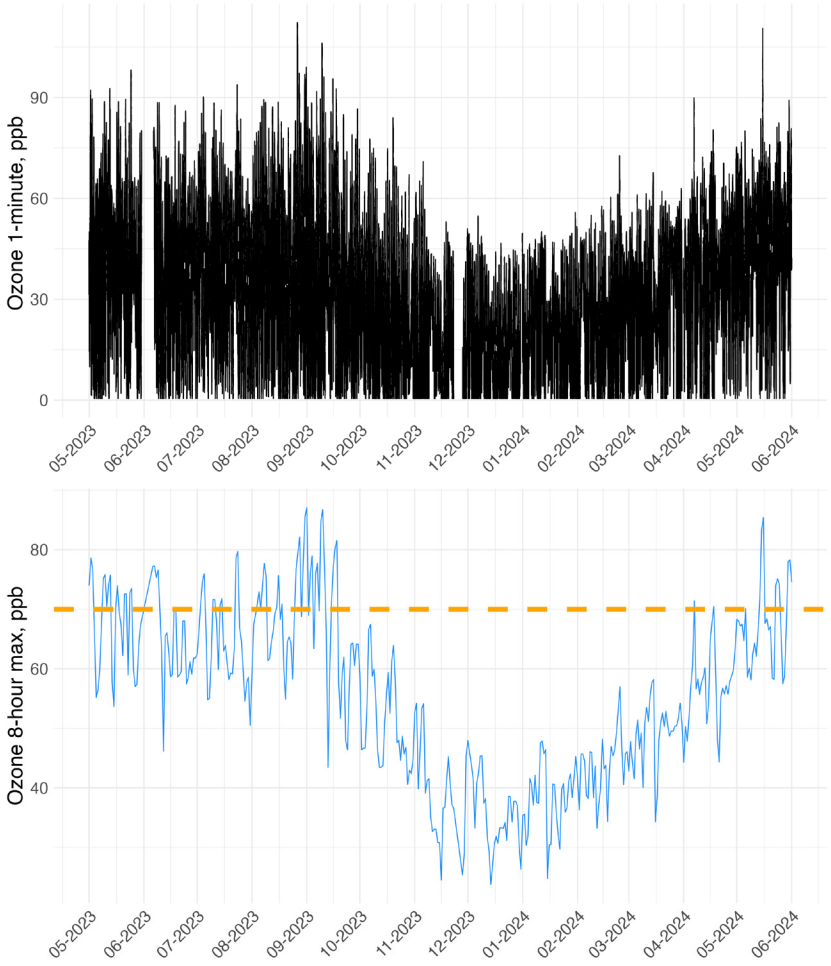

Figure 21. Time series plot showing the full ozone record at LNM, both 1-minute (top) and 8-hour maximum (bottom), with orange dashed line delineating 70 ppb. An area will exceed the National Ambient Air Quality Standard for ozone if the 4th highest maximum daily 8-hour concentration each year, averaged over 3 years, is greater than 70 ppb.

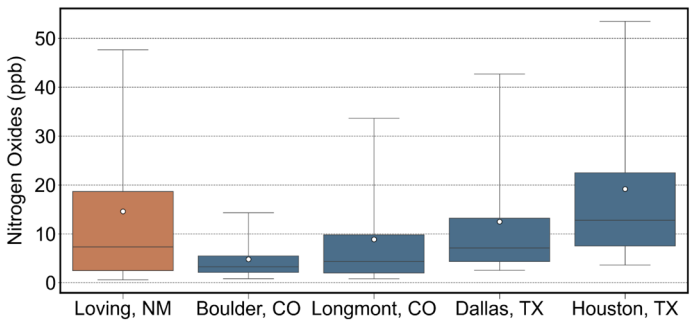

Figure 22. Box-whisker plot comparing LNM nitrogen oxides to other sites in the Colorado Front Range and Texas urban areas. Loving, Boulder, and Longmont data are from the campaign period (4/15/2023–5/31/2024); Dallas data are from 1/1/2023–12/31/2023, and Houston data are from 1/1/2022– 12/31/2022.

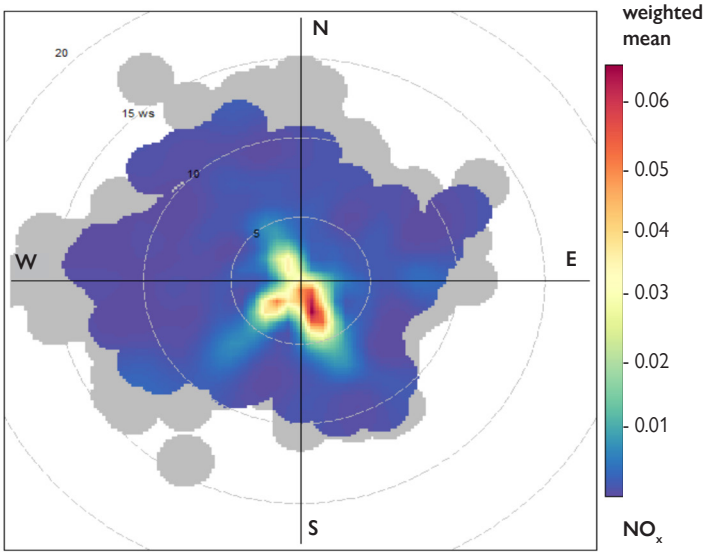

Figure 23. Weighted mean NO_x abundance by wind speed and wind direction, highlighting the three directions contributing most to elevated values across the complete measurement period at LNM.

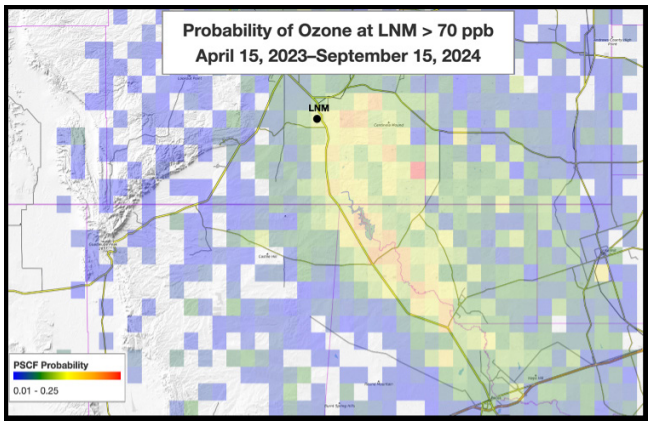

Figure 24. Potential Source Contribution Function (PSCF) analysis, accumulating 3-km resolution HRRR-based HYSPLIT back trajectories paired with ozone occurrences >70 ppb at LNM. Note that this corresponds favorably to the Residence Time Analysis by Pan and colleagues (2023).

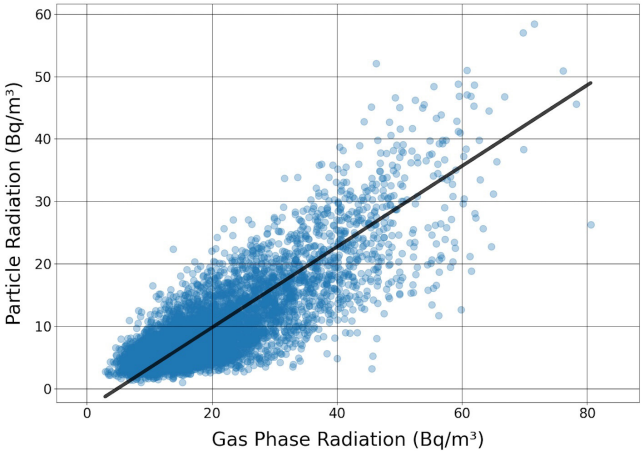

Figure 25. Correlation analysis between gas-phase and particle-associated radioactivity measured at LNM using 90-minute averages. The regression slope from the shown orthogonal distance regression was 0.65.

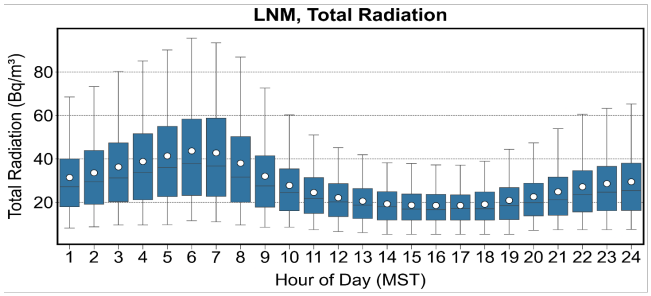

Figure 26A. Box plots of total radioactivity binned by hour of day. The boxes at each hour reflect the 25–75 percentile distribution of the measurements. The horizontal line indicates the median value, the white circle the mean, and the endpoints of the whiskers the 5th and 95th percentile values.

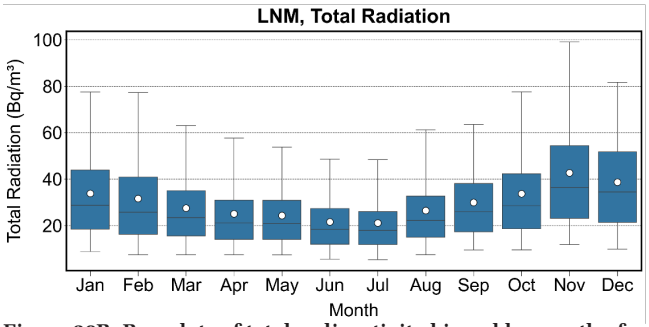

Figure 26B. Box plots of total radioactivity binned by month of year. Boxes as described in Figure 26A.

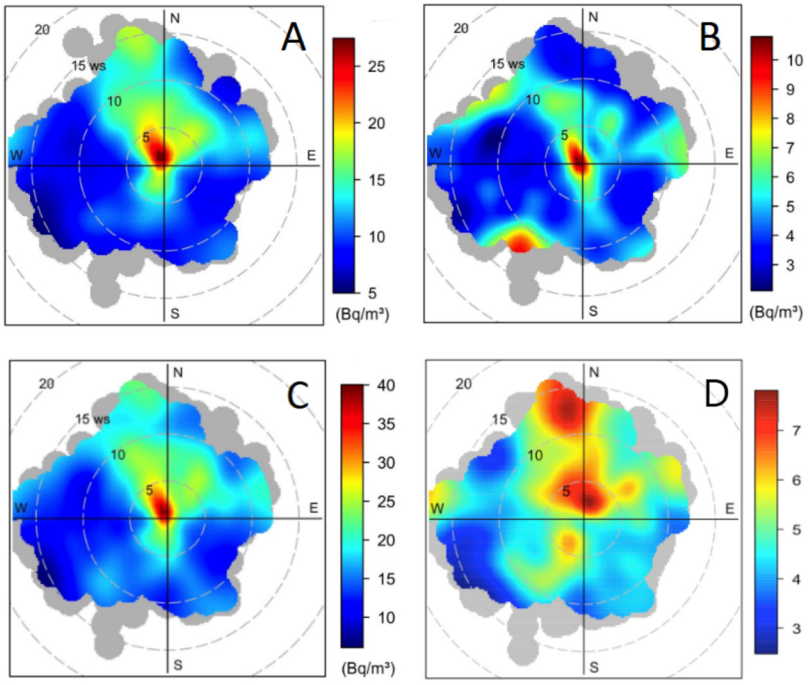

Figure 27. Bivariate plots of gas-phase radioactivity (A), particle-associated radioactivity (B), total radioactivity (C), and gas-phase to particle-associated radioactivity ratio (D) measured at LNM. Wind speeds are shown in m s–1. (A)–(C) use median values to color each bin while (D) uses the mean ratio values.

gas-phase radioactivity was associated with the direction of the small gas flare on the neighboring well pad and was more diffusely present from northern wind directions.

Observations of total radioactivity correlated with several petroleum hydrocarbons, as shown in **Figure 28**. Of the analyzed compounds, the most significant correlation was observed with methane (residual variance = 28%), followed by toluene and benzene (32%), then ethane (34%), n-hexane (36%), and acetylene (38%). Other compounds generally had lower correlation coefficients compared to the hydrocarbons, with nitrogen oxides (residual variance = 37%) showing the most significant correlation, followed by carbon monoxide (40%), hydrogen sulfide (47%), and sulfur dioxide (96%). The correlations with methane and ethane and the correlation with flaring occurrences (see below) may signify a contribution from regional oil and gas exploration sites; however, it is important to note that correlations may arise between two pollutants due to both being controlled by the atmospheric mixing state, rather than signifying a shared emission source.

Figure 29 shows a PSCF analysis, pairing the top 50% of data for total radioactivity observations with airflow trajectories. The highest density of computed back-trajectories was observed to the north–northwest of the site in a swath approximately 40 km long, 15 km wide, and centered around the city of Carlsbad, New Mexico, which generally has lower UOGD activity compared to areas south and east of the LNM site. The radioactivity PSCF results show geographical overlap with the results for methane (Figure 13), with both methane and radioactivity showing their highest contributing sources to the northwest and southeast direction of the LNM site location, albeit with a slightly higher contribution from the northwest sector for the radioactivity source.

Interestingly, this (northwest) swath overlaps with an area where radiometric equivalent uranium (eU) measurements in surface soil and rocks by an airborne gamma-ray detector (collected as part of the Department of Energy National Uranium Resource Evaluation (NURE) program of the 1970s and early 1980s) were found to be highest compared to nearby areas (USGS 1993). While these regionally elevated surface uranium occurrences in limestone are well documented, they are considered minor, and the US Geological Survey classified Eddy County as having a *moderate* radon index based on measurements in the Carlsbad area. The USGS report's "pixel density map" of surface equivalent uranium (page 106) does not allow for a straightforward quantification of regional differences.

Source Apportionment

The analytic dataset for NMF consisted of 27 compounds with 7,408 observations of complete hourly data over the May 2023 to June 2024 sampling period at LNM. We identified five source factors in our analysis, which explained 95% of the overall variance in the data. These factors, illustrated in **Figure 30**, represent different sources of emissions from UOGD.

Factor 1 represented fugitive and venting emissions and explained the highest marginal proportion of the variance (45%). It loaded on light alkanes (ethane, propane, butane), some higher alkanes (pentanes, hexanes, heptane), and methane, a signature typical of venting and leakage from oil and gas operations.

Factor 2 explained 39% of the total variance and was dominated by aromatics (BTEX) and octane, with smaller contributions from n-hexane, n-heptane, and radioactivity. These loadings suggested this factor represented handling, storage, and evaporation from produced water ponds (Lyman et al. 2018; Ma et al. 2024), where aromatic hydrocarbons partially partition into water and then volatilize into the atmosphere.

Factor 3 accounted for 10% of the variance and represented traffic as it expressed on internal combustion products ethene and propene, with contributions from incomplete combustion products CO_2, CO, acetylene, and some NO_x.

Factor 4 explained 9% of the variance and had a high loading of 1,3-butadiene coupled with ethene, propene, NO_x, and some acetylene, another signature of incomplete combustion that is likely attributed to flaring.

Finally, **Factor 5**, which represented 4% of the variance, was dominant in CO_2 and radioactivity, with contributions from sulfur compounds SO_2 and H_2S. This factor may reflect widespread combustion across the Permian basin and widespread soil respiration (CO_2) and radon emissions (Nazaroff 1992).

Examining the source factors by wind direction revealed further insights (**Figure 31**). First, we observed that the westerly wind directions (WSW 240 degrees to WNW 285 degrees) uniformly had very low factor expressions. This is the region's clean air sector, advecting air into the region from across the Rocky Mountains, including Carlsbad Caverns National Park, with little to no UOGD activity and no major roads. On the other hand, winds from the east, east-southeast, south, and south-southeast (90 to 180 degrees) brought air from the central UOGD production areas in the Permian basin. Under these conditions, we saw expressions in oil and gas fugitive emissions (Factor 1), produced water (Factor 2), as well as gas flaring (Factor 4) that coincided with the highest density of flares east of the LNM site (Figure 5). We also observed that the flaring factor showed elevated expression in the northwest (300–340 degrees), where there was distant flaring closer to Carlsbad. Interestingly, the general combustion source (Factor 5) had a nearly flat pattern by wind directions, suggesting a ubiquitous source of emissions. Lastly, the traffic factor (Factor 3) was expressed along the main traffic corridor — to the east and east-southeast around 100–130 degrees where US Route 285 is just 350 m from LNM and the city of Loving is 1–2 km distant, and to the north-northwest around 300–340 degrees where US Route 285 continues north to the city of Carlsbad.

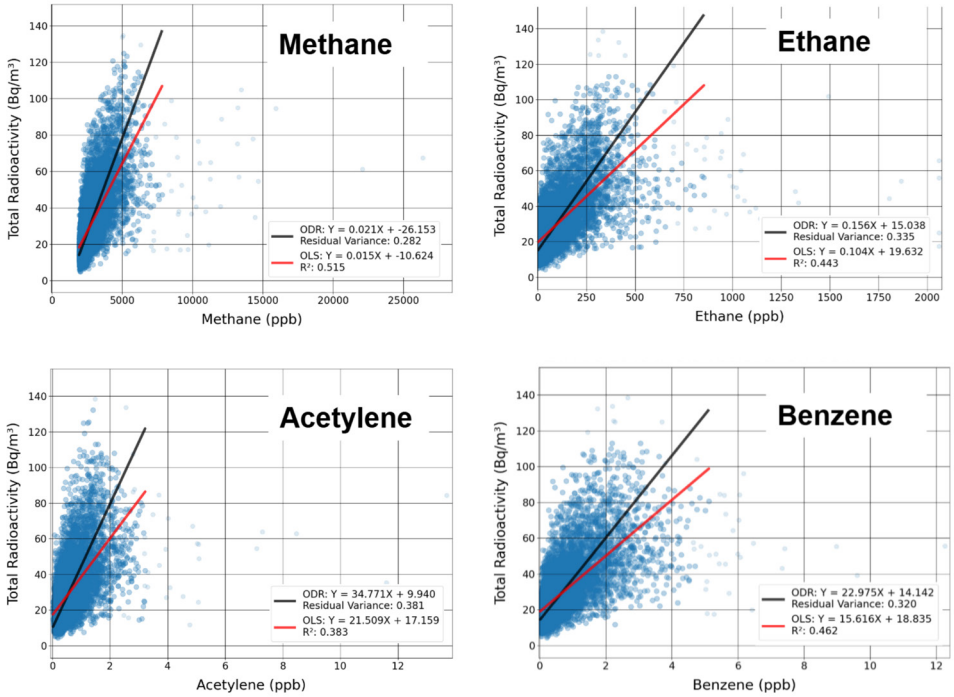

Figure 28. Correlation between total radioactivity and methane, ethane, acetylene, and benzene, using both ordinary least squares (OLS) and orthogonal distance regression (ODR) analyses.

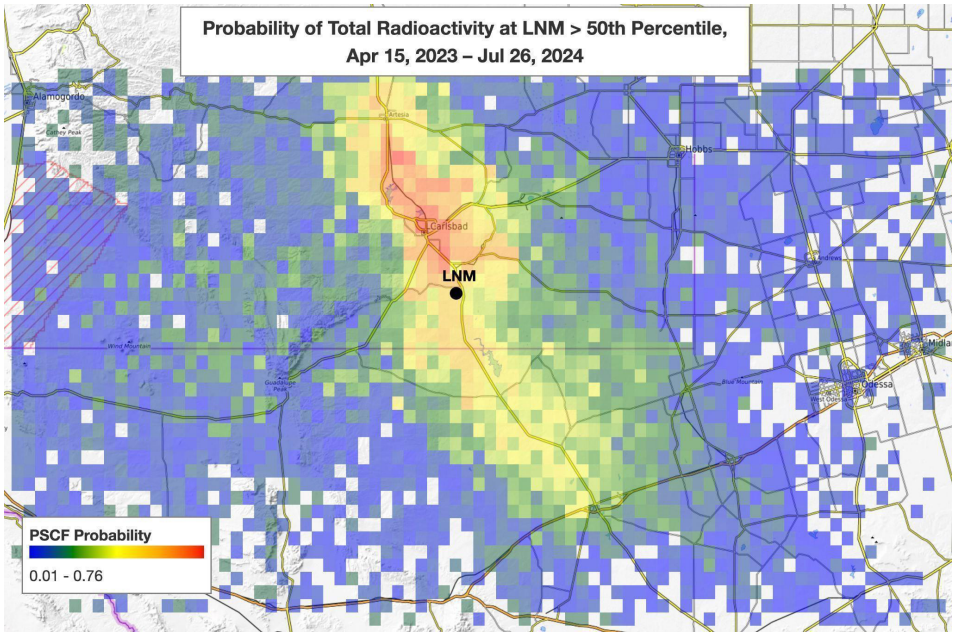

Figure 29. Potential Source Contribution Function (PSCF) analysis, using 3-km-resolution HRRR-based HYSPLIT back trajectories paired with total radioactivity measured above the 50th percentile at the LNM site.

A fingerprint plot (**Figure 32**) illustrates the relative proportions of each compound contributing to the five factors. We observed that the oil and gas fugitive/venting emissions factor, which explained the single largest source of the total variance in the data, consisted of 60 to 80% of the short-chained alkanes (C2–C6), methane, and, to a lesser extent, heavier alkanes. The produced water factor also contributed to the higher alkanes (>C6) and BTEX, consistent with volatilization from stored water. Traffic contributed significantly to ethene and propene, and contributed to CO, acetylene, benzene, and NO_x, typical of internal combustion exhaust. Flaring enhanced alkenes, especially 1,3-butadiene, as well as NO_x, and to a lesser extent, CO and the sulfur compounds. The combustion/respiration factor dominated CO_2 and the sulfur compounds, as well as radioactivity. This could reflect stationary fossil fuel combustion in the area, including from gas turbine engines, and because both CO_2 and radon are also naturally emitted from soils, these processes likely contribute to this factor. However, it is hard to quantify this from our data.

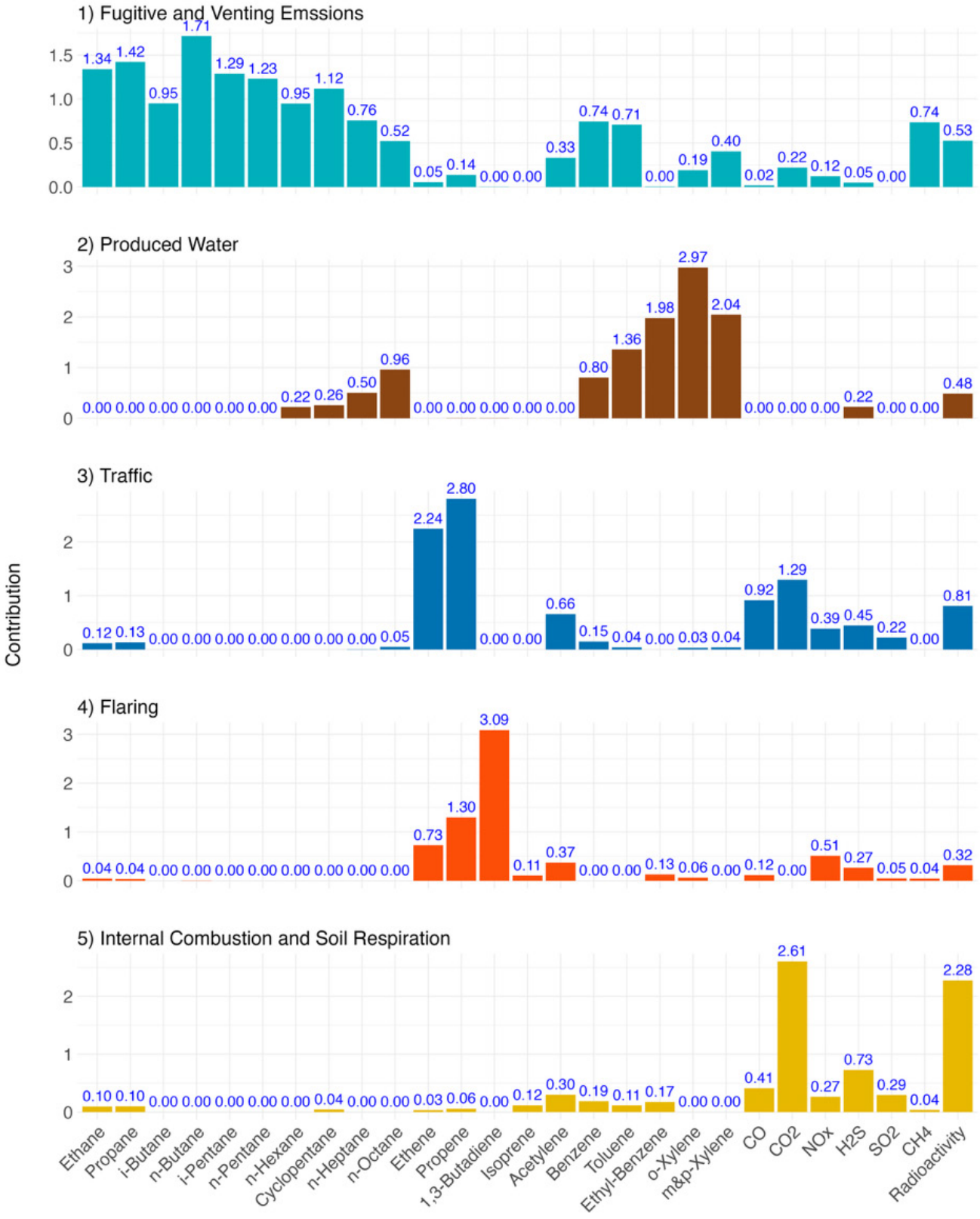

Figure 30. Non-negative matrix factorization source profiles showing component contributions to each factor.

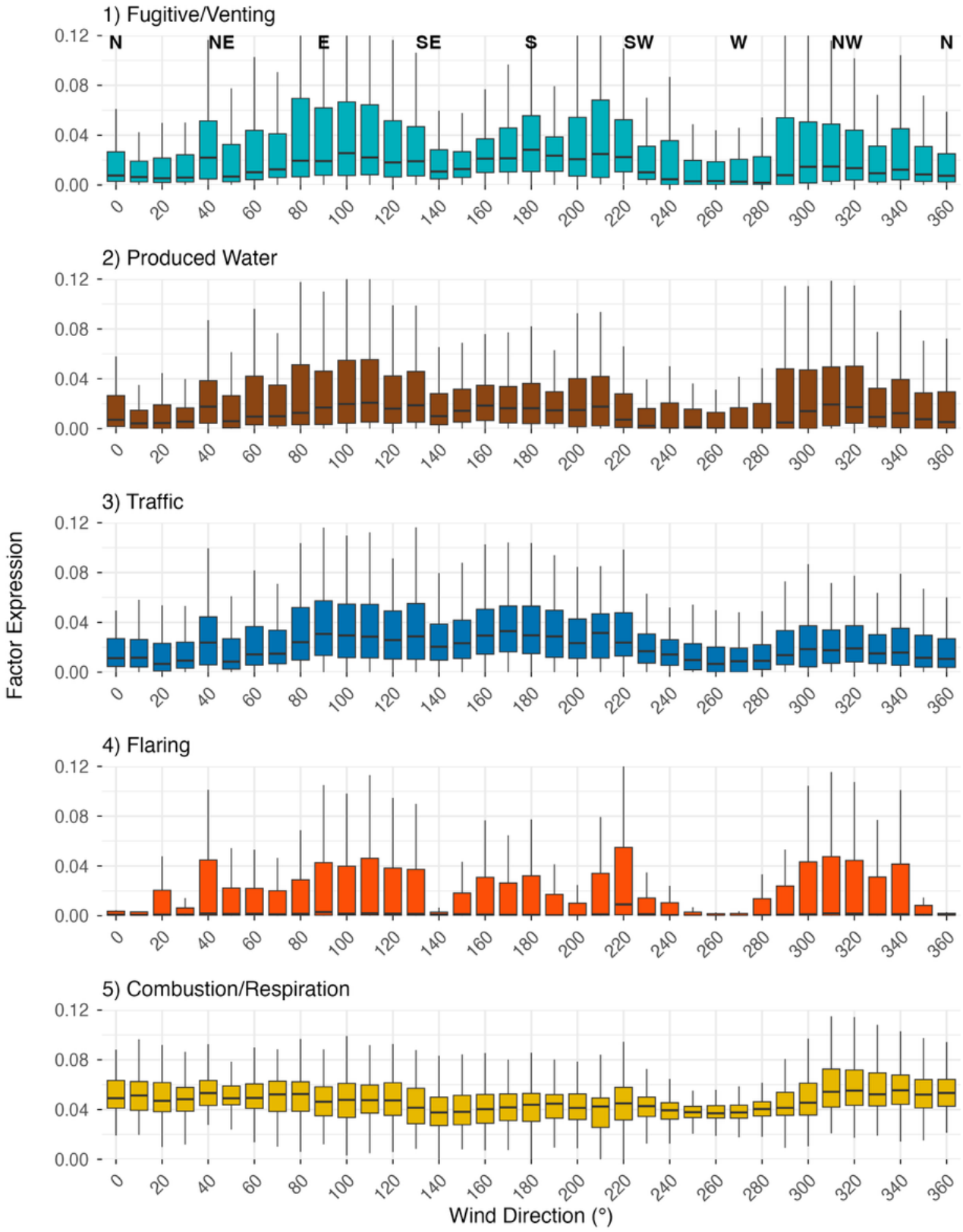

Figure 31. NMF loadings binned by wind directions for all five factors derived from LNM measurements.

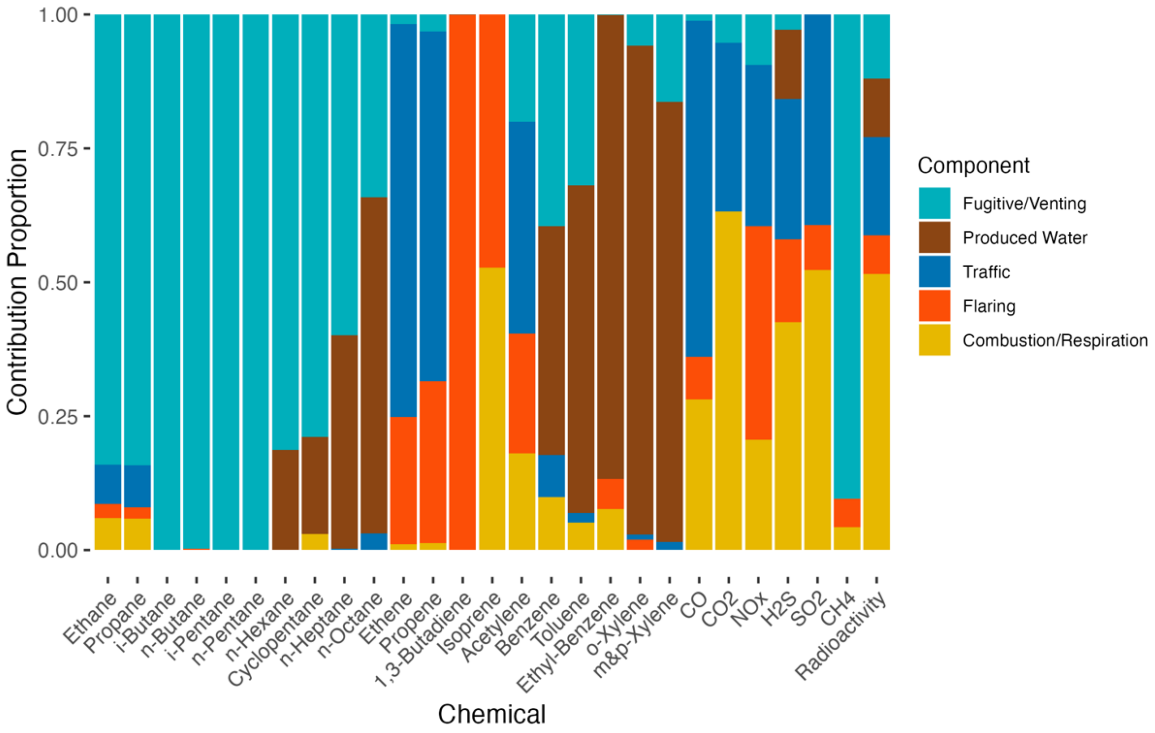

Figure 32. Contribution proportions of each compound to the five NMF-derived source factors at LNM.

Noise Frequency Analysis

There were over 300,000 1-minute observations of A- and C-weighted sound levels (LAeq, LCeq, LAFmax, LAFmin, LCpeak) and individual ⅓ octave band sound frequencies (LZeq 12.5 Hz through LZeq 16 kHz). We created a merged dataset with NO_2, CO_2, CO, CH_4, H_2S, SO_2, O_3, and meteorology (wind direction, wind speed, temperature, relative humidity, atmospheric pressure). Summary tables of the 1-minute data in the merged dataset are shown in Appendix A, Tables A1 through A3. Mean and median LAeq levels (which emphasize mid-frequencies) were about 60 dB, while LCeq (which includes low frequencies) were 70 dB. Peaks in the C-weighted levels topped 133 dB, suggesting the dominance of low-frequency sound at LNM (**Figure 33**). The noted shift in sound levels from April to June 2023 was a result of moving the instrument to a higher elevation on the tower. We removed the earlier data (April 2023 through June 2023) to ensure consistency in the analyses.

Medians and interquartile ranges of the sound levels at each frequency separated by day and night (day: 11:00 to 17:59, night: 18:00 to 10:59 Mountain Time) further illustrate the dominance of lower frequencies and greater variability at frequencies below 125 Hz (**Figure 34**). We observed daytime peaks in lower frequencies that exceeded nighttime values. At middle and high frequencies, there was very little difference in the day and night medians, except at 12 kHz and 16 kHz, where we observed slightly higher levels and greater variability during daytime.

Spectrograms over different lengths of time further illustrate the dominance and periodicity of lower frequency amplitudes at LNM. There was far more temporal variability in the lower frequencies as well, suggesting multiple UOGD processes contributing to this range. In the long-term plot (**Figure 35A**) we noted variability in the frequencies between 12.5 Hz and 100 Hz, changing to an on-and-off pattern at 125 Hz and then a near complete lack of variability at 160 Hz. The cycling pattern at 125 Hz may be due to the AC unit on the trailer, which would be nearly constantly ON during warm months but ON and OFF when temperatures drop at night. Zooming into the 1-month and 1-week plots in September 2023 (**Figure 35B and C**), we see this pattern more distinctly.

The 4-month-long time series shows some fluctuations in middle frequencies around 500 Hz–1.6 kHz, which could be related to truck engine noise from nearby US Route 285. High frequencies from 2 to 16 kHz were very intermittent, possibly only occurring from the nearby flare SW of the trailer or due to sirens.

The 1-day spectrogram (**Figure 35D**) shows the highest intensity at low frequencies occurring at various times of the day, with a peak in late afternoon. Spearman correlations between the frequencies showed clustering of high correlations within groups of frequencies 1.2–16 kHz (high), 8–10 kHz (high), 160–800 Hz, and 12.5–20 Hz (low), and 25–80 Hz (low-mid) (**Figure 36**). LZeq at 125 Hz stood out as it was not in a correlation cluster with any other frequencies.

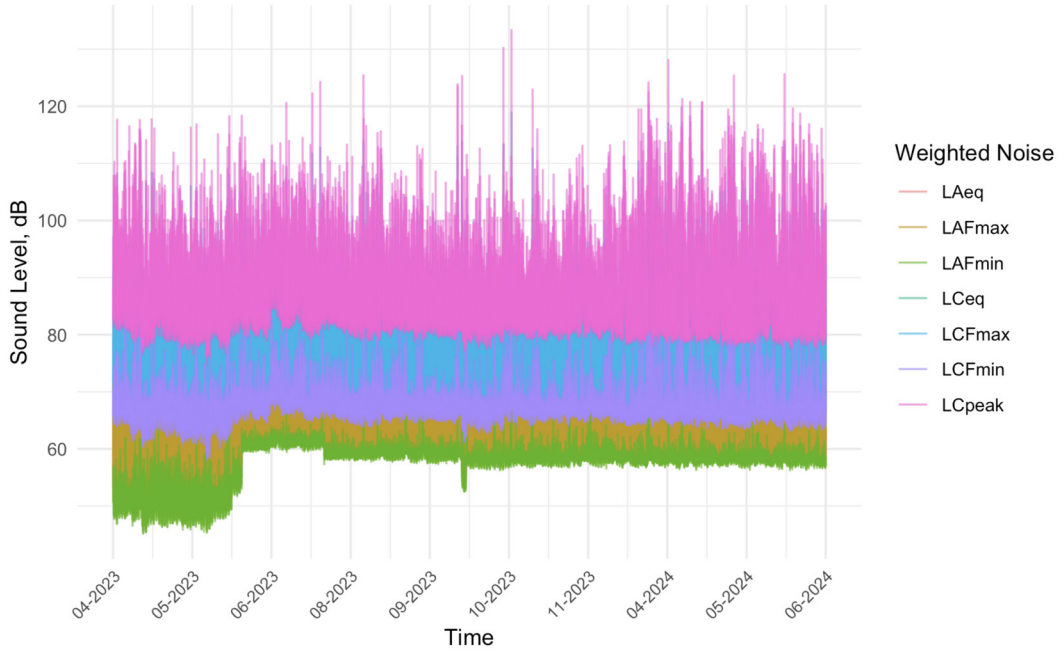

Figure 33. Time series of A- and C-weighted noise measured at LNM showing the dominance of low frequencies in LCpeak, which have highest levels. The jump in frequencies in the time series in June 2023 was due to moving the instrument up higher on the tower, and a gap between November 2023 to March 2024 due to an instrument issue (gap removed from plot).

A 4-factor NMF explained 90% of the overall variance in the LZeq frequencies (**Figure 36**). Factor 1 loaded on a range of some low but mostly mid-to-high frequencies, likely capturing general industrial operational noise. Factor 2, the most important contributor, dominates in the low-frequency range, characteristic of gas compressors, pumps, and vibrations from diesel-powered equipment. Factor 3 is weighted in the low-to-mid frequencies, likely reflecting transportation sources or episodic activities from fracturing stages or maintenance. Factor 4 loads on a mix of low and high frequencies. This could also reflect short-term mechanical sources from high-pressure gas venting.

The XGB models that associated noise with major gas components measured at 1-minute resolution at LNM were fit on two different sets of predictors: 1) all individual LZeq frequencies, and weighted measures LCpeak, LCeq, LAFmax, and LAFmin, and 2) the 4 NMF factors and weighted measures LCpeak, LCeq, LAFmax, and LAFmin. Overall, they performed similarly in terms of test R^2 and RMSE, and the top 10 variables highlighted the role of meteorology as important predictors, particularly pressure, temperature, and winds (**Table 4**).

The best performing models were for CO_2 (R^2 = 0.91–0.94), followed by NO_2, CH_4, H_2S, NO_x, SO_2, and CO. In the models with the full frequency set, the most important noise variables included LCpeak, LAFmax, LAFmin, LCeq, LZeq 12.5 Hz, and meteorology (temperature, pressure, wind, humidity). The uniform importance of LCpeak across pollutants suggests that instantaneous sound peaks, particularly in low frequencies corresponding to compressors, venting, and pumps, were strong predictors of emissions.

In the models with the NMF noise factors, Factors 2 and 4 were frequently top-ranked, suggesting again that low-frequency noise (Factor 2) and episodic high-frequency noise (Factor 4) are general indicators of emissions across pollutants. However, meteorology was consistently ranked as the best predictor variable, above the sound factors.

We found distinguishing features for each pollutant. NO_2 and NO_x were always better predicted with the full frequency set that included a differenced LZeq 25 Hz – LZeq 12 kHz, likely capturing more detailed engine/exhaust profiles and different combustion types (notably NO_x had similar contribution to the combustion and flare factors, Figure 30). On the other hand, CH_4 performed better with the NMF factors as predictors, particularly Factor 2, which had dominant loadings on 12.5–160 Hz, a broad low-frequency pattern signature of venting and flowback operations, leaks, and fugitive emissions from compressors. CO_2, the best-performing model, was well predicted by both model approaches, likely because it is a well-mixed background pollutant associated with combustion and not prone to sharp spatial or temporal spikes like CH_4. The dominance of low-frequency 12.5 Hz (and Factors 2, 4) suggests a source related to compressors, which have combustion as well as venting, especially in midstream operations.

PASSIVE SAMPLING

Spatial and Temporal Trends in Permian Basin (PB), Comparisons to TCEQ Data from Large Cities in Texas

Total measured hydrocarbon mole fractions (tracking 15 compounds) from passively collected samples ranged from 1.1 to 43.3 ppb in the PB; n-hexane and 2-methyl-pentane exhibited the highest concentrations and the highest variability, while ethylbenzene and the xylenes were detected at the

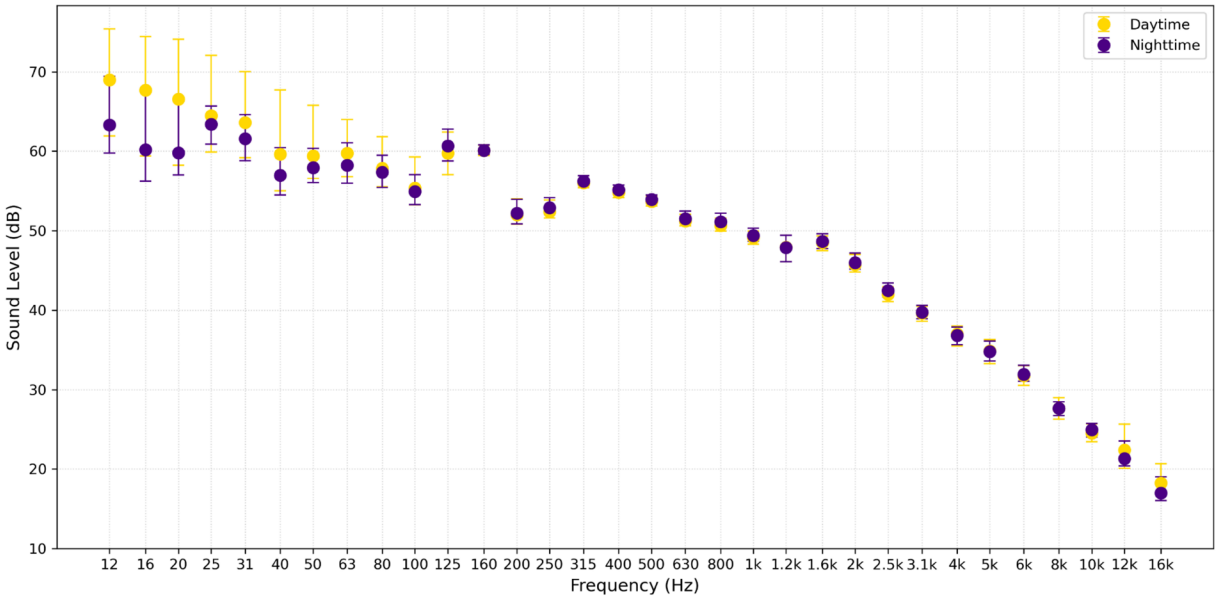

Figure 34. Median sound levels (dB) measured at LNM separated by ⅓ octave band frequency (Hz) and by day and night with error bars representing the interquartile range (25th percentile to 75th percentile).

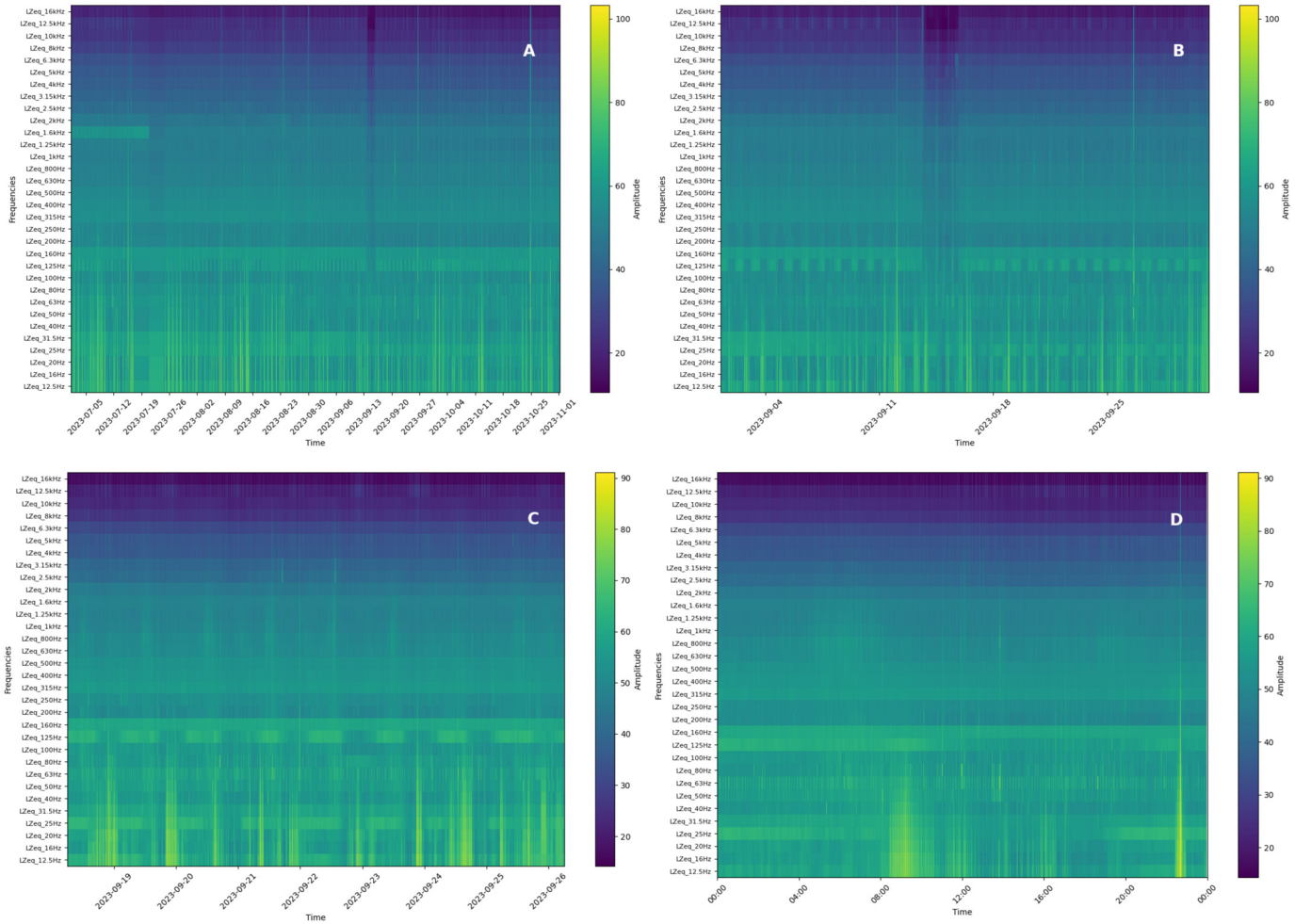

Figure 35. Spectrograms of ⅓ octave bands measured at LNM (A) 4 months, July through October, 2023; (B) 1 month, September, 2023; (C) 1 week, September 18–25, 2023, and (D) 1 day, September 20, 2023.

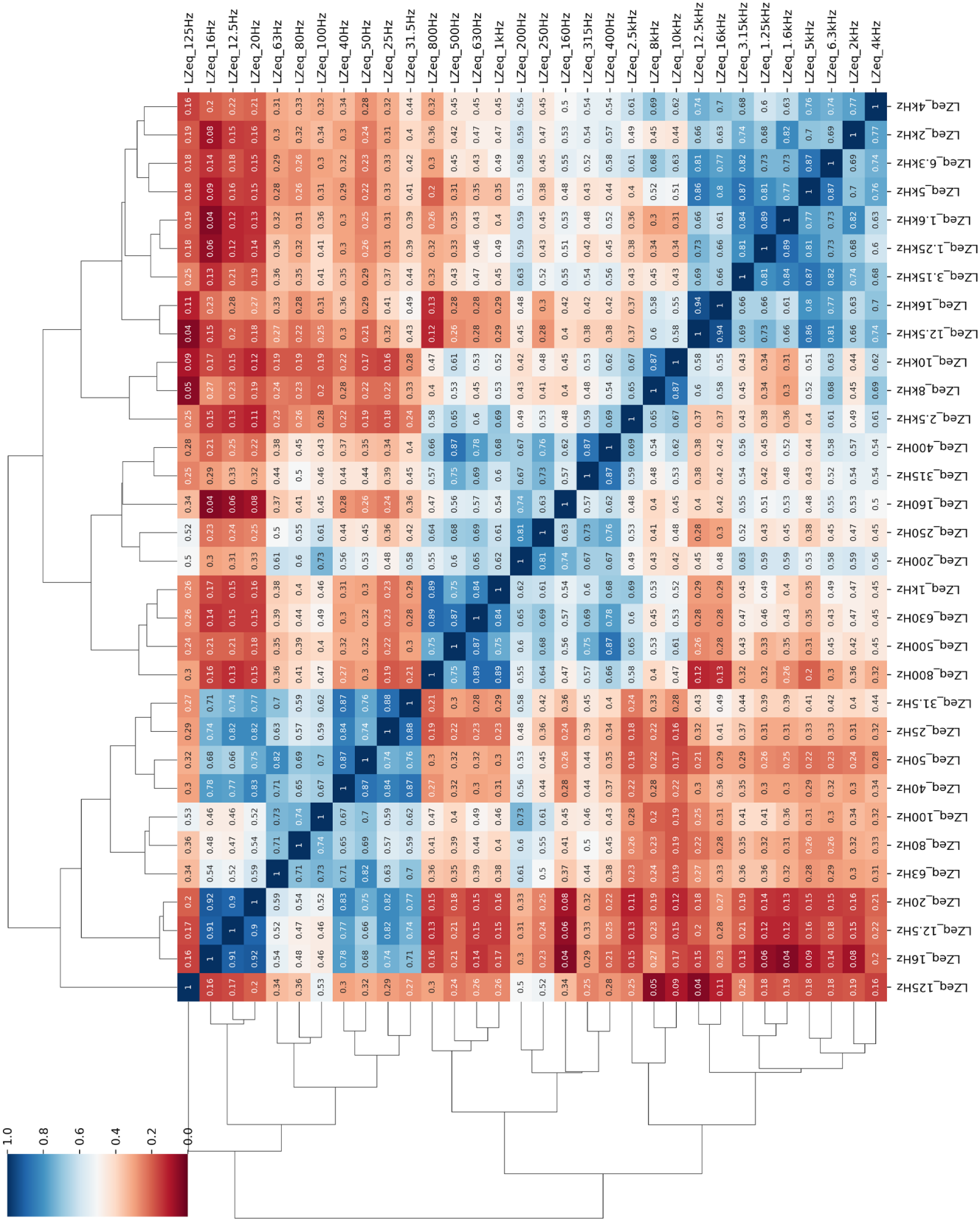

Figure 36. Above: Spearman correlation heatmap with hierarchical clustering of noise frequencies; next page: Non-negative matrix factorization source profiles of the sound data showing frequency contributions to each factor.

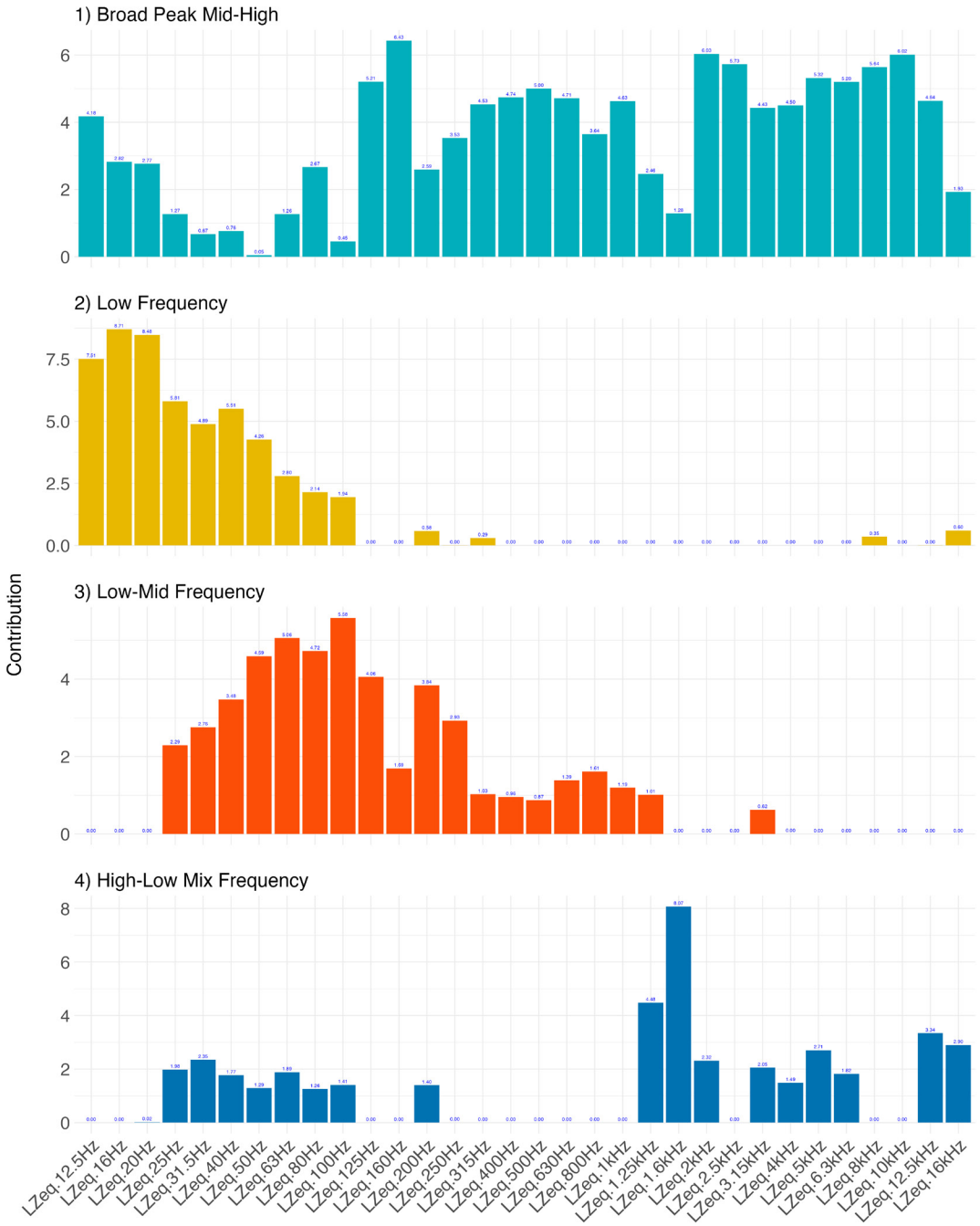

Figure 36. *(continued)*

lowest mole fractions. Statistics are summarized in Table B1 in the Appendix. Here, we focus on selected hydrocarbons with higher abundances and/or toxicity.

Most hydrocarbons measured in our passive sampling network were highly correlated with each other. A matrix of regression coefficients is included in the Appendix. **Figure 37** shows an example correlation between n-hexane, toluene, and methylcyclohexane across all sites and samples, illustrating that toluene showed a weaker correlation with saturated hydrocarbons, which dominated local abundances at all sites.

An exemplary spatial distribution of a typical oil-production related hydrocarbon, the naphthene methylcyclohexane, is shown in **Figure 38**. Bubbles and their shade indicate the average local abundance of the plotted compound, indicating general concentration gradients dropping from south to north and east to west. Such gradients correlate spatially with the

Table 4. XGB Results from Noise Frequencies and a 4-Source NMF on Select UOGD Pollutants Measured at 1-Minute Intervals at LNM

Pollutant	Test R^2 (RMSE) Full Set[a]	Test R^2 (RMSE) NMF Set[a]	Top 10 Important Variables in the Full Set (ordered)	Top 10 Important Variables in the NMF Set (ordered)
CH_4	0.66 (589.38)	0.71 (538.80)	LCpeak, Atmospheric Pressure, Temperature, LAFmax, LCeq, Wind Direction, LAFmin, Wind Speed, LZeq 12.5Hz, Relative Humidity	Temperature, Atmospheric Pressure, Wind Direction, Relative Humidity, Factor2, Factor4, Factor1, LAFmin, Wind Speed, LCeq
CO	0.58 (70.62)	0.54 (71.58)	LCpeak, Atmospheric Pressure, Temperature, Relative Humidity, Wind Direction, LAFmin, Wind Speed, LZeq 12.5Hz, LCeq, LAFmax	Temperature, Atmospheric Pressure, Wind Direction, Relative Humidity, Factor4, Factor2, Wind Speed, LAFmin, Factor1, Factor3
CO_2	0.94 (2.34)	0.91 (2.81)	LCpeak, Atmospheric Pressure, Temperature, Relative Humidity, Wind Direction, LAFmax, LAFmin, LCeq, Wind Speed, LZeq 12.5Hz	Temperature, Atmospheric Pressure, Relative Humidity, Wind Direction, Factor2, Factor4, Wind Speed, LAFmin, Factor1, LCeq
NO_2	0.81 (4.15)	0.79 (4.33)	LCpeak, Atmospheric Pressure, LAFmax, Wind Direction, Temperature, LCeq, LAFmin, Relative Humidity, LZeq 12.5Hz, LZeq 25-2 kHz difference	Temperature, Atmospheric Pressure, Wind Direction, Relative Humidity, Wind Speed, Factor2, Factor4, Factor1, LAFmin, Factor3
NO_x	0.65 (14.75)	0.57 (15.61)	LCpeak, Wind Direction, LAFmax, LCeq, Atmospheric Pressure, LAFmin, Temperature, Wind Speed, LZeq 12.5Hz, LZeq 25-2 kHz difference	Temperature, Wind Direction, Atmospheric Pressure, Relative Humidity, Wind Speed, Factor2, Factor4, LAFmin, Factor3, Factor1
H_2S	0.51 (0.80)	0.66 (0.56)	LCpeak, LAFmax, LAFmin, LCeq, Atmospheric Pressure, Wind Direction, Temperature, LZeq 25-2 kHz difference, LZeq 125Hz, Wind Speed	Temperature, Atmospheric Pressure, Wind Direction, Relative Humidity, Factor4, Wind Speed, LAFmin, Factor2, Factor3, Factor1
SO_2	0.62 (0.33)	0.59 (0.33)	LCpeak, Atmospheric Pressure, Temperature, Relative Humidity, LAFmax, LAFmin, Wind Direction, LCeq, LZeq 125Hz, Wind Speed	Atmospheric Pressure, Temperature, Relative Humidity, Wind Direction, Factor4, LAFmin, Wind Speed, Factor3, Factor2, Factor1

LNM = Loving, New Mexico; NMF = non-negative matrix factorization; ppb = parts per billion; ppm = parts per million; RMSE = root mean square error; UOGD = unconventional oil and gas development; XGB = extreme gradient boosting.

[a] Modeling approach with higher R^2 in **bold.**

area's density of oil and gas production well sites (Figure 5), which increases toward the southeast of urban Carlsbad along Highway 285.

The seasonal changes to the local hydrocarbon concentrations are illustrated in **Figure 39** for the aromatic compound, and air toxic, benzene. Benzene is emitted both at hydrocarbon production sites, including from gas flares, and in tailpipe emissions from on-road vehicles. Consequently, sources are both evaporative and combustion-related. Our results show higher values during fall and winter periods and lower values during spring and summer periods. This is largely driven by seasonality in atmospheric dynamics, providing deeper, more turbulent atmospheric boundary layers (BLs) and stronger dilution of surface emissions in spring and summer, and more shallow boundary layers with weaker dilution in fall and winter. Therefore, even under seasonally unchanging emissions, their accumulation into shallower BLs causes higher concentrations. In this example, winter to summer abundance ratios of approximately 5 ± 2 (and similar ratios for other hydrocarbons) suggest strong regional BL dynamics alongside seasonally reduced atmospheric removal rates,

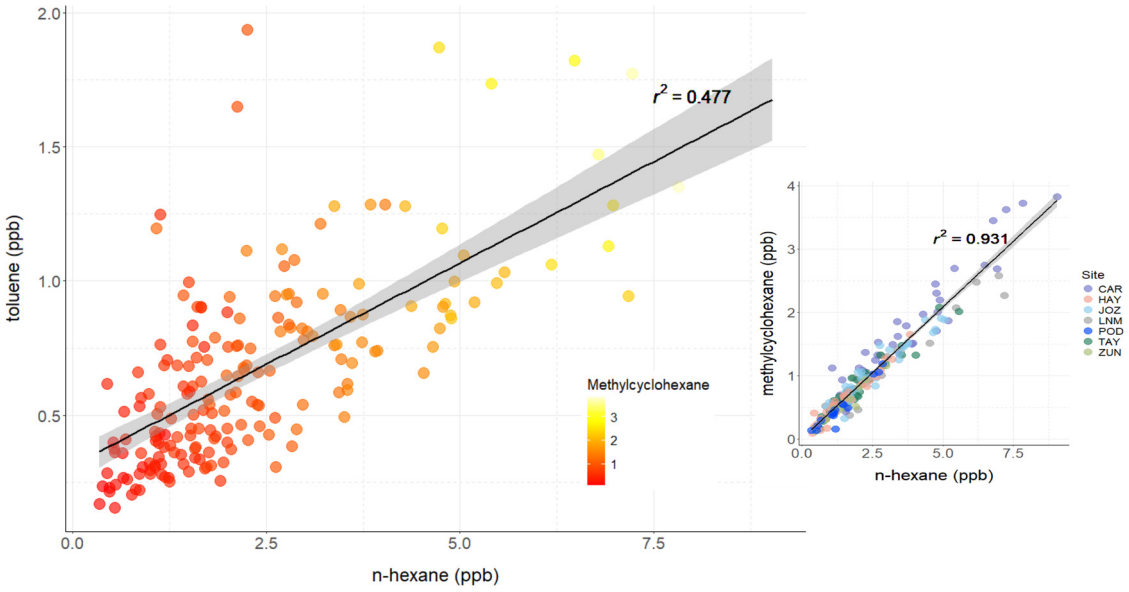

Figure 37. Correlations between passive samples of n-hexane and toluene (main graph; color-coded by methylcyclohexane abundance), and n-hexane and methylcyclohexane (inset; color-coded by network site) across the seven passive monitoring sites in the Permian Basin demonstrating lower correlation between toluene and n-hexane. Trend lines represent linear regressions, including 95% prediction intervals. A correlation matrix is included in the Appendix.

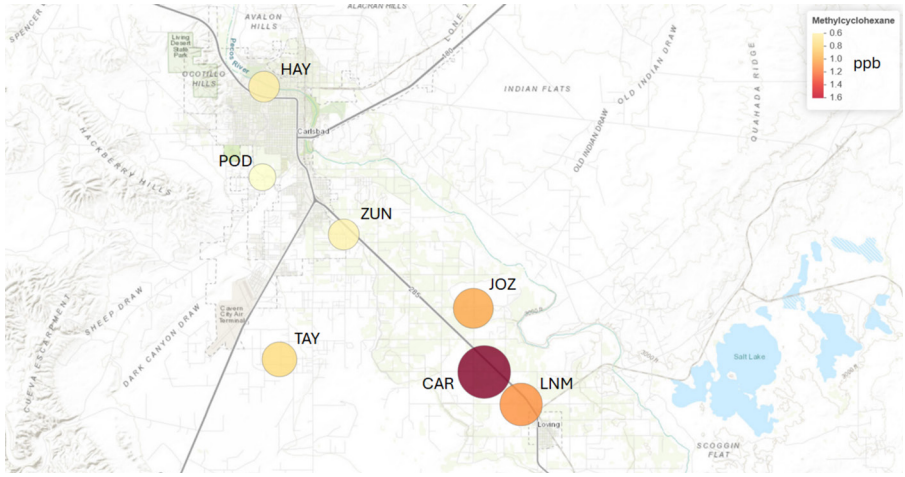

Figure 38. Average annual (or biannual in the case of sites POD and ZUN) methylcyclohexane levels across the network near Carlsbad, New Mexico. Biannual data were representative, meaning using only biannual data for all sites did not change this result meaningfully. Similar maps for other measured hydrocarbons are included in the Appendix.

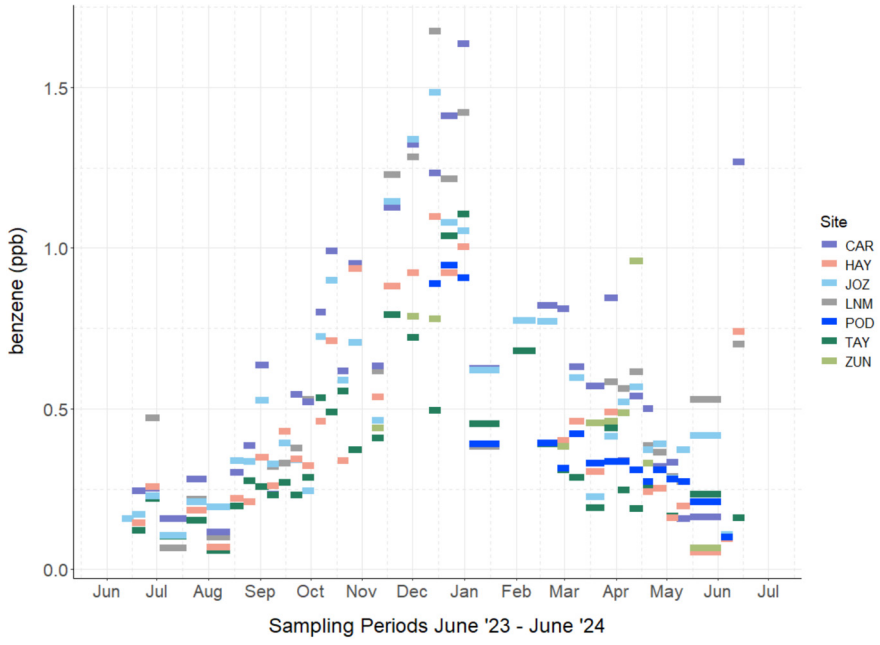

Figure 39. Seasonal changes of surface atmosphere benzene abundances across the Carlsbad, New Mexico area, Permian Basin, network sites. Each sampling period is represented by a horizontal bar, and most periods were 1-week long. Longer sampling periods and gaps occurred due to an inability of the volunteer to collect samplers earlier, or repair and replace samplers at damaged sites, respectively.

although a contribution from seasonally changing emission rates cannot be excluded.

Notably visible in **Figure 39** are both the gradients between sites (different benzene levels in each period) and the strong seasonal changes, starting with increasing levels in September, maximizing in December and January, then dropping back to the previous spring and summer minima by May the next year. Site-level data distributions are shown in **Figure 40**, ordered from high to low site averages. Sites located near Highway 285 and farthest into the oil and gas production area south of Carlsbad had the highest benzene mole fractions. Sites located farther north and west had lower mole fractions. The urban site in Carlsbad (HAY) had among the lowest benzene levels, although it was located mostly downwind of any emissions in the city itself (southerly airflows dominate in the region).

Lastly, **Figure 41** represents a comparison of benzene levels measured at air quality monitoring stations in large Texas cities in 2023 to our data as obtained across the passive sampling network sites ("network") and our own stationary, hourly measurements obtained at the LNM site, which are directly compatible in methodology to the TCEQ-run urban sites in Texas.

Figure 41 shows that benzene exposure levels in the Carlsbad, New Mexico, PB area were substantially higher than at air quality stations in large Texas cities. Included are three health-based reference values: (1) the EPA noncancer reference concentration for chronic inhalation exposure of 9 ppb,* (2) the Agency for Toxic Substances and Diseases (ATSDR) chronic noncancer minimal risk level of 3 ppb,† and (3) the World Health Organization (WHO) cancer guidance level of 0.5 ppb, representing the lower level of life-time exposure at which one new cancer case is expected per 100,000 people.‡ Because benzene is a carcinogen, no amount of exposure is considered without risk. At the hourly time resolution LNM site, the acute exposure level was exceeded a few times, and the chronic level was exceeded many times, similar to observations in Houston (the "Clinton" site located near petrochemical industry facilities in the Houston ship channel). All other urban sites' hourly measurements generally remained below 3 ppb, but only one site, in San Antonio, consistently remained below the WHO's cancer guidance value. Four of our network sites had averages above 0.5 ppb, one had a median above 0.5 ppb, and most upper quartiles were above 0.5 ppb, while none of the urban Texas upper quartile benzene measurements were above 0.5 ppb in 2023.

Spatial and Temporal Trends in the Eagle Ford Shale

Here, we show three results from the field data: (1) strong correlations between saturated hydrocarbons, (2) the spatial distribution of methylcyclohexane in comparison to the PB, and (3) the seasonal changes to benzene and toluene.

Figure 42 shows the correlation between n-hexane and n-heptane, color-scaled by methylcyclohexane, like in Figure 37. All saturated hydrocarbons were similarly strongly correlated across sites, suggesting small emission ratio differences in the area. Correlations to and among the aromatic hydrocarbons measured were slightly noisier, also comparable to our results from the Carlsbad area network in the PB. Summary statistics (Table B2) and a correlation matrix are provided in the Appendix.

Field measurements showed clear spatial gradients. As demonstrated in **Figure 43**, ambient concentrations increased from the most southern (KEN) to the most northern (FPS) site, particularly for saturated hydrocarbons but also for the aromatic compounds (**Figure 44**). The College Station urban reference site was in the Northeast EFS area, but with the most distant oil and gas production activity surrounding it, it showed the lowest mole fractions and best overall air quality. Notably, while the KAC, HEL, and FPS sites had a significant number of active gas flares surrounding them (Figure 9), few gas flares at larger distances could have affected the KEN and COL sites.

Seasonal changes in benzene and toluene are shown in Figure 44. Unlike in the PB, only weak seasonality was observed during our 5 months of measurements. Unlike the New Mexico location, South Central Texas is strongly affected by southerly flows from the Gulf of Mexico, even during winter. We did not measure for a long enough period to capture winter phases of sustained low temperatures under northerly flows when BL depths would have been lower. Most measurement periods were strongly influenced by southerly flows, which may explain why we found a rather consistent south-to-north increase in concentrations across the four central EFS network sites. Such a gradient is expected under southerly flows due to the increasing concentration fetch overlap with the shale oil and gas production area; while the KEN site has few oil and gas production sites upwind under dominant southerlies, the FPS site has nearly the whole shale area width's oil and gas production sites upwind. Statistically, both the FPS and KAC sites showed higher concentrations than the KEN site, the FPS site showed higher levels than the HEL site, but not the KAC site, and all central Eagle Ford sites showed higher values than what we observed in central College Station.

Lastly, the seasonal observations of benzene and toluene depicted in Figure 44 showed very similar results. Both the above-described gradient and the lack of a strong seasonality are observable. Overall, the abundances of these compounds, as well as the measured saturated hydrocarbons, were lower than what we observed in the Carlsbad area in the PB.

Relationship with Well Density

Seasonal average hydrocarbon abundance across the network was compared to well counts (active only, or active and "new" wells (i.e., wells established during the measurement period) in three buffer sizes: 2-, 5-, and 10-km buffers. In general, the averages of the more abundant hydrocarbons were

*https://iris.epa.gov/static/pdfs/0276_summary.pdf.

†https://www.epa.gov/sites/default/files/2014-03/documents/benzene_toxicological_profile_tp3_3v.pdf.

‡https://iris.who.int/server/api/core/bitstreams/1e953091-0810-4f45-91c7-98507bccc2de/content.

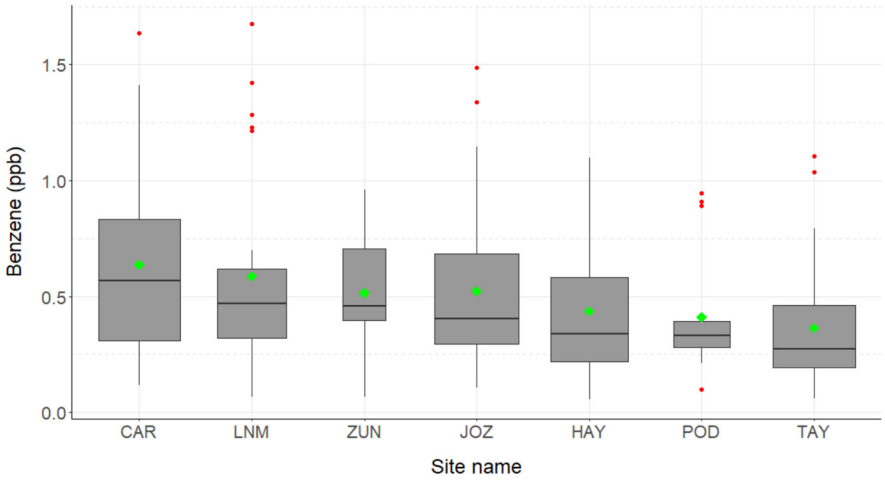

Figure 40. Site-level benzene distributions ordered by observed site averages (green circles). Box plot shows median (horizontal bar), upper and lower quartiles (gray box), and 95% levels (vertical lines). Red dots are outliers, and the width of the box represents how much data were available from each site in comparison.

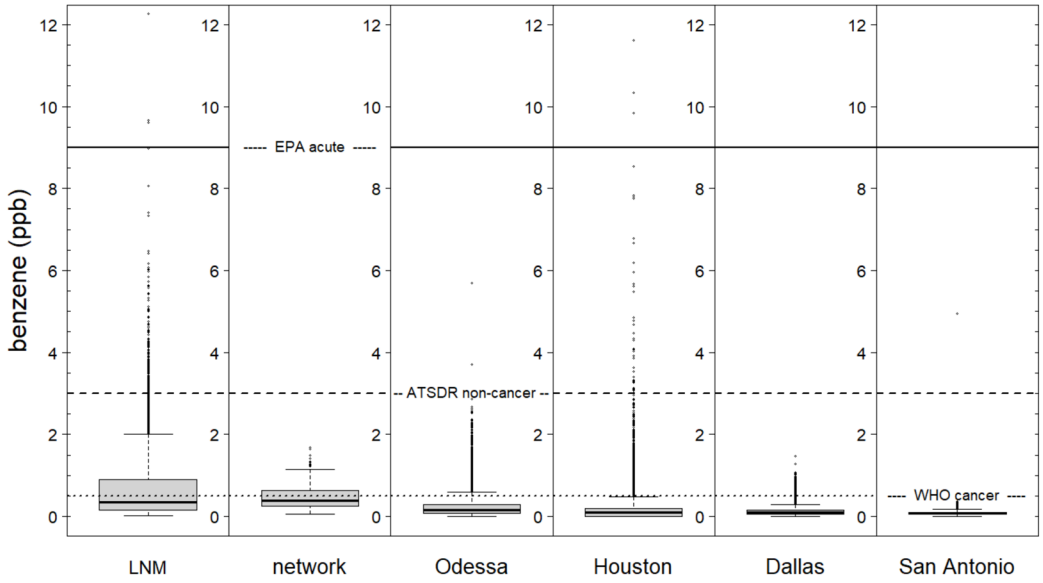

Figure 41. Box plot comparison of ambient air benzene levels as measured at our stationary platform (LNM) and across all network sites (network) compared to 2023 data obtained in four Texas cities. Horizontal dashed lines mark health-based reference values discussed in the text.

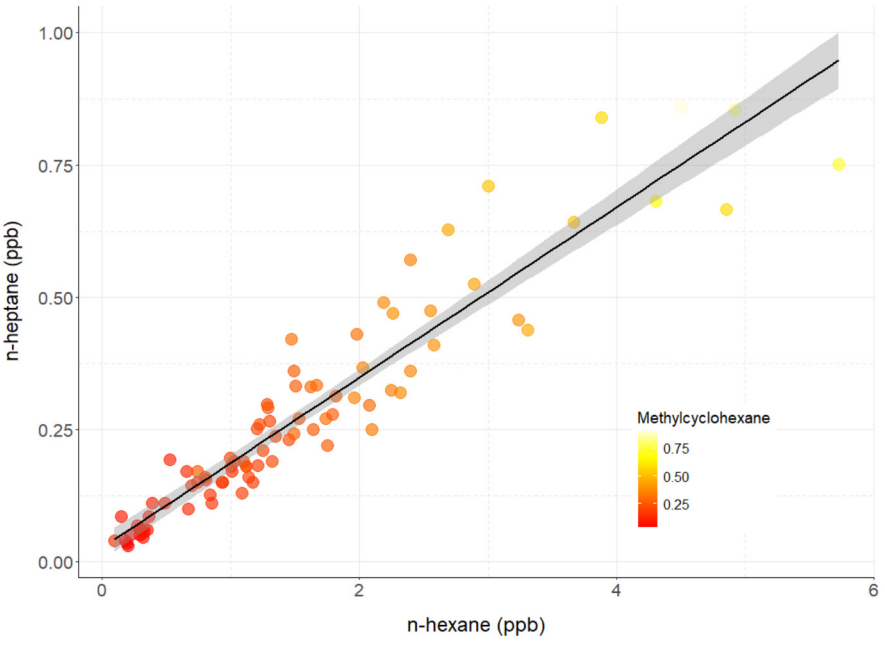

Figure 42. Saturated alkane (nC6 vs. nC7) correlation across all five Eagle Ford sites, color-scaled by methylcyclohexane data. The solid line and gray swath shows a linear correlation with 95% confidence levels (compare to abundances in the PB shown in Figure 37).

Figure 43. Average methylcyclohexane abundances (in ppb) across the Eagle Ford network sites, on Google Earth background. Inset bordered by white line shows the urban College Station location. Note that oil and gas production pad sites are visible as white blotches and, as such, demarcate the EFS boundaries. The KEN site is close to the southern boundary, the FPS site close to the northern boundary. Although the shown averages are similar between the KAC and HEL sites, the median was lower for the KAC site.

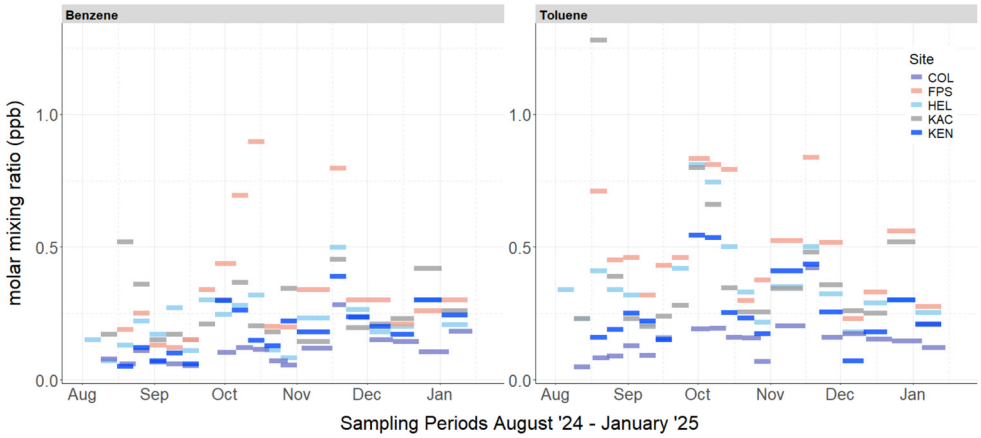

Figure 44. Benzene (left) and toluene (right) seasonal change of mixing ratios across all EFS field sites. Note the south-to-north gradient, generally showing lowest concentrations at the Kenedy site (KEN) and highest concentrations at the FPS site. In nearly all cases, the reference site in College Station (COL) showed the lowest concentrations.

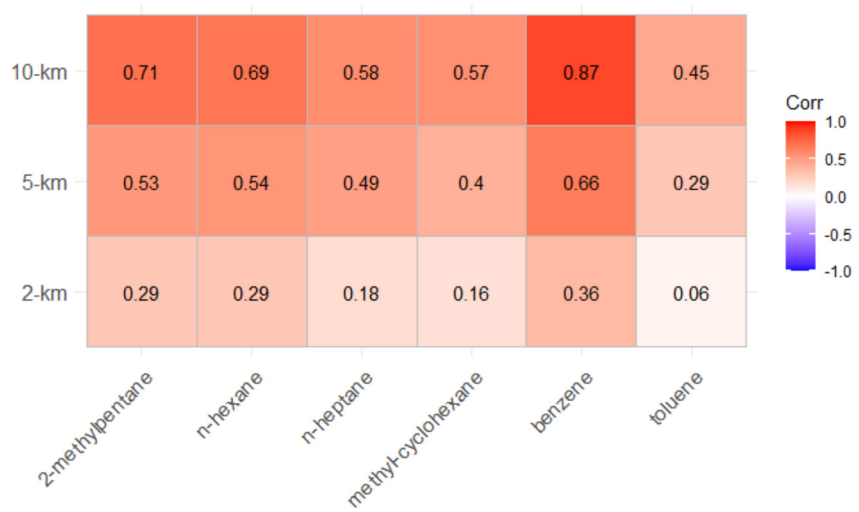

Figure 45. Correlation matrix between the half-annual averages of five abundant hydrocarbons across the seven field sites in the PB and their surrounding well counts in buffer sizes of 2, 5, and 10 km.

statistically significantly correlated ($P > 0.95$) with the surrounding well counts, and determination coefficients tended to increase with buffer size (**Figure 45**). To demonstrate this correlation further, two examples are presented in **Figure 46**.

Notably, two field sites tended to deviate more from the relationship than the others, namely the CAR and TAY sites. The former showed higher than expected and the latter often lower than expected mixing ratios. This may be explained by two unique factors, one at each site — the CAR site may be affected by hydrocarbon emissions from a large midstream facility only 600 m to its west–northwest. Considering the amount of hydrocarbons handled at that midstream facility and the traffic it generates, emissions at the CAR site may be equivalent to numerous ordinary well pad sites. In contrast, the lower-than-average hydrocarbon levels at the TAY site may reflect its location toward the western edge of the oil and gas production region (Figure 5) and away from major traffic-generating roads. Unlike at other field sites, the well sites surrounding the TAY site cluster are in its east and south sectors. The TAY site may thus benefit more often from air masses advecting from the west and northwest, especially during calmer nights when airflows tend to follow the slight terrain slope from north–northwest to south–southeast.

In the EFS as well, average hydrocarbon abundances were statistically significantly ($P > 0.95$) correlated to the number of wells surrounding each site to various degrees. In this case, there was no clear tendency for increasing correlation coefficients with increasing buffer size for the same hydrocarbons. A correlation matrix similar to Figure 45 is provided in the Appendix, and two examples are depicted in **Figure 47**.

In neither the PB nor the EFS were hydrocarbon production volumes at the surrounding well sites significantly correlated with the average hydrocarbon mole fractions measured, regardless of buffer size.

FLARING

The data processing steps taken on VIIRS Nightfire observations during our LNM sampling period, May 1, 2023, through May 31, 2024, including filtering by temperature (HDBSCAN clustering, is outlined in **Figure 48)**. The optimal minimum number of points in a cluster was determined to be four based on the balance between minimizing noise and the number of clusters (Appendix C, Table C3). After processing and clustering, there were 69,815 VNF detections in the PB during this time. All detections had individual flare temperature, source area, and radiant heat. Approximately half of the detections (35,932) included methane equivalents (methane_eq).

The fitted polynomial regression equation used to estimate the missing values of methane equivalents is presented in **Table 5** with test statistics. Predicted vs. observed scatterplots are shown in Appendix C, Figure C2.

Buffers of radius 5 km, 10 km, 20 km, 30 km, and 50 km around LNM allowed us to link the measured air pollutants with local and regional flare counts and median methane equivalents (**Figure 49**).

Within 5 km of LNM, there were 190 clustered flares representing 168 nights of flaring during our study period. Extending to 30 or 50 km resulted in a significant jump in flare counts and the number of nights with flaring that occurred during our study period. Spearman correlation analyses (**Figure 50**) indicated that nightly averages of CH_4, benzene, NO_x, H_2S, ethane, and total radioactivity within small buffers (5 km and 10 km) were moderately correlated with the number of flares and methane equivalents (R = 0.14–0.21). Additionally, in these smaller buffers, NMF source factors 3 and 4 (flaring) were correlated with methane equivalents (R = 0.19 and 0.12, respectively) and the number of flares (R = 0.16).

We fit 130 multivariate regression models adjusting for important nighttime meteorological factors as well as oil and gas production inversely weighted by well distance to LNM to further examine the correlations between these pollutants and flare counts or methane equivalents in buffers.

The models revealed that several of the pollutants measured at LNM were significantly associated with satellite-derived flaring activity, local oil and gas production, and meteorological conditions (**Table 6**). Radioactivity, ethane, and CH_4 exhibited the highest explained variance (adjusted R^2 = 0.40 to 0.50), with the strongest predictors being wind speed, wind direction, weighted oil production, and methane-equivalent flaring estimates within 5–20 km. Notably, radioactivity showed strong associations, probably reflecting the co-emission of radon during flaring and oil extraction. Radon, mobilized from geological formations, can be entrained in vented or combusted gas streams and is subsequently co-advected downwind, especially under stable nighttime meteorological conditions. Methane and ethane, as primary constituents of natural gas, were also well predicted, with methane equivalents showing stronger associations than flare counts. Similarly, NMF Factor 5, the fugitive emissions factor loading on ethane, CH_4, and radioactivity, had a similar R^2 = 0.42. Factor 4, representing flaring, was also associated with methane equivalents in small buffers (R^2 = 0.39 to 0.40), suggesting it captures a flaring-related VOC mixture because it was weighted on ethene, propene, and acetylene. Benzene, ethene, CO, and NO_x showed moderate associations (R^2 = 0.30 to 0.39), particularly with flare activity in larger spatial buffers (up to 50 km), consistent with their formation during combustion and subsequent atmospheric transport. Factor 3, the other NMF-derived flaring factor that showed high unadjusted correlation with methane equivalents, had R^2 = 0.24. In contrast, H_2S and SO_2 were weakly associated ($R^2 < 0.09$), likely reflecting their episodic nature and the need for finer-resolution source data.

Given these promising results, we suggest that the broader use of the VIIRS Nightfire properties, such as flare temperature and source area, could enhance the estimation of per-flare methane equivalents. This approach offers a valuable metric that is more detailed than flare counts that can be used to quantify flaring, particularly in regions lacking direct monitoring.

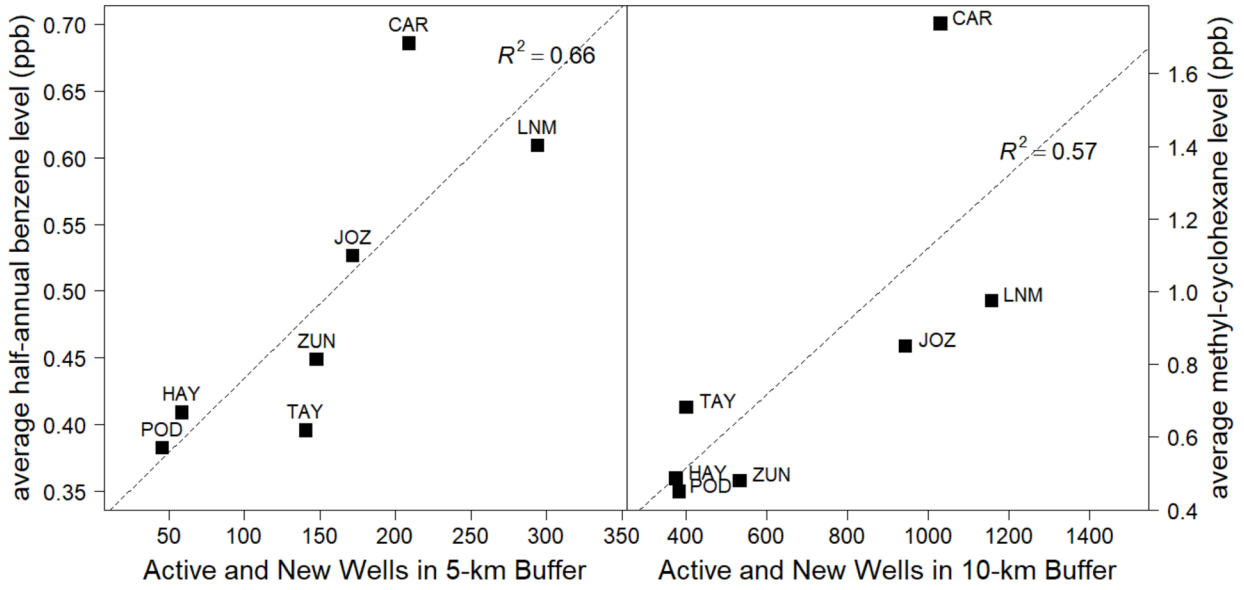

Figure 46. Example correlations between average benzene (left) and methylcyclohexane (right) mixing ratios as a function of well counts in two different buffer sizes in the PB.

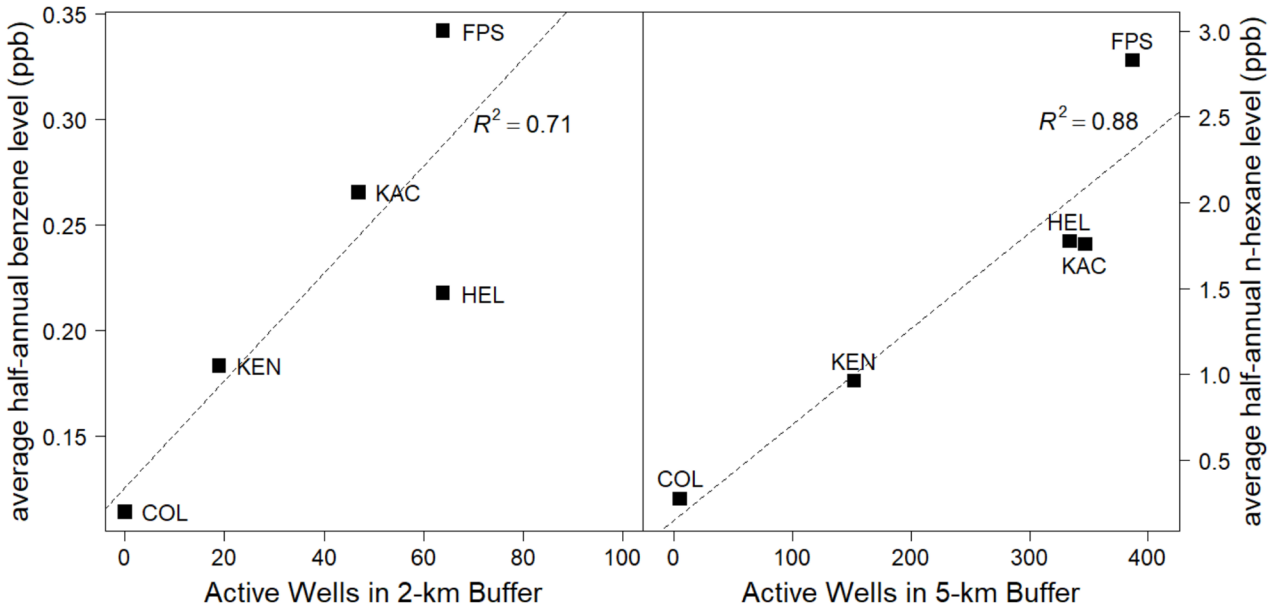

Figure 47. Same as Figure 46 but for the EFS correlations between average benzene and n-hexane abundances as a function of well counts in two buffer sizes.

Table 5. Summary Statistics of Model Performance and Polynomial Regression Equation to Estimate Methane Equivalents from VIIRS Nightfire Temperature and Source Area

	Train R^2/Test R^2	Test RMSE (m^3/s)	Observed Mean (m^3/s)	Observed variance	Preidcted Mean	Predicted Variance
Summary	0.80/0.77	0.06	0.1	0.01	0.11	0.01
Regression equation	Methane equivalents = $-1.05 + 1.59 \times 10^{-2}T - 7.93 \times 10^{-6}T^2 + 1.30 \times 10^{-10}T^3 + 9.51 \times 10^{-2}S$					

RMSE = root mean square error; VIIRS = Visible Infrared Imaging Radiometer Suite.

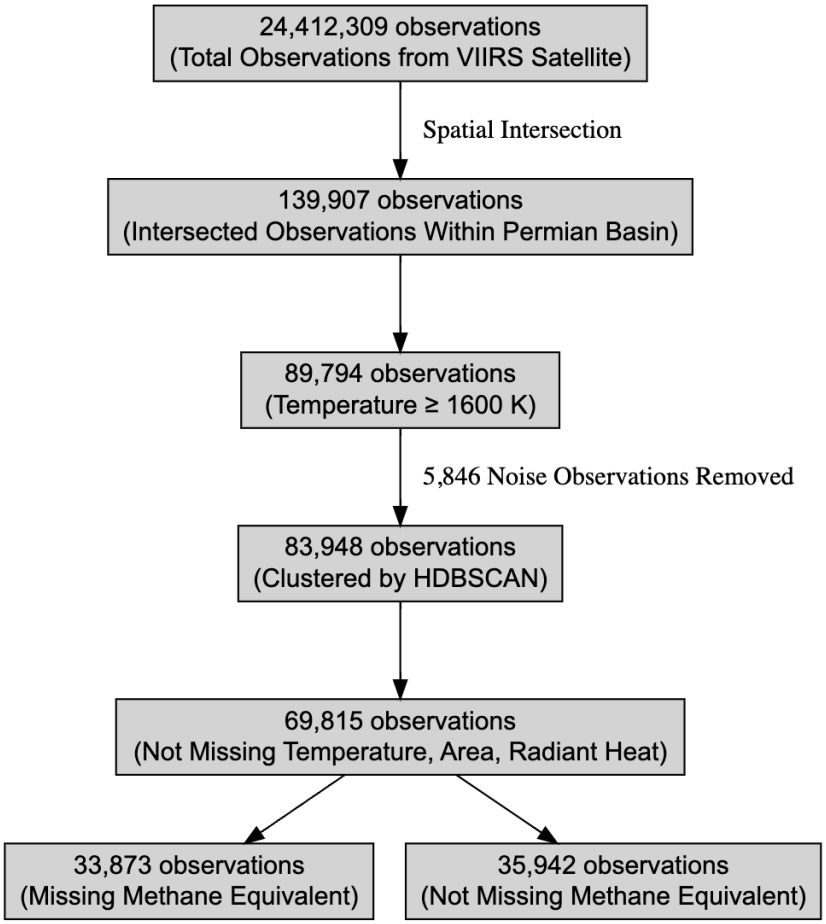

Figure 48. Data processing flow diagram of VIIRS Nightfire v.3.5 May 1, 2023 to May 31, 2024.

LNM Buffer	# Flares	# Nights
5	190	168
10	567	239
20	1,543	317
30	2,331	334
50	10,286	367

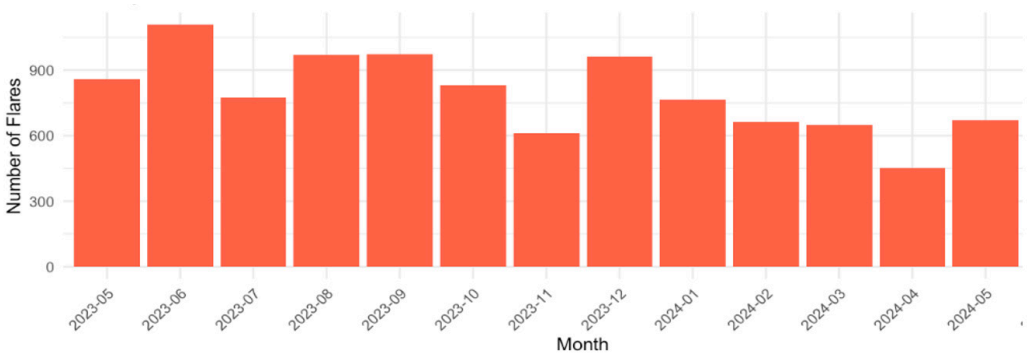

Figure 49. Left: Numbers of clustered flares and nights within different distance buffers around LNM; Right: monthly trend in flare counts within 50-km buffer of LNM.

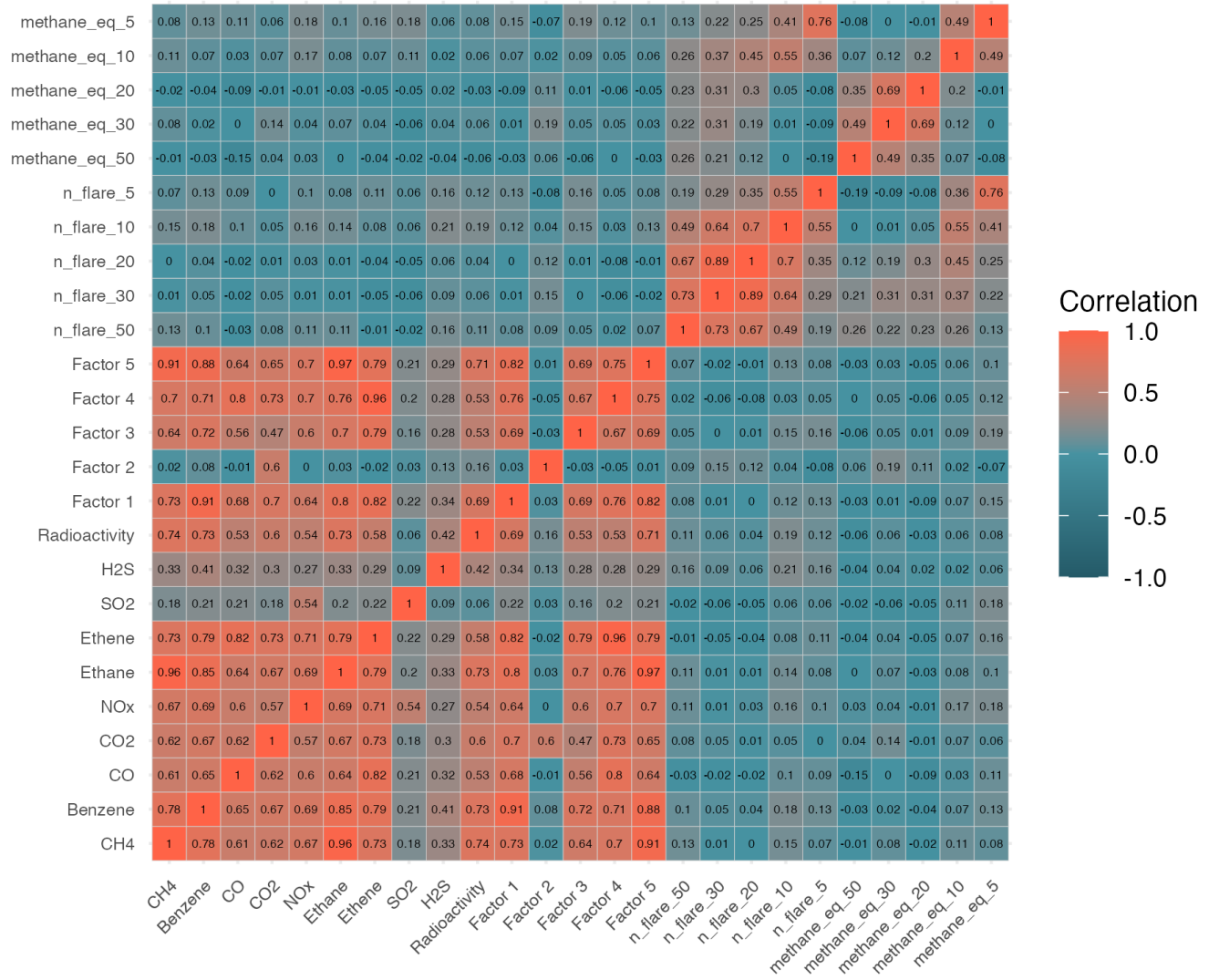

Figure 50. Correlation heatmap of nighttime LNM measurements (averaged 00:00 to 6:00), VNF flare count (n_flare), and VIIRS methane equivalents (methane_eq) in 5 km to 50 km buffers around the trailer.

DISCUSSION AND CONCLUSIONS

Our project studied air quality and noise impacts from inside a highly active oil and gas production area in the PB. Numerous previous studies have evaluated air emissions from upstream oil and gas industry activities, but the majority of these studies have focused on methane emissions (e.g., Allen et al. 2013; Alvarez et al. 2012, 2018; Brandt et al. 2016; Caulton et al. 2014; Daniels et al. 2024; de Gouw et al. 2020; Frankenberg et al. 2016; Johnson et al. 2017; Karion et al. 2013; Kort et al. 2014; Lan et al. 2015; Lavoie et al. 2017; Lyon et al. 2015, 2021; Miller et al. 2013; Omara et al. 2018, 2022; Peischl et al. 2015, 2016; Robertson et al. 2017; Smith et al. 2015; Turner et al. 2016; Varon et al. 2023; Vaughn et al. 2018; Vogt et al. 2022; Yacovitch et al. 2015; Zaimes et al. 2019; Zavala-Araiza et al. 2015; Zhang et al. 2020). This project focused instead on nonmethane hydrocarbon emissions, other common air pollutants associated with the upstream oil and gas industry, such as NO_x and H_2S, and less common aspects, such as radon and noise emissions. Our monitoring location revealed larger-than-expected air pollutant concentrations for numerous compounds investigated compared to other studies that have investigated such emissions using air quality monitoring (Lim et al. 2019; Schade and Roest 2016; Swarthout et al. 2013; Vinciguerra et al. 2015; Zaval-Araiza et al. 2014). Our major findings include the following:

1. Unusually frequent ozone NAAQS exceedances that appear to be clearly linked to oil and gas industry emissions of hydrocarbons and NO_x

Table 6. Multiple Linear Regression Results for the Associations Between Compounds and NMF Source Factors with VIIRS Nightfire Flares in Several Buffers Around LNM

Compound	Radius (km)	Adj R^2	Significant Variables
Radioactivity	20	0.50	wind direction, wind speed, weighted_monthly_oil, methane_eq_20
Ethane	5	0.44	wind direction, wind speed, weighted_monthly_oil, methane_eq_5
Ethane	10	0.44	wind direction, windspeed, weighted_monthly_oil, methane_eq_10
Ethane	20	0.43	wind speed, weighted_monthly_oil, methane_eq_20
Ethane	30	0.43	wind direction, windspeed, weighted_monthly_oil, methane_eq_30
Ethane	50	0.43	wind direction, wind speed, weighted_monthly_oil, methane_eq_50
Factor 5	5	0.42	wind speed, methane_eq_5
CH_4	5	0.41	wind speed, weighted_monthly_oil, methane_eq_5
CH_4	10	0.41	wind speed, weighted_monthly_oil, methane_eq_10
CH_4	20	0.41	wind speed, weighted_monthly_oil, methane_eq_20
CH_4	30	0.40	wind speed, weighted_monthly_oil, methane_eq_30
CH_4	50	0.40	wind speed, weighted_monthly_oil, methane_eq_50
Factor 4	5	0.40	wind direction, wind speed, methane_eq_5
Factor 4	10	0.39	wind direction, wind speed, methane_eq_10
Benzene	10	0.39	wind speed, weighted_monthly_oil, n_flare_10
Benzene	5	0.38	wind speed, weighted_monthly_oil, n_flare_50
Benzene	50	0.38	wind speed, weighted_monthly_oil, n_flare_50
Factor1	5	0.36	wind speed, weighted_monthly_gas, methane_eq_5
Ethene	5	0.35	wind direction, wind speed, weighted_monthly_oil, weighted_monthly_gas, methane_eq_5
Factor1	10	0.35	wind speed, weighted_monthly_gas, methane_eq_10
NO_x	5	0.32	wind speed, methane_eq_5
CO	50	0.30	wind direction, wind speed, weighted_monthly_oil, weighted_monthly_gas, methane_eq_50
NO_x	10	0.30	wind direction, wind speed, methane_eq_10
NO_x	50	0.30	wind direction, wind speed, n_flare_50
Factor 3	5	0.24	wind speed, weighted_monthly_oil, methane_eq_5
H_2S	5	0.09	wind speed, n_flare_5
H_2S	10	0.09	wind speed, n_flare_10
SO_2	5	0.05	n_flare_5, methane_eq_5
Factor 2	30	0.04	wind speed, n_flare_30
SO_2	10	0.03	weighted_monthly_oil, methane_eq_10

LNM = Loving, New Mexico; NMF = non-negative matrix factorization; VIIRS = Visible Infrared Imaging Radiometer Suite.

Variable definitions: wind speed (m/s) averaged from 0:00 to 6:00, wind direction (º) averaged using circular mean from 0:00 to 6:00, weighted_monthly_oil & weighted_monthly_gas (inverse distance weighted sum of monthly oil and gas production at wells within 10 km from LNM), n_flare (number of flares in 10-, 20-, 30-, 50-km buffers around LNM), methane_eq (VIIRS methane equivalent in 10-, 20-, 30-, 50-km buffers around LNM).

2. Unusually frequent encounters of hydrocarbon emissions plumes
3. Unusually high levels of toxic hydrocarbons, particularly benzene, when compared to air monitoring in areas historically considered more polluted (i.e., in densely populated cities)
4. A strong relationship between observed hydrocarbon concentrations and regional well density
5. A significant impact of regional gas flaring on air quality and noise
6. A prevalence of low-frequency noise, likely from various UOGD equipment sources in the region, as determined from correlational analysis
7. Airborne radon radioactivity measurements revealing detectable impacts from gas flaring and a regionally elevated surface source

We discuss these findings below in turn:

1. High ozone concentrations continue to affect air quality in many parts of the nation. Effects of upstream oil and gas production emissions on ozone formation have been previously evaluated by Ahmadi and John (2015), McDuffie and colleagues (2016), Cheadle and colleagues (2017), Roohani and colleagues (2017), Pozzer and colleagues (2020), Buonocore and colleagues (2023), Marsavin and colleagues (2024), and Modi and colleagues (2024). In Southeast New Mexico in particular, detailed measurements at Carlsbad Caverns National Park in 2017 and 2019 (Benedict et al. 2020; Pan et al. 2023; Pollack et al. 2023; Marsavin et al. 2024) revealed dominant impacts of oil and gas development-related emissions under frequent southeasterly winds during summer on local ozone concentrations. Ozone formation was found to be mostly NO_x-sensitive except for a few morning hours, and alkanes were found to be the dominant "fuel" for ozone formation chemistry (Pollack et al. 2023). Our measurements strongly support these conclusions for the LNM site, approximately 34 km east–northeast of the National Park. Ozone at LNM was strongly seasonal and predictably reached high concentrations whenever winds came out of southeasterly directions across the Permian-Delaware Basin. Based on the subset of VOCs we measured and its median composition and OH (hydroxy radical) reactivity during summer (May to October) daytime hours of full boundary layer development (12:00–19:00 local time), the regional ozone formation potential as initiated by VOC oxidation was overwhelmingly dominated by petrochemical hydrocarbons (**Figure 51**). Average VOC reactivity was a moderate 1.65 (0.62–1.80 interquartile range) s^{-1}. On the 33 unique days in 2023 when afternoon ozone levels exceeded 80 ppb, the interquartile range (IQR) of total VOC reactivity was 1.3–2.5 s^{-1}, with an average of 2.0 s^{-1} and a maximum of 4.57 s^{-1}. Compared to all other summer days, these high-ozone days exhibited similar NO_x concentrations, slightly higher temperatures and humidity, marginally lower wind speeds, and winds predominantly from the south to east on 80% of the days. A positive correlation was observed between afternoon ozone and alkane abundance. On nearly all of these days, ambient air temperatures exceeded 30°C in the afternoon. It's important to note that the reported VOC reactivities likely underestimate total atmospheric reactivity, as measurements did not include formaldehyde and other oxygenated VOCs (e.g., methanol), nor CO and CH_4. Given that high ozone and elevated temperatures shorten VOC atmospheric lifetimes — and that meteorological differences between high ozone days and the broader summer period were minimal — the elevated VOC abundances on high ozone days were likely driven by increased emissions from upwind sources relative to the LNM site.

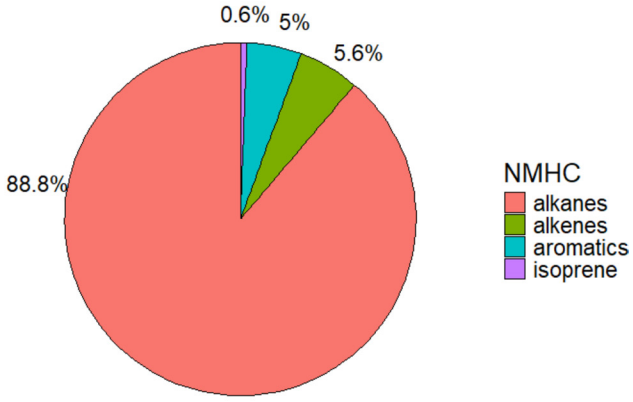

Figure 51. Average relative hydrocarbon OH radical reactivity during summer of 2023 as measured at the LNM site (afternoon hours only when the atmospheric boundary layer was fully developed).

This conclusion is consistent with the findings from the Carlsbad Caverns National Park studies, which identified high ozone days with higher photochemical activity and associated secondary processing of oil and gas activity-related emissions (Marsavin et al. 2024; Pollack et al. 2023).

While our data cannot be used to evaluate whether upwind ozone production depended more on NO_x or hydrocarbons (NO_x- vs. VOC-limitation), the Carlsbad Caverns National Park data identified mostly NO_x-limited conditions for ozone formation. However, this can be inferred, and thus locally confirmed, from our data due to high hydrocarbon to NO_x ratios observed at virtually all times of the day (mean of 55, IQR of 27 to 63 ppb per ppb NO_x) compared to typical ratios of 10–15 delineating VOC-limited from NO_x-limited ozone formation conditions.

2. Creating sufficient photochemical reactivity to form excessive ozone in the boundary layer requires a higher abundance of low-reactivity alkanes compared to regions in the United States, which contain highly reactive VOCs

(i.e., isoprene, due to emissions from vegetation). In the PB, these conditions are created via high emissions of petrochemical hydrocarbons. This manifested itself at our research site via higher average and median mixing ratios compared to the reference sites in Colorado and urban Texas, and the observation of frequent high-concentration plumes from all directions and at all daytimes. We do not know which processes, at which distances, and by which companies produced these emission plumes, and whether they violated existing emission permits or not. However, in their entirety, our hydrocarbon measurements confirm high regional concentrations observed from satellite data for methane (Robertson et al. 2020; Zhang et al. 2020; Irakulis-Loitxate et al. 2021; Chen et al. 2022; Varon et al. 2023) and ethane (Brewer et al. 2024) in the PB. In addition, a consistently low i-/n-pentane ratio (median and mean <1) further confirms that regional methane and hydrocarbon concentrations are almost entirely driven by UOGD-related emissions.

The additional contribution of our observations to these prior works consists not only of the ground-truthing of these remotely sensed data, but in their extension to higher hydrocarbons, including air toxics such as n-hexane and benzene, and the finding that emissions are rather "constant" and invariant, meaning the observed plume composition was nearly unchanging as demonstrated via tight correlations between all hydrocarbons. Furthermore, it is important to realize that our stationary measurements provided one "fixed point" dataset. The site was chosen partially for logistical reasons, and it is possible that VOC concentrations were and are higher in other locations in the PB compared to the point measurements that we are reporting here, as there is no reason to believe that we coincidentally measured at the most polluted site in the PB. Therefore, the LNM site measurements need to be considered as an exemplary dataset and not necessarily as representative of the most polluted conditions that can be encountered in the PB.

3. Tight correlations between the observed hydrocarbons were also demonstrated through our passive sampler network, which displayed consistent across-site relationships that can only be explained by the dominant hydrocarbon sources in the area having highly similar hydrocarbon compositions. This included the toxic hydrocarbon benzene. While our stationary platform's hourly measurements revealed benzene levels that twice exceeded the EPA reference concentration for chronic inhalation exposure of 9 ppb, and often exceeded the ATSDR reference value for chronic inhalation exposure of 3 ppb, the mean, median, and 95th percentile mixing ratios stayed below that value. However, both the stationary and passive sampler sites' benzene mixing ratios statistically significantly ($P < 0.001$) exceeded benzene levels at all reference sites in Colorado and Texas. While most reference sites had long-term average mixing ratios below the WHO cancer guidance value of 0.5 ppb, our PB averages across the passive sampler network and at the LNM site were at or above the WHO guidance value, respectively. In comparison, benzene levels in the Texas EFS were also significantly lower.

   This raises significant concern about benzene exposures in the PB compared to areas not affected by UOGD activities, because, as our NMF analysis showed, benzene emissions from road traffic do not dominate ambient concentrations in this area. As a significant, probably dominant fraction of on-road traffic in the PB is likely generated by the oil and gas industry itself, we surmise that benzene levels in the Carlsbad area are mainly driven by UOGD and its associated generation of on-road traffic via trucks and other vehicles used by its supply industry.

4. Further evidence of UOGD-related hydrocarbon emissions affecting population exposure comes from our passive sampler networks. As both networks reflected sites with widely varying numbers of well pad sites in their surroundings, we were able to correlate average hydrocarbon mixing ratios at the sampler locations with well pad numbers in various buffer sizes. The results in both shale production basins showed that increasing well density led to increasing hydrocarbon concentrations. This relationship held for various buffer sizes and improved with buffer size in the PB, suggesting that distant emission sites significantly contribute to the overall mixing ratio observed at the recipient location. Similarly, in the Texas network, increasing the upwind region (concentration fetch) contributing to emissions had a strong influence on the local hydrocarbon mixing ratio, while the urban reference site in a much less active part of the EFS had the best air quality.

5. Gas flaring has previously been identified as a source of air pollutants with potential health impacts (e.g., Cushing et al. 2020). Satellite-based detection of gas flaring provides a critical tool for understanding the spatial distribution of UOGD-related flaring across large areas. Spatial density maps of the flare locations supported this project, particularly with respect to interpreting the source apportionment results. Because our stationary measurement site was located just 150 m from a comparatively small and infrequently operating flare, we observed strong flaring impacts only from a narrow sector under southwest wind directions, but often enough to identity the gas flare as a source of NO_x, unsaturated hydrocarbons, methane and ethane, hydrogen sulfide, CO and CO_2, and radon. Our NMF analysis identified several combustion factors, one related to the nearby flare and one related to combustion sources, including flaring, that were likely co-located with other, more distant hydrocarbon sources, particularly toward the east. By coupling our LNM data to VIIRS satellite flaring, we could quantify more specifically that flare counts and methane equivalents are associated with regional concentrations of methane, ethane, benzene, and radioactivity. This conclusion is further supported by the associations NMF source factors 3 and 4 (flaring/incomplete combustion) as well as their variation with wind direction.

For comparison, traffic emissions (Factor 1) showed a wind direction distribution alignment with urban sources and the nearby highway. While our VOC measurements were not detailed enough to differentiate gasoline engine cars from diesel truck emissions, the comparatively low levels of short-chain alkanes, together with a lack of a higher i/n-pentane ratio in Factor 1, suggest a dominance of diesel-powered vehicles contributing to the traffic emissions factor. This further supports our above conclusion about the industry's dominant overall contribution to ambient hydrocarbon mixing ratios.

6. Our noise measurements showed a predominance of low-frequency sound (<100 Hz), with daytime levels exceeding nighttime levels. This pattern was reinforced in the NMF decomposition, where the factor explaining the greatest variability in the frequencies was composed almost entirely of frequencies below 100 Hz. Multiple UOGD sources contribute to low-frequency noise, including compressors, active drilling rigs, and pumps. Similar observations were reported in prior studies (Hays et al. 2017; Radtke et al. 2017). When linking the frequency data to air pollutant concentrations using XGB modeling, we observed the highest predictive performance for CO_2, with key predictors including LCpeak (which emphasizes low frequencies) and individual low frequencies (12.5 Hz). Similarly, the XGB using NMF-derived noise factors showed the strongest performance with the factor dominated by low frequencies. This suggests a shared combustion-based source with compressors and other mechanical processes producing both CO_2 emissions and low-frequency noise. This interpretation is further supported by the NMF-based pollutant source apportionment, where the combustion-related factor was dominated by CO_2 and showed little variability by wind direction. The ubiquitousness of this factor points to a regional source; low-frequency sound similarly has long-distance propagation and would be regional. These results build on our previous work (Fallah Shorshani et al. 2024), highlighting the novelty of using noise measurements in machine learning models to better uncover frequency signals that help to understand source-specific emissions.

7. The ratio between gas-phase and particle-phase measurements suggests that the flare on the neighboring well pad site to the southwest was a small source of radon. Its absolute signal did not lead to significant radioactivity increases, which instead were elevated from north–northwesterly wind directions. The radioactivity PSCF results show geographical overlaps (northwest and southerly directions of the LNM site location) with the PSCF results for methane, as well as with a USGS map of enhanced surface radioactivity, a proxy for radon emission density. In a 10-km buffer around LNM, the correlation between VIIRS flares and total radioactivity was $R = 0.19$. When adjusted for winds and oil production in a linear regression, the association strengthened ($R^2 = 0.52$), providing another indication of flaring being a contributing source of airborne radioactivity. Lastly, the NMF analysis confirmed radioactivity impacts from flaring, but a larger portion of its variability was explained by a general combustion factor that may include the ubiquitous ground source of carbon dioxide (from respiration) and radon (from uranium).

IMPLICATIONS OF FINDINGS

To the best of our knowledge, our project represents the most detailed and extensive air quality research study carried out in New Mexico to date. It was also one of the most detailed air quality studies carried out to date in an active US oil and gas production region during a peak production period after the prior maximum production in the prepandemic year of 2019. The results paint a rather bleak picture of the upstream oil and gas air quality impacts, particularly concerning two issues: (1) the creation of an ozone problem where there previously was none, and (2) the re-emergence of high atmospheric benzene levels, which had previously been effectively reduced via EPA regulations limiting benzene in gasoline.

Our results confirm prior work that associated the region's increasing ozone levels (as identified in 2017) with the growing oil and gas development in the PB. This development has caused an increasing ozone design value since then. The US EPA calculates ozone design values for a monitoring site as the 3-year average of the annual fourth-highest daily maximum 8-hour average ozone concentration (US EPA 2025). Although we did not have 3 years of measurement, based on the 13 months of data collected at LNM, the 4th highest 8-hour ozone concentration measured was well above the design values generated from measurements at the nearby Carlsbad Caverns National Park (**Figure 52**). Thus, our measurements strongly suggest that ozone is significantly higher in the Carlsbad region than at the reference site in the National Park to its southwest. Furthermore, higher ozone formation in this region is related to higher hydrocarbon emissions under otherwise similar NO_x conditions. With respect to benzene levels, prior work by us (Schade and Roest 2016, 2018) and others (Bolden et al. 2015; Halliday et al. 2016; Lyu et al. 2021; Rich and Orimoloye 2016; Thompson et al. 2014) has highlighted the increase and importance of benzene emissions from the upstream oil and gas industry, leading to atmospheric levels dominated by this new source even in areas of substantial traffic emissions contributions. Our findings in this project further support this unfortunate development.

Taken together with prior studies, these observations underscore the benefits of targeted reductions in hydrocarbon emissions from oil and gas operations. Further improvements could be achieved by also addressing NO_x emissions, such as by minimizing gas flaring and reducing diesel combustion sources in stationary engines, which may help lower ozone design values and support progress toward meeting NAAQS standards in the region and reduce health risks for local and regional populations.

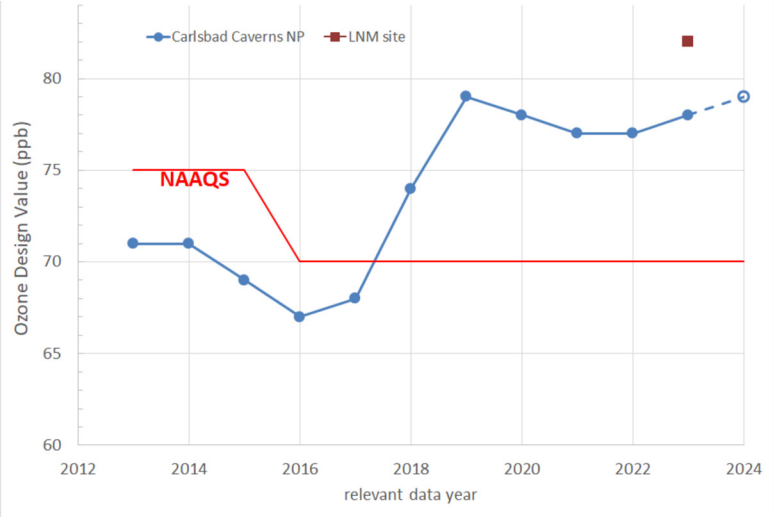

Figure 52. Historic ozone design value development (blue dots and line) at the Carlsbad Caverns National Park site, used by EPA as the relevant regulatory reference site for southeast New Mexico. The 2024 value was estimated based upon data published by the New Mexico Environmental Department. The LNM site's 4th highest 8-hr maximum value was added for comparison. The prior and current ozone National Ambient Air Quality Standard (NAAQS) is outlined in orange.

DATA AVAILABILITY STATEMENT

Continuous monitoring data: All data from the stationary monitoring in Loving, New Mexico, can be explored through *https://meredithfranklin.github.io/UOGD-source-contributions* and downloaded from the supporting GitHub repository *https://github.com/meredithfranklin/UOGD-source-contributions*.

The DJB data used in this study will be available from the EBAS repository, accessible through the following webpage: *https://ebas.nilu.no/data-access/*. On the homepage, click the "Data search and display" icon. Next, under the "Station" drop-down menu, select one of the sites from the study (e.g., Longmont Union Reservoir or Broomfield North Pecos) and click the "List datasets" button. This will return a list of available datasets, which can be downloaded by selecting the desired dataset(s) and then clicking the "Download" button.

Passive sampling data: Passive sampling datasets can be found in the Texas data repository at *https://doi.org/10.18738/T8/WEIZWA*.

Code: All Python code, R code, and analytic datasets for the source apportionment, noise analysis, and flaring analysis are maintained on the GitHub repository *https://github.com/meredithfranklin/UOGD-source-contributions*.

ACKNOWLEDGMENTS

We are grateful to all volunteers providing access to their private properties for us to install passive sampler setups. We are indebted to Ms. J. Dominguez Zuniga, whose contributions to passive sampler collection and shipment enabled this part of the project.

We are also grateful to Boulder AIR team members Dani Caputi, Ryan Daly, Lisa Darby, Gabriel Greenberg, Jacques Hueber, Katherine Potter, Susan Simoncic, and Michel Stahli for their vital assistance in setting up, as well as decommissioning, the field research site in Loving, NM, and their contribution to data acquisition, data quality control, data analyses and reporting.

REFERENCES

Adgate JL, Goldstein BD, McKenzie LM. 2014. Potential public health hazards, exposures and health effects from unconventional natural gas development. Environ Sci Technol 48:8307–8320, *https://doi.org/10.1021/es404621d*.

Agency for Toxic Substances Control Registry. 2007. Toxicological Profile for Benzene.

Ahmadi M, John K. 2015. Statistical evaluation of the impact of shale gas activities on ozone pollution in North Texas. Sci Total Environ 536:457–467, *https://doi.org/10.1016/j.scitotenv.2015.06.114*.

Allen DT, Torres VM, Thomas J, Seinfeld JH. 2013. Measurements of methane emissions at natural gas production sites in the United States. Proc Natl Acad Sci USA 110:17768–17773, *https://doi.org/10.1073/pnas.1304880110*.

Allen DT, Torres VM, Thomas J, Sullivan DW, Harrison M, Hendler A, et al. 2015. Methane emissions from process equipment at natural gas production sites in the United States: pneumatic controllers. Environ Sci Technol 49:633-640.

Allshouse WB, McKenzie LM, Barton K, Brindley S, Adgate JL. 2019. Community noise and air pollution exposure during the development of a multi-well oil and gas pad. Environ Sci Technol 53:7126–7135, *https://doi.org/10.1021/acs.est.9b00052*.

Alvarez RA, Pacal SW, Winebreak JJ, Chameides WL, Hamburg SP. 2012. Greater focus needed on methane leakage from natural gas infrastructure. Proc Natl Acad Sci USA 109:6435–6440, *https://doi.org/10.1073/pnas.1202407109*.

Alvarez RA, Zavala-Araiza D, Lyon DR, Allen DT, Barkley ZR, Brandt AR, et al. 2018. Assessment of methane emissions from the US oil and gas supply chain. Science 361:186–188, *https://doi.org/10.1126/science.aar7204*.

Baillie J, Risk D, Atherton E, O'Connell E, Fougère C, Bourlon E, et al. 2019. Methane emissions from conventional and unconventional oil and gas production sites in southeastern Saskatchewan, Canada. Environ Res Commun 1:011003, *https://doi.org/10.1088/2515-7620/ab01f2*.

Benedict KB, Prenni AJ, El-Sayed MMH, Hecobian A, Zhou Y, Gebhart KA, et al. 2020. Volatile organic compounds and ozone at four national parks in the Southwestern United States. Atmos Environ 239, *https://doi.org/10.1016/j.atmosenv.2020.117783*.

Blomberg AJ, Li L, Schwartz JD, Coull BA, Koutrakis P. 2020. Exposure to particle beta radiation in Greater Massachusetts and factors influencing its spatial and temporal variability. Environ Sci Technol 54:06575–6583, *https://doi.org/10.1021/acs.est.0c00454*.

Boggs PT, Rogers JE, Schnabel RB. 1992. User's Reference Guide for ODRPACK Version 2.01: Software for Weighted Orthogonal Distance Regression. *https://docs.scipy.org/doc/external/odrpack_guide.pdf*.

Bolden AL, Kwiatkowski CF, Colborn T. 2015. New look at BTEX: are ambient levels a problem? Environ Sci Technol 49:5261–5276, *https://doi.org/10.1021/es505316f*.

Brandt AR, Heath GA, Cooley D. 2016. Methane leaks from natural gas systems follow extreme distributions. Environ Sci Technol 50:12512–12520, *https://doi.org/10.1021/acs.est.6b04303*.

Brandt AR, Heath GA, Kort EA, O'Sullivan F, Pétron G, Jordaan SM, et al. 2014. Methane leaks from North American natural gas systems. Science 343:733–735, *https://doi.org/10.1126/science.1247045*.

Brewer JF, Millet DB, Wells KC, Payne VH, Kulawik S, Vigouroux C, et al. 2024. Space-based observations of tropospheric ethane map emissions from fossil fuel extraction. Nat Commun 15:7829, *https://doi.org/10.1038/s41467-024-52247-z*.

Brown DR, Lewis C, Weinberger BI. 2015. Human exposure to unconventional natural gas development: a public health demonstration of periodic high exposure to chemical mixtures in ambient air. J Environ Sci Health Part A 50:460–472, *https://doi.org/10.1080/10934529.2015.992663*.

Buonocore JJ, Reka S, Yang D, Chang C, et al. 2023. Air pollution and health impacts of oil and gas production in the United States. Environ Res Health 1:021006, *http://dx.doi.org/10.1088/2752-5309/acc886*.

Carslaw DC, Ropkins K. 2012. OpenAir — An R package for air quality data analysis. Environ Modell Softw 27–28:52–61, *https://doi.org/10.1016/j.envsoft.2011.09.008*.

Caulton DR, Shepson PB, Santoro RL, Miller BR. 2014. Toward a better understanding and quantification of methane emissions from shale gas development. Proc Natl Acad Sci USA 111:6237–6242, *https://doi.org/10.1073/pnas.1316546111*.

Chan Y-C, Cohen DD, Hawas O, Stelcer E, Simpson R, Denison L, et al. 2008. Apportionment of sources of fine and coarse particles in four major Australian cities by positive matrix factorisation. Atmos Environ 42:374–389, *https://doi.org/10.1016/j.atmosenv.2007.09.030*.

Cheadle LC, Oltmans SJ, Pétron G, Schnell RC, Mattson EJ, Herndon SC, et al. 2017. Surface ozone in the Colorado Northern Front Range and the influence of oil and gas development during FRAPPE/DISCOVER-AQ in summer 2014. Elementa (Wash DC) 5:61, *https://doi.org/10.1525/elementa.254*.

Chen Y, Sherwin ED, Berman ESF, Jones BB, Gordon MP, Wetherley EB, 2022. Quantifying regional methane emissions in the New Mexico Permian basin with a comprehensive aerial survey. Environ Sci Technol 56:4317–23, *https://doi.org/10.1021/acs.est.1c06458*.

Cushing LJ, Vavra-Musser K, Chau K, Franklin M, Johnston JE. 2020. Flaring from unconventional oil and gas development and birth outcomes in the Eagle Ford Shale in South Texas. Environ Health Perspect 128:077003, *https://doi.org/10.1289/EHP6394*.

Czolowski ED, Santoro RL, Srebotnjak T, Shonkoff SBC. 2017. Toward consistent methodology to quantify populations in proximity to oil and gas development: a national spatial analysis and review. Environ Health Perspect 125:086004, *https://doi.org/10.1289/EHP1535*.

Daniels WS, Jia M, Hammerling DM. 2024. Detection, localization, and quantification of single-source methane emissions on oil and gas production sites using point-in-space continuous monitoring systems. Elementa (Wash DC) 12:00110, *https://doi.org/10.1525/elementa.2023.00110*.

de Gouw JA, Veefkind JP, Roosenbrand E, Dix B, Lin JC, Landgraf J, et al. 2020. Daily satellite observations of methane from oil and gas production regions in the United States. Sci Rep 10:1379, *https://doi.org/10.1038/s41598-020-57678-4*.

Dix B, de Bruin J, Roosenbrand E, Vlemmix T, Francoeur C, Gorchov-Negron, et al. 2020. Nitrogen oxide emissions from US oil and gas production: recent trends and source attribution. Geophys Res Lett 47:e2019GL085866, *https://doi.org/10.1029/2019GL085866*.

Dix B, Francoeur C, Li M, Serrano-Calvo R, Levelt PF, Veefkind JP, et al. 2022. Quantifying NO_x emissions from US oil and gas production regions using TROPOMI NO_2. ACS Earth Space Chem 6:403–414, *https://doi.org/10.1021/acsearthspacechem.1c00387*.

Elvidge CD, Zhizhin M, Hsu F-C, Baugh KE. 2013. VIIRS nightfire: satellite pyrometry at night. Remote Sens (Basel) 5:4423–4449, *https://doi.org/10.3390/rs5094423*.

Fallah-Shorshani M, Fruin S, Yin X, McConnell R, Franklin M. 2024. Estimating near-roadway air pollution from multi-frequency noise measurements. Sci Total Environ 944:173900, *https://doi.org/10.1016/j.scitotenv.2024.173900*.

Fallah-Shorshani M, Yin X, McConnell R, Fruin S, Franklin M. 2022. Estimating traffic noise over a large urban area: an evaluation of methods. Environ Int 170:107583, *https://doi.org/10.1016/j.envint.2022.107583*.

Faruolo M, Falconieri A, Genzano N, Lacava T, Marchese F, Pergola N. 2022. A daytime multisensor satellite system for global gas flaring monitoring. IEEE Trans Geosci Remote Sens 60:1–17, *https://doi.org/10.1109/TGRS.2022.3143167*.

Fawole OG, Cai X-M, MacKenzie AR. 2016. Gas flaring and resultant air pollution: a review focusing on black carbon. Environ Pollut 216:182–197, *https://doi.org/10.1016/j.envpol.2016.05.075*.

Francoeur CB, McDonald BC, Gilman JB, Zarzana KJ, Dix B, Brown SS, et al. 2021. Quantifying methane and ozone precursor emissions from oil and gas production regions across the contiguous US. Environ Sci Technol 55:9129–9139, *https://doi.org/10.1021/acs.est.0c07352*.

Frankenberg C, Thorpe AK, Thompson DR, Hulley G, Kort EA, Vance N, et al. 2016. Airborne methane remote measurements reveal heavy-tail flux distribution in Four Corners region. Proc Natl Acad Sci USA 113:9734–9739, *https://doi.org/10.1073/pnas.1605617113*.

Franklin M, Chau K, Cushing L, Johnston JE. 2019. Characterizing flaring from unconventional oil and gas operations in South Texas using satellite observations. Environ Sci Technol 53:2220–2228, *https://doi.org/doi:10.1021/acs.est.8b05355*.

Ghosh B. 2018. Impact of changes in oil and gas production activities on air quality in northeastern Oklahoma: ambient air studies in 2015–2017. Environ Sci Technol 52:3285–3294, *https://doi.org/10.1021/acs.est.7b05726*.

Gillman MW. 2005. Developmental origins of health and disease. N Engl J Med 353:1848–1850, *https://doi.org/10.1056/NEJMe058187*.

Gilman JB, Lerner BM, Kuster WC, de Gouw JA. 2013. Source signature of volatile organic compounds from oil and natural gas operations in northeastern Colorado. Environ Sci Technol 47:1297–1305, *https://doi.org/10.1021/es304119a*.

Global Monitoring Laboratory. 2025. Trends in CH4 - NOAA Global Monitoring Laboratory. *https://gml.noaa.gov/ccgg/trends_ch4/index.html* [accessed 3 February 2025].

Graves JD, Kimura Y, Modi M, Stokes S, Meyer M, Hildebrandt Ruiz L, et al. 2025. Source attribution of elevated ethane concentrations detected by regional monitors in oil and gas production regions. ACS ES&T Air 2:2038–2046, *https://doi.org/10.1021/acsestair.5c00235*.

Gray PR. 1993. NORM contamination in the petroleum industry. J Pet Technol 45:12–16, *https://doi.org/10.2118/22880-PA*.

Guha A, Gentner DR, Weber RJ, Provencal R, Goldstein AH. 2015. Source apportionment of methane and nitrous oxide in California's San Joaquin Valley at CalNex 2010 via positive matrix factorization. Atmos Chem Phys 15:12043–12063, *https://doi.org/10.5194/acp-15-12043-2015*.

Halliday HS, Thompson AM, Wisthaler A, Blake DR, Hornbrook RS, Mikoviny T, et al. 2016. Atmospheric benzene observations from oil and gas production in the Denver-Julesburg Basin in July and August 2014. J Geophys Res 121:11055–11074, *https://doi.org/10.1002/2016JD025327*.

Harrison J, Leggett R, Lloyd D, Phipps A, Scott, B. 2007. Polonium-210 as a poison. J Radiol Prot 27:17–40, *https://doi.org/10.1088/0952-4746/27/1/001*.

Hays J, McCawley M, Shonkoff SBC. 2017. Public health implications of environmental noise associated with unconventional oil and gas development. Sci Total Environ 580:448–456, *https://doi.org/10.1016/j.scitotenv.2016.11.118*.

Hecobian A, Clements AL, Shonkwiler KB, Zhou Y, MacDonald LP, Hilliard N, et al. 2019. Air toxics and other volatile organic compound emissions from unconventional oil and gas development. Environ Sci Technol Lett 6:720–726, *https://doi.org/10.1021/acs.estlett.9b00591*.

Helmig D. 2020. Air quality impacts from oil and natural gas development in Colorado. Elementa (Wash DC) 8:4, *https://doi.org/10.1525/elementa.398*.

Helmig D, Greenberg G, Hueber J, Blanchard B, Chopra J, Simoncic S, et al. 2025. Methane and volatile organic compounds and their influence on air quality in Boulder, Colorado. Elementa (Wash DC) 13:00117, *https://doi.org/10.1525/elementa.2023.00117*.

Helmig D, Nobel J, Caputi D, Brown D, Daly RW, Darby LS, et al. 2024. Elevated airborne radioactivity downwind of a Colorado oil refinery. J Air Waste Manage Assoc 74:920–931, *https://doi.org/10.1080/10962247.2024.2393194*.

Helmig D, Thompson CR, Evans J, Boylan P, Hueber J, Park J-H. 2014. Highly elevated atmospheric levels of volatile organic compounds in the Uintah Basin, Utah. Environ Sci Technol 48:4707–4715, *https://doi.org/10.1021/es405046r*.

Intergovernmental Panel on Climate Change (IPCC). 2021. Climate Change 2021: The Physical Science Basis. Available: *https://www.ipcc.ch/report/ar6/wg1*.

Irakulis-Loitxate I, Guanter L, Liu YN, Varon DJ, Maasakkers JD, Zhang Y, et al. 2021. Satellite-based survey of extreme methane emissions in the Permian basin. Sci Adv 7:eabf4507, *https://doi.org/10.1126/sciadv.abf4507*.

Johnston JE, Chau K, Franklin M, Cushing L. 2020. Environmental justice dimensions of oil and gas flaring in South Texas: disproportionate exposure among Hispanic communities. Environ Sci Technol 54:6289–6298, *https://doi.org/10.1021/acs.est.0c00410*.

Johnson MR, Tyner DR, Conley S, Schwietzke S, Zavala-Araiza D. 2017. Comparisons of airborne measurements and inventory estimates of methane emissions in the Alberta upstream oil and gas sector. Environ Sci Technol 51:13008–13017, *https://doi.org/10.1021/acs.est.7b03525*.

Jones NF, Pejchar L, Kiesecker JM. 2015. The energy footprint: how oil, natural gas, and wind energy affect land for biodiversity and the flow of ecosystem services. Bioscience 65:290–301, *https://doi.org/10.1093/biosci/biu224*.

Karion A, Sweeney C, Pétron G, Frost G, Hardesty M, Kofler J, et al. 2013. Methane emissions estimate from airborne measurements over a western United States natural gas field. Geophys Res Lett 40 4393–4397, *https://doi.org/10.1002/grl.50811*.

Kim K-H, Jahan SA, Kabir E, Brown RJC. 2013. A review of airborne polycyclic aromatic hydrocarbons (PAHs) and their human health effects. Environ Int 60:71–80, *https://doi.org/10.1016/j.envint.2013.07.019*.

Knighton WB, Herndon SC, Wood EC, Fortner EC, Onasch TB, Wormhoudt J, et al. 2012. Detecting fugitive emissions of 1,3-butadiene and styrene from a petrochemical facility: an application of a mobile laboratory and a modified proton transfer reaction mass spectrometer. Indust Engineer Chem Res 51:12706–12711, *https://doi.org/10.1021/ie202794j*.

Kort EA, Frankenberg C, Costigan KR, Lindenmaier R, Dubey MK, Wunch D. 2014. Four corners: the largest US methane anomaly viewed from space. Geophys Res Lett 416898–6903, *https://doi.org/10.1002/2014GL061503*.

Lal S, Patil RS. 2001. Monitoring of atmospheric behaviour of NO_x from vehicular traffic. Environ Monit Assess 68:37–50, *https://doi.org/10.1023/A:1010730821844*.

Lan X, Talbot R, Laine P, Torres A. 2015. Characterizing fugitive methane emissions in the Barnett Shale area using a mobile laboratory. Environ Sci Technol 49:8139–8146, *https://doi.org/10.1021/es5063055*.

Lavoie TN, Shepson PB, Cambaliza MOL, Stirm BH, Conley S, Mehrota S, et al. 2017. Spatiotemporal variability of methane emissions at oil and natural gas operations in the Eagle Ford Basin. Environ Sci Technol 51:8001–8009, *https://doi.org/10.1021/acs.est.7b00814*.

Lekinwala NL, Bhushan M. 2022. Generalised non-negative matrix factorisation for air pollution source apportionment. Sci Total Environ 839:156294, *https://doi.org/10.1016/j.scitotenv.2022.156294*.

Leventhall G, Pelmear P, Benton S. 2003. A review of published research on low-frequency noise and its effects. *http://www.defra.gov.uk/environment/noise/research/lowfrequency/pdf/lowfreqnoise.pdf* [accessed 3 February 2025].

Li L, Blomberg AJ, Spengler JD, Coull BA, Schwartz JD, Koutrakis P. 2020. Unconventional oil and gas development and ambient particle radioactivity. Nature Commun 11:5002, *https://doi.org/10.1038/s41467-020-18226-w*.

Lim GQ, Matin M, John K. 2019. Spatial and temporal characteristics of ambient atmospheric hydrocarbons in an active shale gas region in North Texas. Sci Total Environ 656: 347–363, *http://dx.doi.org/10.1016/j.scitotenv.2018.11.313*.

Lu X, Yao T, Li Y, Fung JCH, Lau AKH. 2016. Source apportionment and health effect of NO_x over the Pearl River Delta region in Southern China. Environ Pollut 212:135–146, *https://doi.org/10.1016/j.envpol.2016.01.056*.

Lupo PJ, Langlois PH, Reefhuis J, Lawson CC, Symanski E, Desrosiers TA, et al. 2012. Maternal occupational exposure to polycyclic aromatic hydrocarbons: effects on gastroschisis among offspring in the National Birth Defects Prevention Study. Environ Health Perspect 120:910–915, *https://doi.org/10.1289/ehp.1104305*.

Lupo PJ, Symanski E, Waller DK, Chan W, Langlois PH, Canfield MA, et al. 2011. Maternal exposure to ambient levels of benzene and neural tube defects among offspring: Texas, 1999-2004. Environ Health Perspect 119:397–402, *https://doi.org/10.1289/ehp.1002212*.

Lyman SN, Mansfield ML, Tran HNQ, Evans JD, Jones C, O'Neil T, et al. 2018. Emissions of organic compounds from produced water ponds I: characteristics and speciation. Sci Total Environ 619–620:896–905, *https://doi.org/10.1016/j.scitotenv.2017.11.161*.

Lyon DR, Hmiel B, Gautam R, Omara M, Roberts KA, Barkley ZR, et al. 2021. Concurrent variation in oil and gas methane emissions and oil price during the COVID-19 pandemic. Atmos Chem Phys 21:6605–6626, *https://doi.org/10.5194/acp-21-6605-2021*.

Lyon DR, Zavala-Araiza D, Alvarez RA, Harriss R, Palacios V, Lan X, et al. 2015. Constructing a spatially resolved methane emission inventory for the Barnett shale region. Environ Sci Technol 49:8147–8157, *https://doi.org/10.1021/es506359c*.

Lyu C, Capps SL, Kurashima K, Henze DK, Pierce G, Hakami A, et al. 2021. Evaluating oil and gas contributions to ambient nonmethane hydrocarbon mixing ratios and ozone-related metrics in the Colorado Front Range. Atmos Environ 246:118113, *https://doi.org/https://https://doi.org.org/10.1016/j.atmosenv.2020.118113*.

Ma L, Hurtado A, Eguilior S, Llamas Borrajo JF. 2024. Acute and chronic risk assessment of BTEX in the return water of hydraulic fracturing operations in Marcellus Shale. Sci Total Environ 906:167638, *https://doi.org/10.1016/j.scitotenv.2023.167638*.

Marsavin A, Pan D, Pollack IB, Zhou Y, Sullivan AP, Naimie LE, et al. 2024. Summertime ozone production at Carlsbad Caverns National Park, New Mexico: influence of oil and natural gas development. J Geophys Res 129:e2024JD040877, *https://https://doi.org.org/10.1029/2024JD040877*.

McDuffie EE, Edwards PM, Gilman JB, Lerner BM, Dubé WP, Trainer M, et al. 2016. Influence of oil and gas emissions on summertime ozone in the Colorado Northern Front Range. J Geophys Res 121:8712–8729, *https://doi.org/10.1002/2016JD025265*.

McKenzie LM, Allshouse WB, Burke T, Blair BD, Adgate JL. 2016. Population size, growth, and environmental justice near oil and gas wells in Colorado. Environ Sci Technol 50:11471–11480, *https://doi.org/10.1021/acs.est.6b04391*.

McKenzie LM, Allshouse WB, Daniels S. 2019. Congenital heart defects and intensity of oil and gas well site activities in early pregnancy. Environ Int 132:104949, *https://doi.org/10.1016/j.envint.2019.104949*.

McKenzie LM, Guo R, Witter RZ, Savitz DA, Newman LS, Adgate JL. 2014. Birth outcomes and maternal residential proximity to natural gas development in rural Colorado. Environ Health Perspect 122:412–417, *https://doi.org/10.1289/ehp.1306722*.

Miller SM, Wofsy SC, Micalak AM, Kort EA, Andrews AE, Biraud SC, et al. 2013. Anthropogenic emissions of methane in the United States. Proc Natl Acad Sci USA 110:20018–20022, *https://doi.org/10.1073/pnas.1314392110*.

Modi M, Kimura Y, Ruiz LH, Allen DT. 2024. Fine scale spatial and temporal allocation of NO_x emissions from unconventional oil and gas development can result in increased predicted regional ozone formation. ACS EST Air, 2:130–140, *https://doi.org/10.1021/acsestair.4c00077*.

Moore CW, Zielinska B, Petron G, Jackson RB. 2014. Air impacts of increased natural gas acquisition, processing, and use: a critical review. Environ Sci Technol 48:8349–8359, *https://doi.org/10.1021/es4053472*.

Nazaroff WW. 1992. Radon transport from soil to air. Rev Geophys 30:137–160, *https://doi.org/10.1029/92RG00055*.

Oltmans SJ, Cheadle LC, Helmig D, Angot H, Pétron G, Montzka SA, et al. 2021. Atmospheric oil and natural gas hydrocarbon trends in the Northern Colorado Front Range are notably smaller than inventory emissions reductions. Elementa (Wash DC) 9:00136, *https://doi.org/10.1525/elementa.2020.00136*.

Omara M, Zavala-Araiza D, Lyon DR, Hmiel B, Roberts KA, Hamburg SP. 2022. Methane emissions from US low production oil and natural gas well sites. Nat Commun 13:2085, *https://doi.org/10.1038/s41467-022-29709-3*.

Omara M, Zimmerman N, Sullivan MR, Li X, Ellis A, Cesa R, et al. 2018. Methane emissions from natural gas production sites in the United States: data synthesis and national estimate. Environ Sci Technol 52:12915–12925, *https://doi.org/10.1021/acs.est.8b03535*.

Pan D, Pollack IB, Sive BC, Marsavin A, Naimie LE, Benedict KB, et al. 2023. Source characterization of volatile organic compounds at Carlsbad Caverns National Park. J Air Waste Manag Assoc 73:914–929, *https://doi.org/10.1080/10962247.2023.2266696*.

Peischl J, Karion A, Sweeney C, Kort EA, Smith ML, Brandt AR, et al. 2016. Quantifying atmospheric methane emissions from oil and natural gas production in the Bakken shale region of North Dakota. J Geophys Res 121:6101–6111, *https://doi.org/10.1002/2015JD024631*.

Peischl J, Ryerson TB, Aikin KC, de Gouw JA, Gilman JB, Holloway JS, et al. 2015. Quantifying atmospheric methane emissions from the Haynesville, Fayetteville, and Northeastern Marcellus shale gas production regions. J Geophys Res 120:2119–2139, *https://doi.org/10.1002/2014JD022697*.

Pekney NJ, Davidson CI, Zhou L, Hopke PK. 2006. Application of PSCF and CPF to PMF-modeled sources of PM2.5 in Pittsburgh. Aerosol Sci Technol 40:952–961, *https://doi.org/10.1080/02786820500543324*.

Pollack IB, Pan D, Marsavin A, Cope EJ, Juncosa Calahorrano J, Naimie L, et al. 2023. Observations of ozone, acyl peroxy nitrates, and their precursors during summer 2019 at Carlsbad Caverns National Park, New Mexico. J Air Waste Manag Assoc 73:951–968, *https://doi.org/10.1080/10962247.2023.2271436*.

Pozzer A, Schultz MG, Helmig D. 2020. Impact of US oil and natural gas emission increases on surface ozone is most pronounced in the central United States. Environ Sci Technol 54:12423–12433, *https://doi.org/10.1021/acs.est.9b06983*.

Radtke C, Autenrieth DA, Lipsey T, Brazile WJ. 2017. Noise characterization of oil and gas operations. J Occup Environ Hyg 14:659–667, *https://doi.org/10.1080/15459624.2017.1316386*.

Rich AL, Orimoloye HT. 2016. Elevated atmospheric levels of benzene and benzene-related compounds from unconventional shale extraction and processing: human health concern for residential communities. Environ Health Insights 10:75–82, *https://doi.org/10.4137/EHI.S33314*.

Robertson AM, Edie R, Field RA, Lyon D, McVay R, Omara M, et al. 2020. New Mexico Permian basin measured well pad methane emissions are a factor of 5–9 times higher than US EPA estimates. Environ Sci Technol 54:13926–13934, *https://doi.org/10.1021/acs.est.0c02927*.

Robertson AM, Edie R, Snare D, Soltis J, Field RA, Burkhart MD, et al. 2017. Variation in methane emission rates from well pads in four oil and gas basins with contrasting production volumes and compositions. Environ Sci Technol 51:8832–8840, *https://doi.org/10.1021/acs.est.7b00571*.

Roohani YH, Roy AA, Heo J, Robinson AL, Adams PJ. 2017. Impact of natural gas development in the Marcellus and Utica shales on regional ozone and fine particulate matter levels. Atmos Environ 155:11–20, *https://doi.org/10.1016/j.atmosenv.2017.01.001*.

Rossabi S, Helmig D. 2018. Changes in atmospheric butanes and pentanes and their isomeric ratios in the continental United States. J Geophys Res 123:3772–3790, *https://doi.org/10.1002/2017JD027709*.

Sablan OM, Schade GW, Holliman J. 2020. Passively sampled ambient hydrocarbon abundances in a Texas oil patch. Atmosphere 11:241, *https://doi.org/10.3390/atmos11030241*.

Schade GW, Heienickle EN. 2023. Passive hydrocarbon sampling in a shale oil and gas production area shows spatially heterogeneous air toxics exposure based on type and proximity to emission sources. Atmosphere 14:744, *https://doi.org/10.3390/atmos14040744*.

Schade GW, Roest G. 2016. Analysis of non-methane hydrocarbon data from a monitoring station affected by oil and gas development in the Eagle Ford shale, Texas. Elementa (Wash DC) 4:000096, *https://doi.org/10.12952/journal.elementa.000096*.

Schade GW, Roest G. 2018. Source apportionment of non-methane hydrocarbons, NO_x and H_2S data from a central monitoring station in the Eagle Ford shale, Texas. Elementa (Wash DC) 6:35, *https://doi.org/10.1525/elementa.289*.

Smith ML, Kort EA, Karion A, Sweeney C, Herndon SC, Yacovitch TI. 2015. Airborne ethane observations in the Barnett Shale: quantification of ethane flux and attribution of methane emissions. Environ Sci Technol 49:8158–8166, *https://doi.org/10.1021/acs.est.5b00219*.

Sorrels J, Coburn J. 2019. EPA Air Pollution Control Cost Manual, Chapter 1: Flares. 71.

Srivastava D, Saksakulkrai S, Acton WJF, Rooney DJ, Hall J, Hou S, et al. 2025. Comparative receptor modelling for the sources of fine particulate matter ($PM_{2.5}$) at urban sites in the UK. Atmos Environ 343:120963, *https://doi.org/10.1016/j.atmosenv.2024.120963*.

Swarthout RF, Russo RS, Zhou Y, Hart AH, Sive BC. 2013. Volatile organic compound distributions during the NACHTT campaign at the Boulder Atmospheric Observatory: influence of urban and natural gas sources. J Geophys Res 118:10,614–10,637, *https://doi.org/10.1002/jgrd.50722*.

Thompson CR, Hueber J, Helmig D. 2014. Influence of oil and gas emissions on ambient atmospheric non-methane hydrocarbons in residential areas of Northern Colorado. Elementa (Wash DC) 2:1–17, *https://doi.org/10.12952/journal.elemanta.000035*.

Turner AJ, Jacob DJ, Benmergui J, Wofsy SC, Maasakkers JD, Butz A, et al. 2016. A large increase in US methane emissions over the past decade inferred from satellite data and surface observations. Geophys Res Lett 43:2218–2224, *https://doi.org/10.1002/2016GL067987*.

US Energy Information Administration. 2018. Petroleum & Other Liquids: Crude Oil Production. *https://www.eia.gov/petroleum/data.php*.

US Energy Information Administration. 2020. US Natural Gas Gross Withdrawals (Million Cubic Feet). *https://www.eia.gov/dnav/ng/hist/n9010us2m.htm* [accessed 16 October 2020].

US Environmental Protection Agency (US EPA). 2022. Ambient concentrations of selected air toxics. Available: *https://cfpub.epa.gov/roe/indicator.cfm?i=90#4* [accessed 21 May 2025].

US Environmental Protection Agency (US EPA). 2025. 40 CFR Part 50, Appendix U — Interpretation of the Primary and Secondary National Ambient Air Quality Standards for Ozone. Available: *https://www.ecfr.gov/current/title-40/chapter-I/subchapter-C/part-50/appendix-Appendix%20U%20to%20Part%2050*.

United States Geological Survey (USGS). 1993. Geologic radon potential of EPA Region 6, Arkansas, Louisiana, New Mexico, Oklahoma, and Texas. *https://doi.org/10.3133/ofr93292F*.

Varon DJ, Jacob JD, Hmiel B, Lyon DR, Omara M, Sulprizio M, et al. 2023. Continuous weekly monitoring of methane emissions from the Permian Basin by inversion of TROPOMI satellite observations. Atmos Chem Phys 23:7503–7520, *http://dx.doi.org/10.5194/acp-23-7503-2023*.

Vaughn TL, Bell CS, Pickering CK, Schwietzke S, Heath GA, Pétron G, et al. 2018. Temporal variability largely explains top-down/bottom-up difference in methane emission estimates from a natural gas production region. Proc Natl Acad Sci USA 115:11712–11717, *https://doi.org/10.1073/pnas.1805687115*.

Vinciguerra T, Yao S, Dadzie J, Chittams A, Deskins T, Ehrman S, et al. 2015. Regional air quality impacts of hydraulic fracturing and shale natural gas activity: evidence from ambient VOC observations. Atmos Environ 110:144–150, *https://doi.org/10.1016/j.atmosenv.2015.03.056*.

Vogt J, Laforest J, Argento M, Kennedy S, Bourlon E, Lavoie M, et al. 2022. Active and inactive oil and gas sites contribute to methane emissions in Western Saskatchewan, Canada. Elementa (Wash DC) 10:00014, *https://doi.org/10.1525/elementa.2022.00014*.

Weyant CL, Shepson PB, Subramanian R, Cambaliza MOL, Heimburger A, McCabe D, et al. 2016. Black carbon emissions from associated natural gas flaring. Environ Sci Technol 50:2075–2081, *https://doi.org/10.1021/acs.est.5b04712*.

Williams BJ, Goldstein AH, Kreisberg NM, Hering SV, Worsnop DR, Ulbrich IM, et al. 2010. Major components of atmospheric organic aerosol in Southern California as determined by hourly measurements of source marker compounds. Atmos Chem Phys 10:11577–11603, *https://doi.org/10.5194/acp-10-11577-2010*.

Willis MD, Carozza SE, Hystad P. 2023. Congenital anomalies associated with oil and gas development and resource extraction: a population-based retrospective cohort study in Texas. J Expo Sci Environ Epidemiol 33:84–93, *https://doi.org/10.1038/s41370-022-00505-x*.

World Health Organization (WHO). 1979. Environmental Health Criteria 13: Carbon Monoxide. Available: *https://iris.who.int/bitstream/handle/10665/336055/9241540737-eng.pdf*.

Yacovitch TI, Herndon SC, Pétron G, Kofler J, Lyon D, Zahniser MS, et al. 2015. Mobile laboratory observations of methane emissions in the Barnett Shale Region. Environ Sci Technol 49:7889–7895, *https://doi.org/10.1021/es506352j*.

Yin X, Fallah-Shorshani M, McConnell R, Fruin S, Franklin M. 2020. Predicting fine spatial scale traffic noise using mobile measurements and machine learning. Environ Sci Technol 54:12860–12869, *https://doi.org/10.1021/acs.est.0c01987*.

Zaimes GG, Littlefield JA, Augustine DJ, Cooney G, Schwietzke S, George FC, et al. 2019. Characterizing regional methane emissions from natural gas liquid unloading. Environ Sci Technol 53:4619–4629, *https://doi.org/10.1021/acs.est.8b05546*.

Zavala-Araiza D, Lyon DR, Alvarez RA, Davis KJ, Harriss R, Herndon SC, et al. 2015. Reconciling divergent estimates of oil and gas methane emissions. Proc Natl Acad Sci USA 112:15597–15602, *https://doi.org/10.1073/pnas.1522126112*.

Zavala-Araiza D, Sullivan DW, Allen DT. 2014. Atmospheric hydrocarbon emissions and concentrations in the Barnett Shale natural gas production region. Environ Sci Technol 48:5314–5321, *https://doi.org/10.1021/es405770h*.

Zhang Y, Gautam R, Pandey S, Omara M, Maasakkers JD, Sadavarte P, et al. 2020. Quantifying methane emissions from the largest oil-producing basin in the United States from space. Sci Adv 6:eaaz5120, *https://doi.org/https://doi.org/10.1126/sciadv.aaz5120*.

Zhang YZ, Gautam R, Zavala-Araiza D, Jacob DJ, Zhang RX, Zhu L, et al. 2019. Satellite-observed changes in Mexico's offshore gas flaring activity linked to oil/gas regulations. Geophys Res Lett 46:1879–1888, *https://doi.org/10.1029/2018gl081145*.

HEI QUALITY ASSURANCE STATEMENT

The conduct of this study was subjected to independent audits by RTI International staff members Dr. David Wilson, Dr. Charbel Harb, and Mr. Ryan Chartier. These staff members are experienced in quality assurance (QA) oversight for air quality monitoring, modeling, exposure assessment, and statistical modeling.

The QA oversight program consisted of a remote audit of the draft final report, the edited final report, and the data processing steps. Key details of the dates of the audit and the reviews performed are listed below.

Audit: Final Remote Audit

Date: March 2025 – April 2025

Remarks: The final remote audit consisted of two parts: (1) review of the final project report and (2) audit of data processing steps. The review of the final report focused on ensuring that the methods are well documented and the report is easy to understand. The review also examined whether the report highlighted key study findings and whether limitations were supported by the data presented.

The data audit included a review of the datasets and codes for data reduction, processing, and analysis, and comparison of the data outputs with reported data. This portion of the audit was restricted to the key components of the study and associated findings. Selected codes for air quality data reduction and modeling were sent to RTI for review.

The codes were reviewed at RTI to verify, to the extent feasible, linkages between the various scripts; confirmation of the models and model variables reported; and verification of key tables, figures, and data outputs. The codes appear to be largely consistent with the models described in the report and follow the overall model development procedures described. The values themselves were verified by RTI using the data and scripts provided by the investigators.

Except for very few minor discrepancies, no major quality-related issues were identified from the review of the codes, data, and the report. Recommendations were made to address noted discrepancies and typographical errors, and included general edits for improved clarity. Those recommendations were addressed in the final version of the report.

A written report was provided to HEI. The QA oversight audit demonstrated that the study was conducted according to the study protocol. The final report appears to be representative of the study conducted.

David Wilson, PhD, Statistician, Quality Assurance Auditor

Charbel Harb, PhD, Environmental Scientist, Quality Assurance Auditor

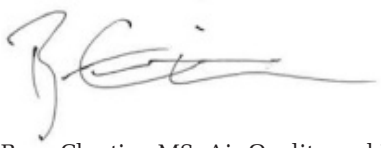

Ryan Chartier, MS, Air Quality and Exposure Scientist, Lead Quality Assurance Auditor

Date: June 11, 2025

SUPPLEMENTARY APPENDICES ON THE HEI WEBSITE

Supplementary Appendices A through C are not included in the main report but can be found on the report's web page at *https://www.healtheffects.org/publications*.

Appendix A: Additional Details on Aim 1, Stationary Sampling at Loving, New Mexico

Appendix B: Additional Details on Aim 2, Passive Sampling in the Permian Basin and Eagle Ford Shale

Appendix C: Additional Materials for Aim 3, Analysis of Satellite Flaring

ABOUT THE AUTHORS

Meredith Franklin holds a BSc in mathematics from McGill University in Montreal, Quebec, an MSc in statistics from the Ottawa-Carleton Institute of Mathematics and Statistics in Ottawa, Ontario, and a PhD in statistics and environmental health from the Harvard T.H. Chan School of Public Health in Boston, MA. She was a postdoc at the University of Chicago and Argonne National Laboratory and a faculty member in the Division of Biostatistics at the University of Southern California before moving to her current position as an associate professor in the Department of Statistical Sciences and the School of the Environment at the University of Toronto in Toronto, Ontario. Her research interests are at the intersection of data science, environment, and health, with a particular focus on developing statistical and machine learning approaches to synthesize multisource data for environmental exposure assessment to be used in epidemiological studies.

Detlev Helmig holds a chemistry diploma degree from the University of Bochum, Germany, and a PhD in environmental chemistry from the University of Duisburg, Germany. He conducted his postdoctoral research at the University of California Statewide Air Pollution Research Center in Riverside and the National Center for Atmospheric Research in Boulder, Colorado. He subsequently received an EPA Young Investigator Award and became a research professor at the University of Colorado. The core of his research is the study of air composition, air quality, atmospheric chemistry, composition changes, and atmospheric transport, with an emphasis

on local to regional air quality. Most recently, he became the founder and owner of Boulder AIR. Boulder AIR has been contracted by local governments to implement the monitoring of air quality indicators at several locations across the Colorado Front Range. Dr. Helmig led the development, deployment, and operation of the Loving stationary air monitoring station. This air monitoring builds on instrumental and data processing advancements that facilitate the real-time reporting of air pollutants at public websites. A particular goal is the assessment of the influence of oil and natural gas development on air quality and tracking atmospheric composition changes from the expansion of the industry and implementation of new policies in Colorado. Data have provided new insight into influences from oil and gas emissions on regional air quality and surface ozone. Dr. Helmig's research has resulted in some 250 peer-reviewed publications. He is the Editor-in-Chief of the Atmospheric Science Domain of the online, nonprofit journal *Elementa-Science of the Anthropocene* that is published by the University of California Press. In that role, he is overseeing the manuscript peer-review in several special features, such as "Oil and Natural Gas Development: Air Quality, Climate Science, and Policy," "Quantification of Urban Greenhouse Gas Emissions: The Indianapolis Flux Experiment," and "Reactive Gases in the Global Atmosphere" (*https://online.ucpress.edu/elementa/pages/specialfeatures*).

Gunnar Schade holds a chemistry diploma and a PhD from the University of Mainz in Germany. As a postdoctoral researcher for Dr. Allen Goldstein at UC Berkeley, he was in charge of an Ameriflux network site's VOC flux measurements in the Sierra Nevada of California from 1998 to 2002 before returning to Germany for a prestigious Emmy-Noether grant in 2003. After a brief 2-year stay at the University of Bremen from 2003 to 2005, he started a tenure-track position in the Atmospheric Sciences department at Texas A&M University in College Station. Now an associate professor, Dr. Schade worked on urban flux measurements of energy and trace gases, including hydrocarbons, at a unique tower site in Houston before switching to research on the impacts of the shale oil and gas boom in the United States on air quality in 2014. He was among the first to point out the potential impacts of oil and gas exploration-related emissions on ozone air quality in 2015, and has since completed a series of air quality measurements and analyses projects related to UOGD-related emissions in Texas.

Jill Johnston is an associate professor of environmental health and spatial sciences and the director of Community Engagement in Environmental Health at the University of Southern California. She completed her PhD in environmental sciences and engineering with a minor in public policy at the University of North Carolina, Chapel Hill. She conducted a postdoctoral research fellowship in environmental epidemiology. She conducts community-driven epidemiology and exposure assessment to address inequitable exposures to harmful contaminants that affect health disparities, including in Latinx, Black, and Asian Pacific Islander communities and among the working poor. Her research examines the community health impacts of upstream oil and gas extraction on vulnerable populations. She serves on the environmental justice advisory board for the South Coast Air Quality Management District and technical advisory panels on energy extraction and climate, the City of Los Angeles, the Los Angeles Department of Public Health, and the State of California.

Lara Cushing is an associate professor in environmental health sciences and the Fielding Presidential Chair in Health Equity at the University of California, Los Angeles. She completed her PhD in energy and resources and MPH in epidemiology at the University of California, Berkeley. Her research focuses on social disparities in exposure to environmental health hazards and has investigated questions of environmental justice in the context of exposure to air pollution, synthetic chemicals, oil and gas development, drinking water quality, extreme heat, and sea level rise. She has assessed the health consequences of environmental and climate-related exposures for pregnant women and infants, including risks of adverse birth outcomes associated with living near oil and gas development in California and Texas. She was involved with the development of CalEnviroScreen, a screening tool developed by the California Environmental Protection Agency to identify communities disproportionately impacted by environmental health hazards in California, and was a contributing author to the Fourth Assessment Report of the UN Intergovernmental Panel on Climate Change (IPCC). She is the recipient of an EPA STAR graduate student fellowship, a former Environmental Fellow of the Robert & Patricia Switzer Foundation, and a JPB Environmental Health Fellow through the Harvard T.H. Chan School of Public Health.

OTHER PUBLICATIONS RESULTING FROM THIS RESEARCH

POSTERS

Schade GW, Helmig D, Johnston J, Cushing L, Caulder E, Franklin M. Poster GH41C-2716. Passive Sampling Derived Toxic Hydrocarbon Abundances Across a New Mexico Frontline Community in the Permian-Delaware Oil and Gas Production Basin. AGU24, Washington DC, 9–13 December 2024.

Franklin M, Wu J, Johnston J, Cushing L, Schade GW, Helmig D. Poster GH41D-2729. Health, Air Pollution, and Environmental Justice Impacts of Oil and Gas Flaring in the Permian Basin. AGU24, Washington DC, December 9–13, 2024.

Schade GW, Helmig D, Caputi D, Franklin M, Greenberg G, Dali R, et al. Poster A23B-1971. Southeast New Mexico Has Become the Second Most Ozone-Polluted Region in the US due to Oil and Gas Emissions. AGU24, Washington DC, December 9–13, 2024.

Greenberg G, Helmig D, Caputi D, Cushing L, Daly R, Darby L, et al. Poster GC51T-0229. Highly Elevated Atmospheric Methane from Oil and Natural Gas Emissions in Loving, NM. AGU24, Washington DC, December 9–13, 2024.

Sung D, Zhai S, Deveraux E, Lin CH, Turner, Konon K, et al. Poster A23B-1968. Novel Spatiotemporal Measurements of Volatile Organic Compounds and Trace Gases in the Permian Basin. AGU24, Washington DC, December 9–13, 2024.

PRESENTATION

Helmig D, Potter KE, Caputi D, Cushing L, Daly R, Darby LS, et al. 2024. Presentation A42E-02. Atmospheric Radioactivity in Loving, NM, and Its Relationship to Oil and Natural Gas Development in the Permian Basin. AGU24, Washington DC, December 9–13, 2024.

Research Report 231, *Assessing Source Contributions to Air Quality and Noise in Unconventional Oil Shale Plays*, M. Franklin et al.

INTRODUCTION

The scale and rate of onshore oil and natural gas development in the United States since the early 2000s differ markedly from earlier periods due to technological changes involving increased use of hydraulic fracturing and horizontal drilling. Although hydraulic fracturing has captured much public attention, the process itself is not new. Neither is horizontal drilling, the extraction of oil and gas from unconventional formations such as tight (i.e., low permeability) sandstone and shale. What is new is the use of high-volume multistage hydraulic fracturing that uses millions of gallons of water per well, combined with horizontal drilling that can extend thousands of m in length.

Unconventional oil and natural gas development (UOGD*), the development and production of oil and natural gas through multistage hydraulic fracturing in horizontal wells, has been associated with a wide range of potential exposures to chemicals (e.g., radioactive material, those found in the wastewater, and odorous compounds) and nonchemical agents (e.g., noise, light, and vibration). The rapid expansion of this development has caused concerns about its potential effects on human health and has created knowledge gaps about exposures that must be addressed to better understand potential impacts on health.

In August 2020, HEI Energy issued Request for Applications *E20-1*, Community Exposures Associated with Unconventional Oil and Natural Gas Development. HEI sought to fund studies that would apply a combination of approaches to quantify the spatial and temporal variability in population exposures to UOGD-generated outdoor air pollutants and noise (see Preface).

Dr. Franklin at the University of Southern California† and colleagues proposed to address critical research needs by improving the spatial and temporal characterization of UOGD-related air pollution, radioactivity, and noise in oil-producing regions via stationary, passive, and satellite monitoring, along with modeling that could be leveraged to ultimately assess human health exposures. The HEI Energy Research Committee recommended the study for funding because it had several strong features. In particular, the blending of a variety of sampling methods using state-of-the-art instruments would result in a robust dataset with information on the variability of ambient chemical concentrations over space and time. Moreover, the data could be used in future health studies. Franklin had assembled a strong team with demonstrated air quality measurement expertise and connections to communities in the study areas.

This Commentary provides the HEI Energy Review Committee's evaluation of the study. It is intended to aid the sponsors of HEI and the public by highlighting the study's strengths and limitations and placing the results presented in the Investigators' Report in a broader scientific and regulatory context.

SCIENTIFIC AND REGULATORY BACKGROUND

UOGD OVERVIEW

UOGD processes occur on and off the well pad and include

- **field development:** exploration, pad preparation, vertical and horizontal drilling, well completion (casing and cementing, perforating, acidizing, hydraulic fracturing, flowback [the fluid mixture of injected water, sand, and chemicals and the natural brines from rock that returns to the surface after a well has been hydraulically fractured], and well testing) in preparation for production and management of wastes
- **production operations:** extraction, gathering, processing, and field compression of gas; extraction and processing of oil and natural gas condensates (byproducts of gas production that include organic compounds that condense from a gas phase into a liquid form); management of wastes and produced water that is naturally present in underground water formations in the soil and brought to the surface during oil and gas extraction; and construction and operation of field production facilities
- **postproduction:** well closure and land reclamation.

Some UOGD operations are regulated at the federal level under the Clean Air Act, the Clean Water Act, and the Safe Drinking Water Act, while state authorities play a major role

Dr. Meredith Franklin's 2-year study, "Assessing Source Contributions to Air Quality and Noise in Unconventional Oil Shale Plays," began in February 2022. Total expenditures were $1,203,523. The draft Investigators' Report from Franklin and colleagues was received for review in February 2025 and accepted by the HEI Energy Review Committee in April 2025.

During the review process, the HEI Energy Review Committee and the investigators had the opportunity to exchange comments and clarify issues in both the Investigators' Report and the Review Committee's Commentary. This Commentary has not been reviewed by public or private party institutions, including those that support HEI Energy, and may not reflect the views of these parties; thus, no endorsements by them should be inferred.

* A list of abbreviations and other terms appears at the end of this report.

† Dr. Franklin is now based at the University of Toronto.

in governing UOGD more generally. UOGD-related rules vary among states, with some defining minimum setback distances between UOGD and specific land uses such as residences and schools to protect local populations.

UOGD PROCESSES

Different UOGD processes release air pollutants, noise, and light into the environment (e.g., outdoor air, soil, surface water, and groundwater) that are complex and highly variable. These releases and resulting human exposures are caused by numerous UOGD process-related factors, including variation in operator practices and regulatory requirements. Releases can also happen due to accidental spills and leaks. The level of UOGD activity can vary widely between and across regions and over time in response to fluctuating market conditions.

The well pad preparation phase involves land clearing and other activities similar to many other types of construction. Various chemicals are used to drill, develop, and complete the well. The completion step often includes the process of hydraulic fracturing. Following hydraulic fracturing, pressure is released and the injected fluids, along with natural brines in the source rock, flowback to the surface during a period referred to as flow or flowback (Guarnone et al. 2012). Once a well is completed, it enters the production phase during which fluids continue to flowback to the surface, with the composition of the fluids increasingly dominated by natural brines over time. This fluid is commonly referred to as produced water and must be managed properly along with flowback, drilling muds, and other wastes.

During the development of a well or production, exposures can be associated with vehicle exhaust and emissions from various types of equipment (e.g., compressors).

UOGD EMISSIONS AND TRANSPORT PATHWAYS

UOGD processes can release methane, volatile organic compounds (VOCs), and other pollutants of concern to human health. UOGD emissions to air can occur on or off well pads and originate from equipment and other points and mobile sources, or releases (e.g., leaks, venting from storage tanks, or volatilization from surface spills). The unloading of liquids can be an important source of emissions; this process involves clearing liquids (i.e., water and liquid hydrocarbons) that have accumulated in mature gas wells and that can slow or even halt gas production. Flaring of natural gas is a major source of emissions in some oil-producing regions where gas is produced along with oil, but insufficient infrastructure is available to transport and sell the gas. For this and other reasons (e.g., safety), natural gas is sometimes burned on-site (i.e., flared).

Chemicals that have been released into the environment then disperse and can react in the atmosphere, leading to widely varying concentrations and potential exposures at local and regional scales (Allen 2014; Bell et al. 2017; Mitchell et al. 2015; Vaughn et al. 2018; Zavala-Araiza et al. 2015). A few studies have used air quality monitoring data or modeling to address regulatory needs, such as assessing setback distances between UOGD and residences (Banan and Gernand 2018; Garcia-Gonzales et al. 2019; Haley et al. 2016; McCawley 2013).

UOGD EXPOSURE

A growing body of scientific literature exists about potential human exposures to a range of chemical and nonchemical agents (e.g., noise, light, and vibration) that can be associated with UOGD (Deziel et al. 2022; HEI Energy Research Committee 2019, 2020). While many of these studies provide valuable information for understanding population exposures, only a small group of studies have been conducted with the direct aim of estimating potential air pollution and noise exposures to UOGD (Allshouse et al. 2019; Maskrey et al. 2016; Paulik et al. 2018; Pennsylvania Department of Environmental Protection 2018). Knowledge gaps remain, however, about how these exposures potentially impact human health.

STUDY OBJECTIVES

The overarching objective of Dr. Franklin's study was to characterize air pollutants, greenhouse gas emissions, airborne radioactivity, and noise associated with UOGD in two shale production basins, the Permian Basin (eastern New Mexico and western Texas) and the Eagle Ford Shale (south-central Texas). These two production basins are among the most active drilling and oil production regions in the United States. Collectively, they have over 180,000 active wells that produce approximately 7 million barrels of oil and over 30 billion cubic feet of gas daily (*US Energy Information Administration*).

The investigators developed the following three aims:

1. Characterize the effect of UOGD activities on ambient air pollution, radioactivity, and noise by collecting high temporal resolution data from a stationary monitoring platform in the Permian Basin
2. Understand the spatial distributions of selected petroleum hydrocarbons in ambient air by leveraging a dense network of passive samplers in the Permian Basin and Eagle Ford Shale
3. Combine satellite observations with surface air pollution data to characterize the location and magnitude of flaring and its impact on air quality and radioactivity in the Permian Basin

To address Aim 1, Franklin and colleagues conducted sampling campaigns at a field laboratory located near an active UOGD well pad in the shale production field and at various locations in populated areas close to UOGD activities. At the field laboratory, they used a combination of continuous fixed-site monitoring instruments to identify UOGD processes that resulted in ambient air pollution, radioactivity, and

noise. This laboratory was operational in an area of active UOGD activity in the Permian Basin from May 1, 2023, to May 31, 2024. They measured approximately 30 different components, including 20 VOCs. They also compared their observations with measurements collected at other UOGD sites and in urban areas.

To address Aim 2, the investigators recruited local volunteers to deploy passive samplers for approximately 1 year at 12 locations in populated areas in the Permian Basin and Eagle Ford Shale. They coupled the resulting measurements of 15 hydrocarbons with data on meteorology and well density within about 10 kilometers (km) of the samplers to better understand the factors influencing UOGD-related exposures in the area and to inform future health studies.

Aim 3 of the study focused on flaring. This is a common waste disposal practice associated with oil and gas development, but its effect on air quality is not well characterized. To address this question, the investigators used remote sensing observations of heat sources to identify locations and timing of UOGD-related flaring. They combined these observations with the stationary data of flaring emissions to identify exposures related specifically to flaring.

SUMMARY OF METHODS AND STUDY DESIGN

Aim 1: Stationary Monitoring at a Field Laboratory to Characterize the Effect of UOGD Activities on Ambient Air Pollution, Radioactivity, and Noise

Franklin and colleagues obtained a year's worth of detailed data on meteorology, air pollutant concentrations, noise, and radioactivity at a location directly associated with UOGD activity. An oil and gas operator in Loving, New Mexico, permitted the investigators to install a field laboratory on its property. This stationary field laboratory (i.e., a mobile trailer) was installed in April 2023 and was in continuous operation from May 1, 2023, through May 31, 2024. The laboratory included meteorological sensors for wind conditions, temperature, relative humidity, rainfall, barometric pressure, and solar radiation, and inlets for ambient air that led to instruments inside the trailer. They measured airborne radioactivity as alpha radiation, both in the gas phase and on a filter collecting airborne particles.

Gas analyzer instruments for measuring ozone, methane, carbon dioxide, carbon monoxide, hydrogen sulfide, sulfur dioxide, and nitrogen oxides were located inside the station. They also measured approximately 20 VOCs with a custom-made gas chromatograph. All instruments collected data continuously at 1-minute time resolution or were averaged to 1-minute intervals, except radioactivity and the VOCs, which were measured over a 10-minute interval once every hour. The data were logged automatically to a computer inside the station and were accessible remotely. **Commentary Table 1** provides an overview of all the components and how they were measured.

The investigators compiled descriptive statistics for all components measured at the station and calculated correlations between selected hydrocarbons. They also compared the Permian Basin observations with measurements collected at five sites in the Denver Julesburg Basin — a large oil- and gas-producing basin that extends through Colorado, Wyoming, Nebraska, and Kansas — that were in operation at the same time.

They monitored sound pressure levels using a unidirectional microphone, a preamplifier, and a main processor. This instrument was positioned on a tower above the laboratory at a height of 4 meters (m). The instrument was able to compute A-weighted (i.e., midfrequencies that are audible by humans) and C-weighted noise levels, which reflect overall loudness. C-weighted noises can cause vibrations and travel greater distances than A-weighted noises.

The investigators leveraged these high temporal resolution noise and air quality data to quantify potential sources of noise associated with specific UOGD activities. Flaring is known to produce sporadic, rapid pressure fluctuations, whereas drilling or truck traffic might produce more frequent, continuous noise levels. To analyze this, they followed an approach they had used previously, using extreme gradient boosting (a machine learning algorithm) to identify sources of air pollution associated with specific frequencies of noise (Fallah-Shorshani et al. 2024). The investigators also used non-negative matrix factorization (NMF) to identify and quantify sources of the various emissions. The goal of NMF is to simplify complex data into a smaller set of factors that collectively explain much of the variance in the underlying data. In this case, the factors are intended to represent sources of UOGD emissions. Here, the investigators included 26 components in the input matrix (i.e., all measured VOCs, sulfur dioxide, hydrogen sulfide, carbon monoxide, carbon dioxide, methane, and nitrogen oxides).

Aim 2: Passive Sampling to Describe Patterns of Petroleum Hydrocarbons in Ambient Air in Populated Areas Close to UOGD Activity

Franklin and colleagues observed patterns of petroleum hydrocarbons at a dozen locations near UOGD activities and populated areas. They recruited local volunteers to help deploy a network of seven passive hydrocarbon sampling stations in the Carlsbad–Loving, New Mexico, region and five in the Texas Eagle Ford Shale area. The Permian Basin stations were installed at different times between the spring of 2023 and summer 2024, with some in operation for a full year. Most were located on private property with the owners' permission; one was next to the main field laboratory described earlier. The Eagle Ford stations were installed in summer 2024 and operated for half a year. Four stations were located across the shale area in Karnes County, and another was located in College Station, Texas, which was considered an urban reference station. The Eagle Ford network covered a 10 km × 27 km area, with the College Station sampler located about 240 km away.

Commentary Table 1. Components Measured at a UOGD Field Laboratory, Instruments Used, and Summary Statistics[a]

Measurement	Unit	Instrument	Annual Mean	Standard Deviation	Minimum	Median	Maximum
Carbon Dioxide CO_2	ppm	PICARRO G2301	432.06	8.67	412.78	430.03	554.01
Methane CH_4	ppb	PICARRO G2301	2,667.62	1,305.26	1,918.60	2,283.10	139,140.00
Carbon Monoxide CO	ppb	Thermo Scientific 48C	170.49	99.40	20.00	149.90	10,420.00
Ethane C_2H_6	ppb	Agilent 6890 TD-GC-FID	93.68	133.08	0.78	43.92	2,060.00
Ethene (Ethylene) C_2H_4	ppb	Agilent 6890 TD-GC-FID	0.74	0.85	0.01	0.47	16.97
Propane C_3H_8	ppb	Agilent 6890 TD-GC-FID	58.22	80.75	0.22	27.88	1,211.00
Propene (Propylene) C_3H_6	ppb	Agilent 6890 TD-GC-FID	0.15	0.18	0.01	0.09	5.53
1,3-Butadiene C_4H_6	ppb	Agilent 6890 TD-GC-FID	0.01	0.02	0.01	0.01	1.21
i-Butane (Isobutane) C_4H_{10}	ppb	Agilent 6890 TD-GC-FID	10.15	15.81	0.03	4.58	376.60
n-Butane C_4H_{10}	ppb	Agilent 6890 TD-GC-FID	26.23	39.39	0.06	11.91	536.90
Acetylene C_2H_2	ppb	Agilent 6890 TD-GC-FID	0.56	0.57	0.02	0.37	13.69
Cyclopentane C_5H_{10}	ppb	Agilent 6890 TD-GC-FID	0.53	0.73	0.01	0.25	13.46
i-Pentane (Isopentane) C_5H_{12}	ppb	Agilent 6890 TD-GC-FID	7.91	11.88	0.02	3.50	215.90
n-Pentane C_5H_{12}	ppb	Agilent 6890 TD-GC-FID	8.98	13.58	0.02	3.90	258.80
n-Hexane C_6H_{14}	ppb	Agilent 6890 TD-GC-FID	2.96	4.51	0.02	1.25	93.36
Isoprene C_5H_8	ppb	Agilent 6890 TD-GC-FID	0.01	0.01	0.01	0.01	0.40
n-Heptane C_8H_{18}	ppb	Agilent 6890 TD-GC-FID	1.09	1.63	0.00	0.46	37.25
Benzene C_6H_6	ppb	Agilent 6890 TD-GC-FID	0.67	0.82	0.01	0.35	12.26
n-Octane C_8H_{18}	ppb	Agilent 6890 TD-GC-FID	0.35	0.48	0.00	0.16	8.87
Toluene $C_6H_5CH_3$	ppb	Agilent 6890 TD-GC-FID	0.65	0.81	0.00	0.32	11.07
Ethylbenzene $C_6H_5C_2H_5$	ppb	Agilent 6890 TD-GC-FID	0.06	0.07	0.00	0.03	0.94
m&p-Xylene $C_6H_4(CH_3)_2$	ppb	Agilent 6890 TD-GC-FID	0.22	0.30	0.00	0.10	5.25
o-Xylene $C_6H_4(CH_3)_2$	ppb	Agilent 6890 TD-GC-FID	0.08	0.10	0.00	0.04	1.19
Ozone O_3	ppb	Thermo Scientific 49C	33.25	21.28	0.50	33.15	112.30
Nitrogen Oxide NO	ppb	Teledyne T200UP	5.08	20.04	0.03	0.39	1,204.00
Nitrogen Dioxide NO_2	ppb	Teledyne T200UP	9.64	9.70	0.03	6.32	335.60
Nitrogen Oxides NO_x	ppb	Teledyne T200UP	14.62	25.00	0.03	7.34	1,382.00
Hydrogen Sulfide H_2S	ppb	Teledyne T101	1.02	1.14	0.20	0.73	78.65
Sulfur Dioxide SO_2	ppb	Teledyne T101	0.37	0.45	0.20	0.20	12.61
Gas Radioactivity Rn-222, Rn-220	Bq m^{-3}	AlphaGUARD/Alpha PM	19.77	13.71	1.00	17.07	173.20
Particle Radioactivity	Bq m^{-3}	AlphaGUARD/Alpha PM	9.59	9.45	1.00	7.00	98.51
Temperature	°C	METSENS500 multi-sensor, pyranometer	19.83	7.56	-11.10	20.23	43.09
Wind Speed	m s^{-1}	METSENS500 multi-sensor, pyranometer	3.50	2.29	0.03	3.01	23.60

Bq m^{-3} = Becquerel; FID = flame ionization detector; GC = gas chromatography; ppb = parts per billion; ppm = parts per million; TD = thermal desorption; UOGD = unconventional oil and gas development.

[a] Sampling was conducted over a 12-month period (May 2023 to May 2024) at a field laboratory located in Loving, New Mexico. Source: Investigators' Report Tables 1a and 2.

Each station consisted of a shepherd hook that supported an assembly holding two samplers with diffusion tubes and adsorption cartridges, covered with a shield to protect the samplers from rain and solar radiation. These instruments measured the following 15 hydrocarbons: the alkanes 2-methylpentane, 3-methylpentane, n-hexane, 2,4-dimethylpentane, 2-methylhexane, n-heptane, and n-octane; the naphthenes cyclohexane and methyl-cyclohexane; and the aromatics benzene, toluene, ethylbenzene, m-, o-, and p-xylene. Temperature data were also collected at four of the stations.

The samplers were exchanged weekly by a local volunteer and shipped to a laboratory in College Station, Texas, for analysis. The general approaches that the investigators followed for installing and operating these stations had been used in earlier studies (Schade and Heienickle 2023).

The investigators also compiled information from several state and commercial databases on nearby oil and gas wells, including location, type (i.e., horizontal, vertical, directional, unknown), status (e.g., active, inactive, permanently closed), and monthly oil and gas production rates. They used these data to identify the active wells and to determine the total oil and gas production during the sampling periods within 2-, 5-, and 10-km buffers around each passive sampling station and within 10 km of the larger, stationary station.

Aim 3: Combining Satellite Observations and Surface Air Pollution Data to Characterize Flaring and Its Effect on Air Quality and Radioactivity

The burning of waste gas (i.e., flaring) is a common waste disposal practice in these study areas, but its effect on air quality is not well characterized. Franklin and colleagues analyzed flaring activities in the Permian Basin by combining satellite observations from the Visible Infrared Imaging Radiometer Suite using the Nightfire algorithm (Elvidge et al. 2013) with the field measurements of air pollutants and VOCs described earlier. Specifically, the investigators sought to estimate flaring activity including the volume of flared gas and the contribution of flaring to observed levels of methane, nitrogen oxides, carbon dioxide, radioactivity, and select VOCs.

Visible Infrared Imaging Radiometer Suite is a multispectral instrument that records near-infrared and short-wave infrared (i.e., radiant heat) data in several spectral bands. Data are collected nightly with a 750-m spatial resolution. The observed signals can be attributed readily to the flaring combustion source. The Nightfire algorithm also allows users to relate the observed radiant heat to the volume of combusted gas. The investigators used these data and tools, along with a method they developed previously (Franklin et al. 2019) to estimate the volume of gas combusted per flare. They also calculated the numbers of nighttime flares within 5-, 10-, 20-, 30-, and 50-km buffers around the field laboratory to model the relationships between satellite-observed flares and ground-observed air pollutant concentrations.

SUMMARY OF KEY RESULTS

OBSERVATIONS OF AMBIENT AIR POLLUTION, RADIOACTIVITY, AND NOISE AT THE UOGD FIELD LABORATORY (AIM 1)

Summary statistics for the components measured at the field laboratory are presented in Commentary Table 1. Franklin and colleagues observed high diurnal and seasonal variability in the observed levels of most components measured during the study period. Many of the observed components experienced frequent occurrences of elevated spikes in concentrations. For example, although the mean concentration of methane over the study period was 2.6 ppm, it exceeded 20 ppm in nearly every month of the study and exceeded 100 ppm on several occasions (**Commentary Figure 1**). Mean concentrations of VOCs with low carbon numbers (e.g., ethane and propane) were the highest, and those with high carbon numbers (e.g., octane and xylenes) were the lowest.

Concentrations of most pollutants measured in this study were higher than those reported at comparison sites in the Denver Julesburg Basin and elsewhere. This was the case for average hourly and annual concentrations, as well as maximum values. For example, the observed annual mean concentrations of benzene (0.67 ppb) were substantially higher than those observed at the Colorado Denver Julesburg Basin sites (all below 0.15 ppb; Investigators' Report Figure 16) and at air quality stations in several large Texas cities that served as reference locations (all below 0.60 ppb; Investigators' Report Figure 40). All carbon monoxide and sulfur dioxide data were below the corresponding short- and long-term NAAQSs for those pollutants.

The radioactivity data showed high diurnal and seasonal variability, with values ranging from below the detection limit up to 173 Bq m^3 for gas-phase radioactivity and up to 99 Bq m^3 for particle-associated radioactivity. For reference, the EPA estimates that the average concentration of indoor radon among homes in the United States is about 50 Bq/m^3, and they recommend that action be taken to mitigate concentrations greater than 150 Bq/m^3 in homes.

Overall, many of the components measured at the field laboratory were correlated significantly with each other, which suggests that nearly all the components measured were emitted from similar or co-located sources.

The investigators collected over 300,000 1-minute observations of A- and C-weighted noise levels during the study period. Mean and median values of A-weighted levels (which emphasize midfrequencies) were approximately 60 decibels (dB), and those for C-weighted levels (which include lower sound frequencies) were approximately 70 dB. Noise levels between 60 and 70 dB correspond to what might be experienced as background noise in a typical office setting (i.e., normal level conversation, background music, or the sounds of common office equipment).

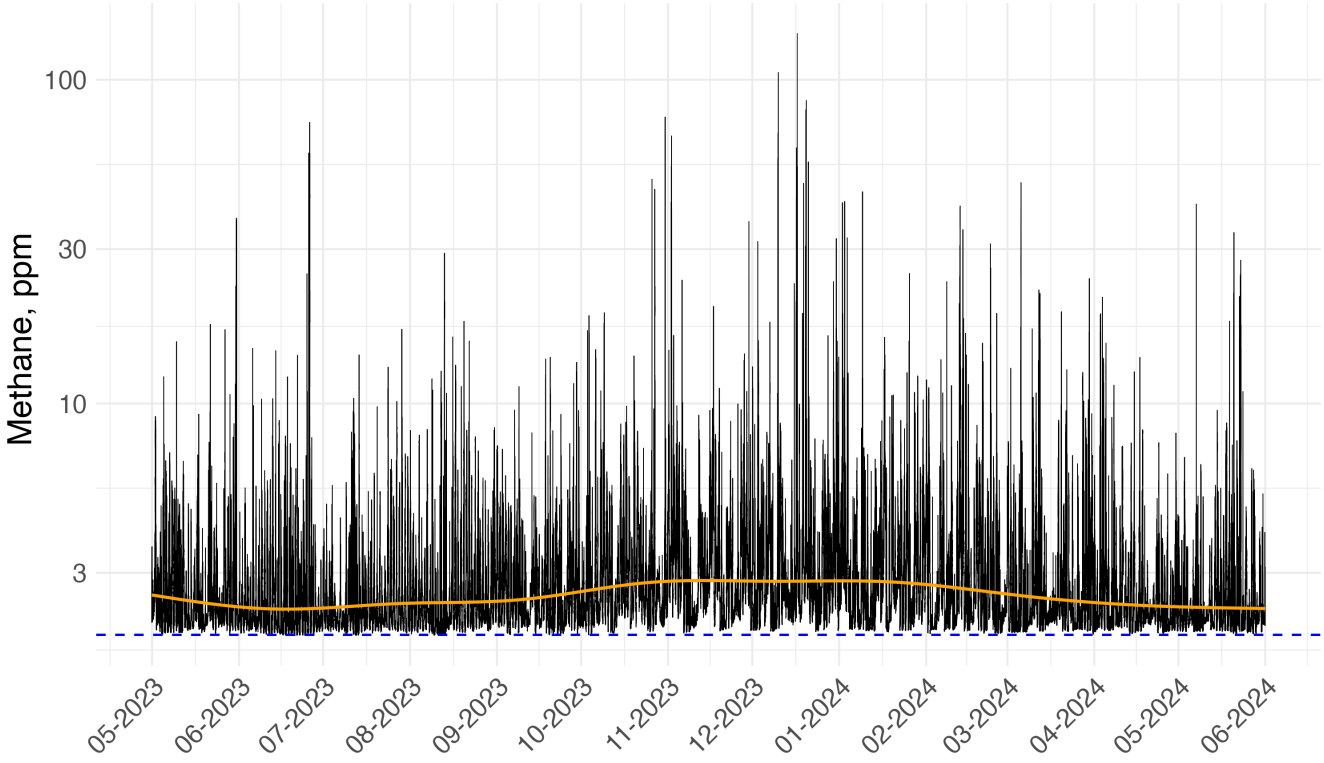

Commentary Figure 1. Time series plot showing methane measurements at the field laboratory located in Loving, New Mexico. The orange line represents the monthly running mean, and the blue dashed line represents the global background level of 1.93 ppm. Source: Investigators' Report Figure 10.

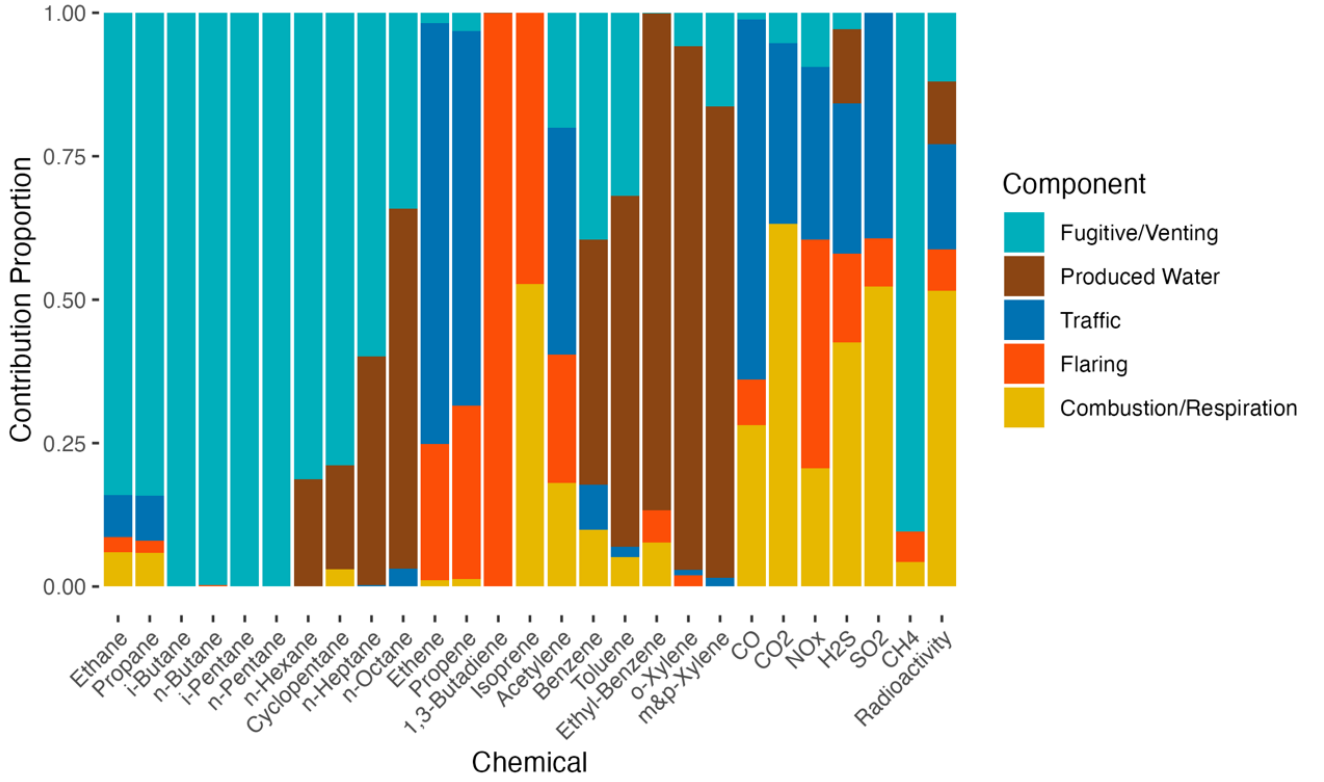

Commentary Figure 2. Contribution proportions of each compound to the five factors identified through the source apportionment analysis. Source: Investigators' Report, Figure 32.

The results of the machine learning models indicated that carbon dioxide was the pollutant whose variability was the most correlated with the noise measurements (i.e., had the best model fit according to R^2 and root mean square error; Investigators' Report Table 4). Nitrogen oxides were the only pollutants to have a high-frequency sound signal, differentiating themselves from carbon dioxide, carbon monoxide, and hydrogen sulfide, which had only low-frequency sound signals. The low frequencies associated with carbon dioxide suggested a source related to compressors, which have combustion as well as venting aspects. Methane was also associated with low-frequency sound signals, which, unlike carbon dioxide, were likely from flowback operations, leaks, and fugitive emissions from compressors.

In the source apportionment analysis, the investigators identified five factors representing various sources of UOGD emissions. These factors together explained about 95% of the overall variance in the data: oil and gas fugitive emissions and venting (45%), handling, storage, and evaporation from produced water ponds (39%), traffic emissions (10%), flaring (9%), and widespread combustion and radon emissions (4%) (**Commentary Figure 2**). Note that the sum of factor-specific variance explained values can exceed 100% due to shared explanatory power between factors.

Overall, most of the pollutants measured showed high variability, with frequent occurrences of elevated concentration spikes.

PATTERNS OF PETROLEUM HYDROCARBONS IN AMBIENT AIR BASED ON PASSIVE SAMPLING IN POPULATED AREAS CLOSE TO UOGD ACTIVITY (AIM 2)

Sampling of hydrocarbons in populated areas close to UOGD activity indicated that concentrations of n-hexane and 2-methylpentane were the highest and most variable among the hydrocarbons collected on the samplers, while concentrations of ethylbenzene and the xylenes were the lowest (Investigators' Report Appendix Tables B1 and B2). The observed concentrations of most hydrocarbons were strongly correlated with each other.

Observed concentrations of benzene were highest during fall and winter and lowest during spring and summer. The investigators attributed these patterns to seasonality in atmospheric dynamics, with deeper, more turbulent atmospheric boundary layers in spring and summer and more shallow boundary layers in fall and winter. Overall median and maximum values for benzene were 0.20 and 0.90 ppb, respectively, at the Eagle Ford Shale sites, as compared with 0.50 and 1.68 ppb at the fixed-site field laboratory.

The investigators found that average hydrocarbon concentrations were correlated positively (and statistically significantly) with the number of wells surrounding each site within several buffer distances examined. For example, concentrations of benzene were correlated (r = 0.87 and 0.66) with well counts within 10- and 5-km buffers, respectively (**Commentary Figure 3**). Average hydrocarbon concentrations were not correlated significantly with the production volumes at the surrounding well sites, however, regardless of buffer size.

Overall, the data collected from the passive sampling network suggested northwest to southeast (i.e., from Carlsbad toward Loving) increases in ambient concentrations of the measured hydrocarbons, which corresponded to the known UOGD and traffic activities in the area.

CHARACTERIZING THE LOCATIONS AND MAGNITUDE OF FLARING AND ITS EFFECT ON AIR QUALITY AND RADIOACTIVITY (AIM 3)

Franklin and colleagues detected a total of 71,401 individual nightly gas signals in the Permian Basin study area during the study period (i.e., May 2023 to June 2024). Their analyses produced estimates of individual flare temperature, source area, and radiant heat for each flare. Unfortunately, however, they were able to estimate methane flared gas volume for only 40% of these (mean volume per time = 0.100 m^3/s). Notably, only 36 flares (recorded over 32 nights) were recorded within 5 km of the field laboratory. That is, most flares were located at greater distances (i.e., between 10 and 50 km) from the sampling station. They found that nightly average concentrations of several VOCs (benzene, ethane, and ethene), methane, carbon monoxide, carbon dioxide, nitrogen oxides, and total radioactivity were correlated with the number of flares and with the estimated flared gas volume within 50 km of the field laboratory (Investigators' Report Figure 50). These findings suggested that the flaring contributed to the concentrations of these components.

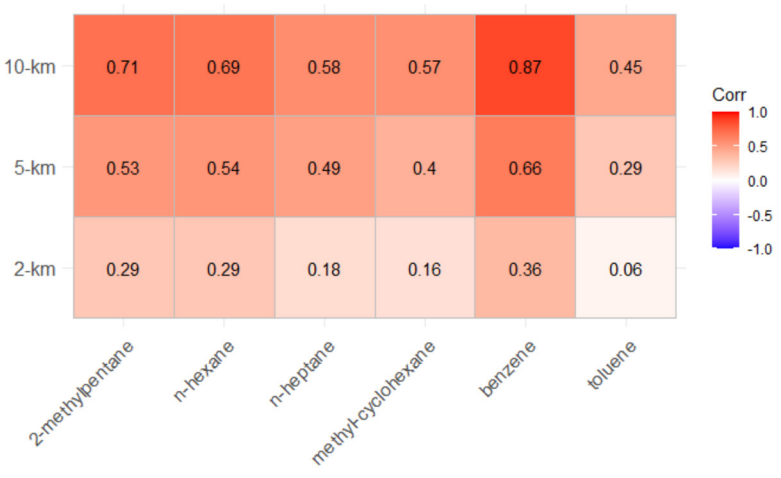

Commentary Figure 3. Correlation matrix (r values) between the half-annual averages of five hydrocarbons measured at the seven passive sampling stations and the counts of wells in 2-, 5-, and 10-km buffers around them. Source: Investigators' Report Figure 44.

HEI ENERGY REVIEW COMMITTEE'S EVALUATION

STUDY DESIGN, DATASETS, AND ANALYTICAL APPROACHES

This study provided important insights into the contributions of UOGD activities to potential local and regional exposures to noise, airborne radioactivity, and many air pollutants in the Permian Basin and Eagle Ford Shale areas. The results of the study document that UOGD, along with older oil and gas operations, are the dominant source for air pollution in the study area, with emissions arising specifically from production and storage activities, gas flaring, and truck traffic.

In its independent evaluation of the report, the HEI Energy Review Committee identified several strengths of the study design. One strength was the use of multiple measurement methods, such as stationary, passive, and satellite monitoring. Others were the long, continuous sampling period of over 1 year and the use of creative and novel exposure modeling approaches. Committee members were impressed with the large number of components the investigators measured, including several criteria air pollutants and many VOCs, along with detailed measurements of weather and noise, using a wide variety of different instruments.

The investigators compiled detailed information on the locations of and activities at well pads throughout the study areas during the sampling period. The Committee appreciated the comparisons of samples collected at the study sites with those collected at locations in other nearby UOGD regions and with urban background air quality stations. An additional strength of the study was the involvement of volunteers from the local communities to support the collection of the passive sampling data.

The Committee recognized that the development and implementation of the approach that combined remote sensing tools, machine learning, and ground-based observations to characterize counts and locations of flaring events and their contributions to regional concentrations of methane was important work. The Committee members also found that the analyses that linked well pad locations and activity with the various components measured were effective for attributing them directly to the UOGD activities. Moreover, the analyses that linked specific noise levels to the timing of individual emissions source were clever and produced original findings.

A limitation of the study was the investigators' use of a single noise monitoring site. Additionally, the instrument used for measuring noise levels could detect A-level frequencies that were only relatively nearby. The device was better able to detect levels of C-weighted frequencies, which can travel longer distances from their source. Finally, the monitoring methods could not distinguish between UOGD and older oil and gas operations

FINDINGS AND INTERPRETATION

Overall, Franklin and colleagues presented their findings very thoroughly and fairly. They included in the report over 50 figures, including a mix of maps, charts, and photographs, along with several tables, to help readers visualize and understand the results clearly. The Committee agrees with the investigators that UOGD activities appear to be the dominant source of air pollution in the study area.

Many of the findings arising from this study were interesting and useful. For example, the temporal richness of the extensive sampling program allowed the investigators to observe and describe both diurnal (short-term) and seasonal (long-term) patterns for many of the components they measured.

Their ability to interpret the relevance of key findings in ways that were meaningful to potential policymakers and industry alike, and to compare their findings with those from other locations and studies, was an additional strength of the report.

CONCLUSIONS

In summary, this study contributed to our knowledge about potential exposures to a variety of emissions from UOGD activities at local and regional scales. The study showed that UOGD activities are the dominant source of air pollution in the study area. The results indicate that communities living near UOGD activities are potentially exposed to pollutants of health concern. The investigators, however, did not investigate specific health effects related to their findings. Further study is therefore needed to determine local exposures to hazardous air pollutants, such as benzene and ozone. The work presented by Franklin and colleagues is among the most detailed air quality sampling to be conducted in an active oil and gas production region during a peak production period. Whereas many previous studies on air emissions from UOGD activities in the Permian Basin focused exclusively on methane emissions, this study added valuable data on a variety of VOCs and other air pollutants such as nitrogen oxides and ozone. It also added information on less-commonly studied exposures associated with this industry, such as airborne radioactivity and noise emissions.

ACKNOWLEDGMENTS

The HEI Energy Review Committee thanks the ad hoc reviewers for their help in evaluating the scientific merit of the Investigators' Report. The Committee is also grateful to Donna Vorhees for oversight of the study, to Dan Crouse for assistance with the review of the report and preparation of its Commentary, to Kristine Nemec for editing the Investigators' Report and its Commentary, and to Kristin Eckles and Hope Green for preparing this Research Report for publication.

REFERENCES

Allen DT. 2014. Atmospheric emissions and air quality impacts from natural gas production and use. Annu Rev Chem Biomol Eng 5:55–75, *https://doi.org/10.1146/annurev-chembioeng-060713-035938*.

Allshouse WB, McKenzie LM, Barton K, Brindley S, Adgate JL. 2019. Community noise and air pollution exposure during the development of a multi-well oil and gas pad. Environ Sci Tech, *https://doi.org/10.1021/acs.est.9b00052*.

Banan Z, Gernand JM. 2018. Evaluation of gas well setback policy in the Marcellus Shale region of Pennsylvania in relation to emissions of fine particulate matter. J Air Waste Manage Assoc 68:988–1000, *https://doi.org/10.1080/10962247.2018.1462866*.

Bell C, Vaughn T, Zimmerle D, Herndon S, Yacovitch T, Heath G, et al. 2017. Comparison of methane emission estimates from multiple measurement techniques at natural gas production pads. Elem Sci Anth 5, *https://doi.org/10.1525/elementa.266*.

Deziel NC, Clark CJ, Casey JA, Bell ML, Plata DL, Saiers JE. 2022. Assessing exposure to unconventional oil and gas development: strengths, challenges, and implications for epidemiologic research. Curr Environ Health Rep 9:436–450, *https://doi.org/10.1007/s40572-022-00358-4*.

Elvidge CD, Zhizhin M, Hsu F-C, Baugh KE. 2013. VIIRS Nightfire: satellite pyrometry at night. Remote Sens 5:4423–4449, *https://doi.org/10.3390/rs5094423*.

Fallah-Shorshani M, Fruin S, Yin X, McConnell R, Franklin M. 2024. Estimating near-roadway air pollution from multi-frequency noise measurements. Sci Total Environ 944:173900, *https://doi.org/10.1016/j.scitotenv.2024.173900*.

Franklin M, Chau K, Cushing LJ, Johnston JE. 2019. Characterizing flaring from unconventional oil and gas operations in South Texas using satellite observations. Environ Sci Technol 53:2220–2228, *https://doi.org/10.1021/acs.est.8b05355*.

Garcia-Gonzales DA, Shonkoff SBC, Hays J, Jerrett M. 2019. Hazardous air pollutants associated with upstream oil and natural gas development: a critical synthesis of current peer-reviewed literature. Annu Rev Public Health 40:283–304, *https://doi.org/10.1146/annurev-publhealth-040218-043715*.

Guarnone M, Rossi F, Negri E, Grassi C, Genazzi D, Zennaro R. 2012. An unconventional mindset for shale gas surface facilities. J Nat Gas Sci Eng 6:14–23, *https://doi.org/10.1016/j.jngse.2012.01.002*.

Haley M, McCawley M, Epstein AC, Arrington B, Bjerke EF. 2016. Adequacy of current state setbacks for directional high-volume hydraulic fracturing in the Marcellus, Barnett, and Niobrara Shale Plays. Environ Health Perspect, *https://doi.org/10.1289/ehp.1510547*.

Health Effects Institute (HEI) Energy Research Committee. 2019. Potential Human Health Effects Associated with Unconventional Oil and Gas Development: A Systematic Review of the Epidemiology Literature. Special Report 1. Boston, MA: Health Effects Institute.

Health Effects Institute (HEI) Energy Research Committee. 2020. Human Exposure to Unconventional Oil and Gas Development: A Literature Survey for Research Planning. Communication 1. Boston, MA: Health Effects Institute.

Maskrey JR, Insley AL, Hynds ES, Panko JM. 2016. Air monitoring of volatile organic compounds at relevant receptors during hydraulic fracturing operations in Washington County, Pennsylvania. Environ Monit Assess 188:1–12, *https://doi.org/10.1007/s10661-016-5410-4*.

McCawley M. 2013. Air, Noise, and Light Monitoring Results. Assessing Environmental Impacts of Horizontal Gas Well Drilling Operations (ETD-10 Project), West Virginia Department of Environmental Protection Division of Air Quality, Charleston, West Virginia. Available: *https://dep.wv.gov/oil-and-gas/Horizontal-Permits/legislativestudies/Documents/WVU%20Final%20Air%20Noise%20Light%20Report.pdf* [accessed 22 April 2025].

Mitchell AL, Tkacik DS, Roscioli JR, Herndon SC, Yacovitch TI, Martinez DM, et al. 2015. Measurements of methane emissions from natural gas gathering facilities and processing plants: measurement results. Environ Sci Tech 49:3219–3227, *https://doi.org/10.1021/es5052809*.

Paulik LB, Hobbie KA, Rohlman D, Smith BW, Scott RP, Kincl L, et al. 2018. Environmental and individual PAH exposures near rural natural gas extraction. Environ Pollut 241:397–405, *https://doi.org/10.1016/j.envpol.2018.05.010*.

Pennsylvania Department of Environmental Protection. 2018. Long-Term Ambient Air Monitoring Project: Marcellus Shale Gas Facilities. Available: *https://files.dep.state.pa.us/air/airquality/aqportalfiles/monitoring%20topics/toxic%20pollutants/docs/final_long-term_marcellus_project_report_071018.pdf* [accessed 22 April 2025].

Vaughn TL, Bell CS, Pickering CK, Schwietzke S, Heath GA, Pétron G, et al. 2018. Temporal variability largely explains top-down/bottom-up difference in methane emission estimates from a natural gas production region. Proc Natl Acad Sci 115:11712–11717, *https://doi.org/10.1073/pnas.1805687115*.

Zavala-Araiza D, Allen DT, Harrison M, George FC, Jersey GR. 2015. Allocating methane emissions to natural gas and oil production from shale formations. ACS Sustain Chem Eng 3:492–498, *https://doi.org/10.1021/sc500730x*.

ABBREVIATIONS AND OTHER TERMS

BC	black carbon
Boulder AIR	Boulder Atmosphere Innovation Research
BTEX	benzene, toluene, ethylbenzene, and xylenes
C_2	ethane
C_8	octane
CH_4	methane
CO	carbon monoxide
CO_2	carbon dioxide
dB	decibel
DJB	Denver Julesburg Basin
ECC	Erie Community Center
EFS	Eagle Ford Shale
FID	Flame Ionization Detector
GC	gas chromatograph/gas chromatography
H_2S	hydrogen sulfide
HDBSCAN	Hierarchical Density-Based Spatial Clustering of Applications with Noise
HRRR	High-Resolution Rapid Refresh
HYSPLIT	Hybrid Single-Particle Lagrangian Integrated Trajectory
Hz	hertz
kHz	kilohertz
LNM	Loving, New Mexico
LUR	Longmont Union Reservoir
NAAQS	National Ambient Air Quality Standards
NMF	non-negative matrix factorization
NO	nitric oxide
NO_2	nitrogen dioxide
NO_x	nitrogen oxides
O_3	ozone
PAH	polycyclic aromatic hydrocarbons
PB	Permian Basin
PCSF	potential source contribution function
ppb	parts per billion
ppm	parts per million
RMSE	root mean square error
SO_2	sulfur dioxide
TCEQ	Texas Commission on Environmental Quality
UOGD	unconventional oil and gas development
VIIRS	Visible Infrared Imaging Radiometer Suite
VOC	volatile organic compound
VNF	VIIRS Nightfire
XGB	extreme gradient boosting

HEI BOARD, ENERGY COMMITTEES, and STAFF

BOARD OF DIRECTORS

Richard A. Meserve, Chair *Senior of Counsel, Covington & Burling LLP; President Emeritus, Carnegie Institution for Science; former Chair, US Nuclear Regulatory Commission*

Stephen Corman *President, Corman Enterprises*

Martha J. Crawford *Operating Partner, Macquarie Asset Management*

Ana V. Diez Roux *Dana and David Dornsife Dean and Distinguished University Professor of Epidemiology, Dornsife School of Public Health, Drexel University; Director, Drexel Urban Health Collaborative*

Michael J. Klag *Dean Emeritus and Second Century Distinguished Professor, Johns Hopkins Bloomberg School of Public Health*

Alan I. Leshner *CEO Emeritus, American Association for the Advancement of Science*

Catherine L. Ross *Regents' Professor Emerita, City and Regional Planning and Civil and Environmental Engineering, Georgia Institute of Technology; Chairman of the Board of Directors of the Auto Club Group, American Automobile Association*

Martha E. Rudolph *Environmental Attorney, Former Director of Environmental Programs, Colorado Department of Public Health and Environment*

Karen C. Seto *Frederick C. Hixon Professor of Geography and Urbanization Science, Yale School of the Environment, Yale University*

Jared L. Cohon *President Emeritus and Professor, Civil and Environmental Engineering and Engineering and Public Policy, Carnegie Mellon University, In Memoriam 1947–2024*

ENERGY COMMITTEE OF THE HEI BOARD OF DIRECTORS

Martha E. Rudolph, Chair *Colorado Department of Public Health and Environment*

Michael J. Klag *Dean Emeritus and Second Century Distinguished Professor Emeritus, Johns Hopkins Bloomberg School of Public Health*

Richard A. Meserve *Senior of Counsel, Covington & Burling LLP; President Emeritus, Carnegie Institution for Science; former Chair, US Nuclear Regulatory Commission*

Jared L. Cohon *President Emeritus and Professor, Civil and Environmental Engineering and Engineering and Public Policy, Carnegie Mellon University, In Memoriam 1947–2024*

HEI ENERGY RESEARCH COMMITTEE

George Hornberger, Chair *Distinguished Professor Emeritus, Vanderbilt University*

Alfred Eustes *Associate Professor Emeritus, Petroleum Engineering Department, Colorado School of Mines*

Julia Haggerty *Associate Professor of Geography, Department of Earth Sciences, Montana State University*

Kirsten Koehler *Professor, Department of Environmental Health and Engineering, Bloomberg School of Public Health, Johns Hopkins University*

Christopher Paciorek *Adjunct Professor and Research Computing Consultant, Department of Statistics, University of California, Berkeley*

Armistead (Ted) G. Russell *Howard T. Tellepsen Chair and Regents Professor of Civil and Environmental Engineering, Georgia Institute of Technology*

Peter S. Thorne *University of Iowa Distinguished Chair and Professor, Department of Occupational and Environmental Health, University of Iowa College of Public Health*

Yifang Zhu *Professor of Environmental Health Sciences, UCLA Fielding School of Public Health, University of California, Los Angeles*

Continues next page

HEI BOARD, ENERGY COMMITTEES, and STAFF

HEI ENERGY REVIEW COMMITTEE

Isabelle Cozzarelli, Chair *Senior Research Scientist Emerita, USGS Geology, Energy, & Minerals Science Center*

Jim Crompton *Affiliate Professor, Petroleum Engineering Department, Colorado School of Mines*

Albert Presto *Director, Center for Atmospheric Particle Studies; Research Professor, Department of Mechanical Engineering, Carnegie Mellon University*

Christine Wiedinmyer *Director of UCAR Community Programs, University Corporation for Atmospheric Research (UCAR)*

Jun Wu *Professor, Department of Environmental and Occupational Health, University of California, Irvine*

STAFF AND CONSULTING SCIENTISTS

Elena Craft *President and CEO*

Ellen K. Mantus *Director of Science*

Donna J. Vorhees *Director of HEI Energy*

Thomas J. Champoux *Director of Science Communications*

Jacqueline C. Rutledge *Director of Finance and Administration*

Emily Alden *Corporate Secretary*

Daniel S. Greenbaum *President Emeritus, In Memoriam 1952–2024*

Robert M. O'Keefe *Vice President Emeritus*

Annemoon M. van Erp *Deputy Director of Science Emerita*

Amy Andreini *Science Communications Specialist*

Hanna Boogaard *Consulting Principal Scientist*

Jacki Collins *Senior Staff Accountant*

Dan Crouse *Senior Scientist*

Cloelle Danforth *Senior Scientist*

Philip J. DeMarco *Compliance Manager*

Kristin C. Eckles *Senior Editorial Manager*

Hlina Kiros *Research Assistant*

Lissa McBurney *Senior Science Administrator*

Samantha Miller *Research Assistant*

Victor Nthusi *Consulting Research Fellow*

Pallavi Pant *Head of Global Initiatives*

Allison P. Patton *Senior Scientist*

Yasmin Romitti *Staff Scientist*

Anna Rosofsky *Senior Scientist and Community Health and Environmental Research Initiatives Lead*

Abinaya Sekar *Consulting Research Fellow*

Continues next page

HEI BOARD, ENERGY COMMITTEES, and STAFF

(*Staff and Consulting Scientists, continued*)

Robert Shavers *Operations Manager*
Eva Tanner *Staff Scientist*
Alexis Vaskas *Digital Communications Manager*

RESEARCH REPORT

NUMBER 231
DECEMBER 2025

HEI energy

Health Effects Institute
75 Federal Street
Suite 1400
Boston, Massachusetts 02110, USA
+1-617-488-2300

www.healtheffects.org
www.HEIenergy.org